QUANTITATIVE HAEMODYNAMIC RESEARCH ON THE TREATMENT OUTCOME ASSESSMENT FOLLOWING EXTRACRANIAL-INTRACRANIAL BYPASS SURGERY FOR MOYAMOYA DISEASE

Fengping Zhu (M.D.)

Faculty of Medicine and Health Sciences

A thesis of The Faculty of Medicine and Health Sciences, Macquarie University, submitted in fulfilment of the requirements for the degree of Doctor of Philosophy.

March 2016

Supervisor:

Itsu Sen (Yi Qian)

Co-supervisor:

Michael Kerin Morgan

Ying Mao (HuaShan Hospital, Fudan University, China)

MACQUARIE University
SYDNEY·AUSTRALIA

Declaration of originality

I hereby declare that the work presented in this thesis has not been submitted for a higher degree to any other university or institution. To the best of my knowledge this submission contains no material previously published or written by another person, except where due reference is stated otherwise. Any contribution made to the research by others is explicitly acknowledged. All the patients' data was collected from Huashan Hospital, Fudan University, China. All the models included in this thesis were created at the Faculty of Medicine and Health Sciences, Macquarie University. Ethics Committee approvals were obtained from ethical committees of Huashan Hospital, Fudan University (Number: KY 2012-230) and Macquarie University (Number: 5201100750).

Fengping Zhu

Faculty of Medicine and Health Sciences
Macquarie University

16/03/2016

Table of Contents

Acknowledgements

I would like to express my deep and sincere gratitude to my supervisors, Professor Yi Qian, Michael Kerin Morgan and Ying Mao. Their vast knowledge and their logical way of thinking have been of great value for me. Their expertise, understanding, patience and encouragement have added considerably to my experience of research and graduation. They always pointed me in the right direction while giving me independence and flexibility that I needed. It has been a great honour to be led by their supervision.

Besides my advisors, I would like to thank the rest of my thesis committee: Professor Liangfu Zhou, Professor Jinsong Wu, Professor Wei Zhu, Professor Bin Xu and Professor Yuxiang Gu, for their insightful comments and encouragement, but also for the hard questions which inspired me to widen my research from various perspectives. Without their continuous support it would not be possible to conduct this research.

My sincere gratitude also goes to Dr. Charlie Teo who provided me an opportunity to join his team, and who gave access to visiting their operation room and research facilities.

I am also greatly grateful to my fellow lab mates for the stimulating discussions, exchanges of knowledge and skills. I would like to also extend my gratitude to David Verrelli for editing the thesis and Kaavya Karunanithi, Liuen Liang for providing a stimulating and fun filled environment and constant support through this study.

Thanks also must be given to Ms. Wendy Shi, Dr. Monica Zhang and Mr. Fenghao Liu for the wonderful friendship and their encouragements during the journey.

The Macquarie Research Excellence Scholarship (MQRES) and Skipper Travel Award were provided by Macquarie University to support my study.

Last but not the least, I would also like to thank my family for the support they provided me through my entire life. Your love, endless support, encouragement and belief in me helped me to achieve my many ambitions. Your contribution is far too great for words.

Publications from this thesis

Journal publications

1. Defeng Wang, **Fengping Zhu (Co-first Author)**, Kaming Fung, Wei Zhu, Yishan Luo, Winnie Chu, Vincent Mok, Jinsong Wu, Lin Shi, Anil Ahuja, Ying Mao. Predicting Cerebral Hyperperfusion Syndrome Following Superficial Temporal Artery to Middle Cerebral Artery Bypass based on Intraoperative Perfusion-Weighted Magnetic Resonance Imaging. Scientific Reports. 2015; 5:14140. **IF=5.078**

2. **Fengping Zhu**, Yu Zhang, Yi Qian, Masakazu Higurashi, Bin Xu, Yuxiang Gu, Ying Mao, Michael Kerin Morgan. Haemodynamic analysis of vessel remodelling in STA-MCA bypass for Moyamoya disease and its impact on bypass patency. Journal of biomechanics. 2014; 47(8):1800-1805. **IF=2.751**

3. **Fengping Zhu**, Yanlong Tian, Wei Zhu, Yuxiang Gu, Bin Xu, Jinsong Wu, Ying Mao, Liangfu Zhou. Application of 3.0T intraoperative high-field magnetic resonance imaging guidance for the surgery of arteriovenous malformation within eloquent areas. Chin Med J (Engl). 2014; 127 (6):1180-1182. **IF=1.016**

4. **Fengping Zhu**, Kaavya Karunanithi, Yi Qian, Ying Mao, Bin Xu, Yuxiang Gu, Wei Zhu, Liang Chen, Yong Wang, Huiwen Pan, Yujun Liao, and Michael Morgan. Assessing Surgical Treatment Outcome Following Superficial Temporal Artery to Middle Cerebral Artery Bypass based on Computational Haemodynamic Analysis. Journal of biomechanics. 2015; 48(15): 4053-4058. **IF=2.751**

5. Kaavya Karunanithi, **Fengping Zhu (Co-first Author)** , Bin Xu, Yuxiang Gu, Yong Wang, Liang Chen, Wei Zhu, Ying Mao, Yi Qian. Characterization of Pressure Drop Index

(PDI) in MMD patients treated with combined direct and indirect revascularization surgery. Medical Engineering & Physics, Submitted.

Articles published in Conference proceedings

Computational Analysis of Haemodynamic Parameters of MMD Patients Treated with STA-MCA Bypass. 37th Annual International Conference of the IEEE Engineering in Medicine and Biology Society, Milan, 2015.

Conference abstracts published in conference proceedings

1. Intraoperative haemodynamic monitoring for the surgery of STA-MCA bypass in the occlusive cerebrovascular disease by 3.0T intraoperative high-field MRI, 15th Interim Meeting of the World Federation of Neurosurgical Societies (WFNS), Rome, 2015.

2. Haemodynamic analysis of vessel remodelling in STA-MCA bypass for Moyamoya disease and its impact on the bypass patency, 15th Interim Meeting of the World Federation of Neurosurgical Societies (WFNS), Rome, 2015.

3. Predicting Cerebral Hyperperfusion Syndrome Following Superficial Temporal Artery to Middle Cerebral Artery Bypass based on Intraoperative Perfusion-Weighted Magnetic Resonance Imaging, 4th International Moyamoya Meeting, Berlin, 2015.

4. Vessel remodelling of STA-MCA bypass for Moyamoya disease, 13th Congress of the World Federation of Interventional and Therapeutic Neuroradiology (WFITN) and 12th Interdisciplinary Cerebrovascular Symposium, Intracranial Stent Meeting (ICS), Gold Coast, 2015.

Declaration of contributions

The contributions of authors in each chapter is as follows:

Chapter 1:

Fengping Zhu: manuscript draft; Yi Qian and Ying Mao academic advisory and manuscript revision; Morgan M: Academic advisory.

Chapter 2:

Fengping Zhu: literature review, manuscript draft; Yi Qian and Ying Mao academic advisory and manuscript revision; Michael Morgan: Academic advisory.

Chapter 3:

Fengping Zhu: manuscript draft; Yi Qian and Ying Mao academic advisory and manuscript revision; Michael Morgan: Academic advisory.

Chapter 4:

Fengping Zhu and Defeng Wang: data collection and analysis, manuscript draft; Yi Qian and Ying Mao: academic advisory and manuscript revision; Kaming Fung: data analysis, manuscript draft; Yishan Luo, Winnie Chu, Vincent Mok and Anil Ahuja: data analysis; Wei Zhu and Jinsong Wu: academic advisory; Lin Shi: manuscript revision.

Chapter 5

Fengping Zhu and Yu Zhang: data collection and analysis, manuscript draft; Yi Qian and Ying Mao: study design, academic advisory and manuscript revision; Masakazu Higurashi: data analysis; Bin Xu and Yuxiang Gu: Performing surgeries, data collection; Michael Morgan: academic advisory and manuscript revision.

Chapter 6:

Fengping Zhu and Kaavya Karunanithi: data collection and analysis, manuscript draft; Yi Qian and Ying Mao: study design, academic advisory and manuscript revision; Masakazu Higurashi: data analysis; Bin Xu and Yuxiang Gu: Performing surgeries, data collection; Wei Zhu, Liang Chen and Yong Wang: manuscript revision; Huiwen Pan and Yujun Liao: data collection; Michael Morgan: academic advisory and manuscript revision.

Chapter 7:

Fengping Zhu and Kaavya Karunanithi: data collection and analysis, manuscript draft; Bin Xu and Yuxiang Gu: Performing surgeries, data collection; Yong Wang, Liang Chen and Wei Zhu: data collection; Yi Qian and Ying Mao: study design, academic advisory and manuscript revision.

Chapter 8:

Fengping Zhu: manuscript draft; Yi Qian and Ying Mao academic advisory and manuscript revision; Michael Morgan: Academic advisory.

List of Figures

List of Tables

List of Abbreviations

2D	two dimensional
3D	three dimensional
ACA	anterior cerebral artery
ASL	arterial spin labelling
AVM	arteriovenous malformations
BA	basilar artery
bFGF	basic fibroblast growth factor
CBF	cerebral blood flow
CBV	cerebral blood volume
CFD	computational fluid dynamics
CHS	cerebral hyperperfusion syndrome
CSF	cerebrospinal fluid
CTP	computed tomography perfusion
DSA	digital subtraction angiography
DSC	dynamic susceptibility contrast imaging
DWI	diffusion weighted imaging
EC-IC	extracranial-intracranial
ECA	external carotid artery
EDAS	encephalo-duro-arterio-synangiosis
EDAGS	encephalo-duro-arterio-galeosynangiosis
EDAMS	encephalo-duro-arterio-myo-synangiosis
EDMAPS	encephalo-duro-myo-arterio-pericranial-synangiosis
EDMS	encephalo-duro-myo-synangiosis
EMS	encephalo-myo-synangiosis
EPCs	endothelial progenitor cells
EDPS	encephalo-duro-periosteal-synangiosis
ELANA	excimer laser-assisted nonocclusive anastomosis
FLAIR	fluid-attenuated inversion-recovery
HGF	hepatocyte growth factor
ICA	internal carotid artery
ICG	indocyanine green
iMRI	intraoperative MRI

MCA middle cerebral artery

MMD moyamoya disease

MMPs matrix metalloproteinases

MMS moyamoya syndrome

MMV moyamoya vessels

MRA magnetic resonance angiography

MRI magnetic resonance image

MRP magnetic resonance perfusion

MTT mean transit time

NIRS near-infrared spectroscopy

NOVA non-invasive optimal vessel analysis

OA occipital artery

PAA posterior auricular artery

PCA posterior cerebral artery

PC-MRI phase-contrast MRI

PDI pressure drop index

PET positron emission tomography

PWI perfusion weighted imaging

QMRA quantitative MRA

RCT randomized controlled trial

ROI region of interest

SMCs smooth-muscle cells

SPCs smooth-muscle progenitor cells

SPECT single photon emission computed tomography

STA superficial temporal artery

TCD trans-cranial doppler ultrasound

TIAs transit ischemic attacks

TTP time to peak

TOF time of flight

Venc velocity encoding

WSS wall shear stress

XeCT xenon-enhanced computed tomography

Abstract

Extracranial-intracranial (EC-IC) bypass surgery is the mainstay of treatment for Moyamoya disease (MMD) which is characterised by progressive steno-occlusive changes of the arteries around the circle of Willis by augmenting cerebral blood flow to the brain. However, bypass failure, postoperative bleeding and cerebral hyperperfusion syndrome (CHS) are common complications following the bypass procedures. Emerging evidence reveals that vessel remodelling and haemodynamic changes of the cerebral circulation play pathogenic roles for postoperative complications aforementioned. This study aimed to use different quantitative haemodynamic techniques, mainly computational fluid dynamics (CFD) and intraoperative perfusion weighted imaging (PWI) to estimate the haemodynamic changes after EC-IC bypass surgery, thereby aid in our understanding of the influence of haemodynamic parameters on the treatment outcomes after bypass procedures, as well as prevention of postoperative complications. Cerebrovascular haemodynamic changes of MMD patients immediately after bypass surgery were confirmed using intraoperative PWI. Immediate great increase of relative cerebral blood flow at middle cerebral artery (MCA)-terminal territory measured using intraoperative PWI might be a sensitive parameter for indicating postoperative CHS. There are vessel auto-remodelling of both superficial temporal artery (STA)-MCA bypass graft and internal carotid artery (ICA). STA-MCA bypass has a characteristic remodelling that usually reduces the flow resistance after surgery. The initial morphology of bypass has a significant effect on the outcome of bypass patency. The remodelling of ICA after bypass is associated with reduction in the volume flow rate and pressure drop, of which the percentage changes are correlated with angiographic treatment outcome grading. Pressure drop index might be regarded as a quantitative haemodynamic indicator for predicting treatment outcome during the follow-up of MMD patients.

Chapter 1

Introduction

Moyamoya is a Japanese mimetic word, meaning ‘something hazy, like a puff of cigarette smoke drifting in the air’. In 1969, Suzuki and Takaku firstly used the term “Moyamoya disease” to describe a progressive occlusive disease of the cerebral vasculature with particular involvement of the circle of Willis and the arteries that feed it [1].

MMD is generally characterized by bilateral stenosis and even occlusions of the terminal portions of the ICA and/or the proximal areas of anterior cerebral artery (ACA), MCA, followed by formation of an abnormal fine vascular network at the base of brain which looks like ‘Moyamoya’ in angiogram. The formation of ‘Moyamoya’ vessels which usually consist of parenchymal, leptomeningeal, and transdural collateral vessels seemingly compensate for reduced perfusion to brain by acting as collateral channels. However, this attempt usually fails, leading to ischemic onsets of stroke or transient ischemic attacks (TIAs). Moreover, the collateral vascular networks are immature and fragile under the long-lasting ischemic status of the brain. This leads to the other well-known clinical manifestation as haemorrhagic stroke. Angiographic examination is still essential for the diagnosis of MMD although many image techniques are used to aid in diagnosis. The aetiology of MMD is yet to be fully elucidated, however, epidemiological studies reveal that MMD might be related to genetic factors due to ethnic distributions and familial clustering. The incidence of MMD has regional differences. It is most prevalent in Asia, including Japan, China, and Korea. However, many studies have shown that MMD also occurs amongst patients of non-Asian backgrounds, including Europe, US and Africa. Surgical revascularization, including direct extracranial-intracranial arterial bypass, e.g. STA – MCA anastomosis, and indirect methods, including encephalo-duro-arterio-synangiosis (EDAS), encephalo-myo-synangiosis (EMS), encephalo-duro-myo-synangiosis (EDMS), encephalo-duro-arterio-myo-synangiosis (EDAMS) and multiple burr holes surgery, are common treatments for reconstructing cerebral blood vessel networks of MMD patients. A number of studies have demonstrated that STA-MCA bypass surgery can prevent ischemic and haemorrhagic stroke in patients with MMD. However, complications

such as cerebral ischemia, recurrent haemorrhage and hyperperfusion have also been reported following this procedure.

Over the years, many quantitative haemodynamic techniques have evolved to assess the treatment outcome and prevent complications. The purpose of this study is to apply different quantitative haemodynamic techniques, mainly and magnetic resonance perfusion to estimate the haemodynamic changes after revascularization surgery of MMD, thereby aid in our understanding of the influence of haemodynamic parameters on the outcomes of bypass operations, as well as the prevention of postoperative complications.

A brief overview of each chapter and its content is provided below, including brief description, aims and methodologies.

Chapter 2. Literature Review

This chapter provides a background to this thesis by reviewing studies conducted by others in the field of Moyamoya disease. A brief overview of the vasculature of cerebral circulation, the Circle of Willis and Moyamoya disease is presented. The recent progress of studies on Moyamoya disease is also reported after comprehensively reviewing the literature, especially in regard to characteristics, aetiology, diagnosis, treatment and outcomes.

Chapter 3. Quantitative Haemodynamic Analysis Techniques

This chapter outlines the quantitative haemodynamic techniques used in this study, including the perfusion weighted image and computational fluid dynamics. The use of these techniques on Moyamoya disease conducted by other researchers are also briefly reviewed.

Chapter 4. Predicting Cerebral Hyperperfusion Syndrome Following Superficial Temporal Artery to Middle Cerebral Artery Bypass based on Intraoperative Perfusion-Weighted Magnetic Resonance Imaging

The role of intraoperative perfusion-weighted magnetic resonance imaging in assessing the haemodynamic changes and early predicting cerebral hyperperfusion syndrome after bypass surgery is discussed in this chapter. Atlas-based method is used to minimize potential selective errors contributed by choosing regions of interest manually when analyzing

perfusion parameters. The relative perfusion parameters namely, cerebral blood flow (CBF), cerebral blood volume (CBV), mean transit time (MTT) and time to peak (TTP) were all quantified to evaluate the haemodynamic changes.

Chapter 5. Haemodynamic Analysis of Vessel Remodelling in STA-MCA Bypass for Moyamoya Disease and its Impact on Bypass Patency

This chapter reports the vessel remodelling characteristics of STA-MCA bypass and correlates the haemodynamic features of bypass with the long-term patency using CFD technique. Patient-specific models immediately after surgery and at 6-months follow-up are studied and haemodynamic parameters, including flow resistance and wall shear stress are investigated.

Chapter 6. Assessing Surgical Treatment Outcome Following Superficial Temporal Artery to Middle Cerebral Artery Bypass based on Computational Haemodynamic Analysis

There is also vessel remodelling of ICA in Moyamoya disease after bypass surgery. This section investigates the vessel remodelling characteristics of ICA and the correlation between the haemodynamic modification and angiographic treatment outcome using CFD technique. Haemodynamic parameters, including the volume flow, pressure drop and wall shear stress are analysed.

Chapter 7. Haemodynamic Assessment of Surgical Treatment Outcome on MMD Patients with Complete Circle of Willis following Revascularization Surgery

Unilateral revascularization surgery on Moyamoya disease has been reported to have effects on the whole cerebral circulation. This chapter investigates the haemodynamic features and vessel remodelling of bilateral ICA for Moyamoya disease with intact circle of Willis following unilateral revascularization surgery. Haemodynamic parameters, including the flow, pressure drop are analysed and correlated with treatment outcome.

Chapter 8. Conclusions and Future Directions

This chapter provides an overview of the findings of this thesis regarding the performance of quantitative haemodynamic analysis in assessing the treatment outcome following extracranial-intracranial bypass surgery for Moyamoya disease using CFD technology and intraoperative PWI. Limitations of each study and suggestions for improvement are also discussed. Overall, in future, the quantitative haemodynamic analysis techniques would be available to predict early postoperative complications and long-term treatment outcome.

Chapter 2

Literature Review

2.1 Moyamoya disease

2.1.1 Cerebral Circulation

The cerebral circulation is the blood movement through cerebral vasculature supplying the brain (Figure 2.1). Cerebral vasculature includes arteries, veins and microcirculatory beds. The arterial circulation delivers oxygenated blood, glucose and other essential nutrients to the brain. It is normally divided into anterior cerebral circulation and posterior cerebral circulation. The anterior cerebral circulation supplies the blood to the anterior portion of the brain, including ICA, ACA and MCA. The posterior cerebral circulation consists of vertebral artery, basilar artery (BA) and posterior cerebral artery (PCA), giving blood supply to the posterior part of the brain. Approximately 20% of the cardiac output circulates in the brain which accounts for about 2% of the body weight [2].

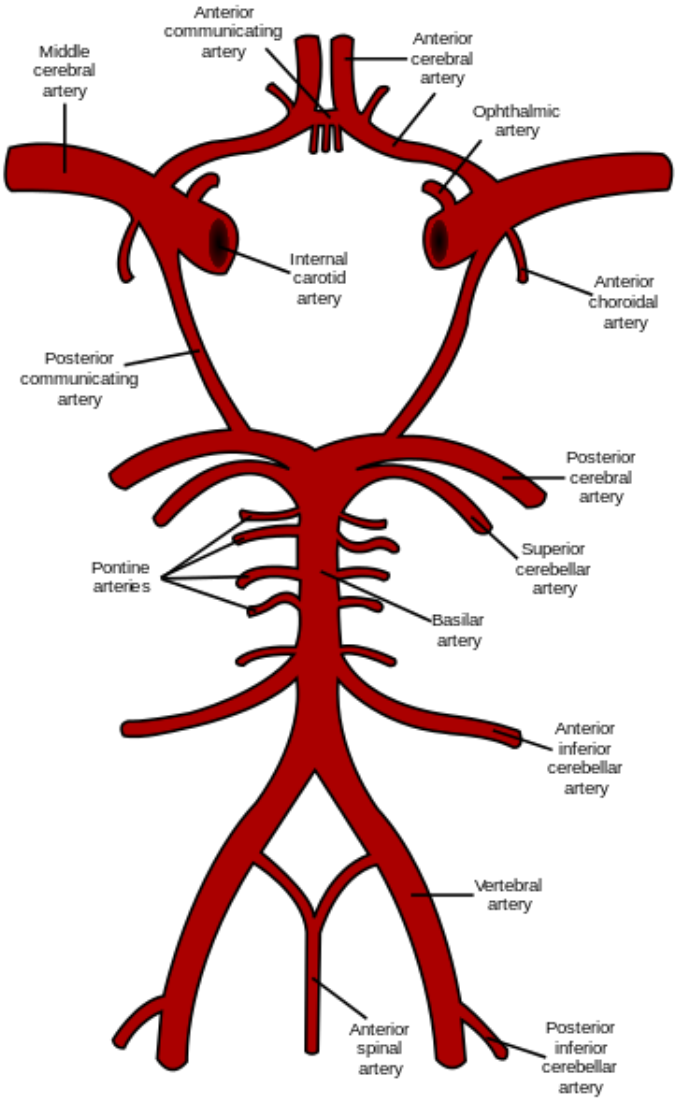

Figure 2.1 Schematic representation of the circle of Willis, arteries of the brain and brain stem [3]

2.1.2 Circle of Willis

The circle of Willis (also called Willis' circle, loop of Willis) is a circulatory anastomosis which lies in the interpeduncular fossa at the base of brain, supplying blood to the brain and surrounding tissues. It is composed of bilateral ACA, anterior communicating artery, bilateral ICA, bilateral PCA and posterior communicating artery. The circle of Willis interconnects the anterior and posterior cerebral circulations, providing backup circulation to the brain in case of occlusion in one of the supply arteries; see figure 2.1. However, there might be variations

in this typical configuration. Berman et al. reported the typical configuration of Circle of Willis is only found in 34.5% of cases [3]. The changes in the normal morphology of the circle of Willis may cause or influence the severity of many cerebrovascular disorders, such as aneurysms, infarcts, MMD and other vascular anomalies.

2.1.3 Moyamoya disease

MMD is a progressive, occlusive disease of the cerebral vasculature with particular involvement of the circle of Willis and the arteries that feed it (Figure 2.2) [4, 5]. The chronic and progressive arterial stenosis or occlusion usually involves the anterior circulation, including terminal portions of the ICA or origins of the ACA or MCA. However, the steno-occlusive changes also involves posterior circulation, especially the PCA and the posterior communicating artery. The vertebral or basilar artery was rarely impacted. Lee et al. reported that posterior cerebral artery involvement were observed in MMD patients. The small angle between the P1 segment and the basilar artery was associated with the progressive stenosis of PCA [6]. Funaki et al. found that preoperative involvement in the PCA was one of the independent risks that predicted future impairment of the postoperative long-term outcomes in paediatric MMD [7]. Outer-diameter narrowing of the involved arteries were observed in MMD patients [8]. Intimal thickening is the typical pathological change, leading to stenosis and/or occlusion of the terminal portion of the internal carotid artery, the middle and anterior cerebral arteries, the posterior communicating artery, and the posterior cerebral artery. The collateral vessels in an attempt to deliver blood to the ischemic brain form in compensation for the narrowing arteries. However, these collateral vessels are tiny and have a hazy, filmy appearance which looks like ‘puff of smoke’ on angiogram (Figure 2.3).

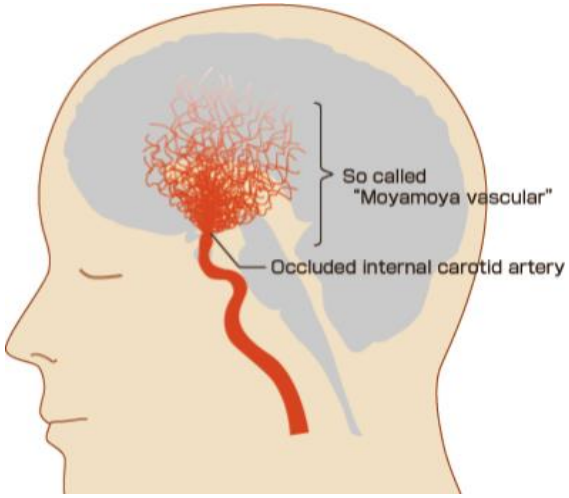

Figure 2.2 Schematic representation of Moyamoya disease [10]

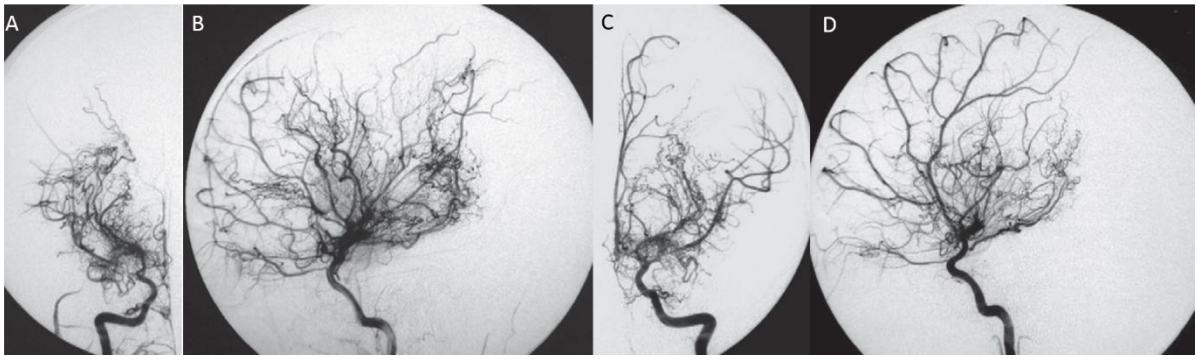

Figure 2.3 Typical findings seen with cerebral angiography in an 8-year-old boy with Moyamoya disease [11]

A, B: Angiogram of the right internal carotid artery. C, D: Angiogram of the left internal carotid artery

2.2 Characteristics of Moyamoya disease

2.2.1 Epidemiological

The prevalence of MMD has regional differences. MMD occurs predominantly in Asian countries, including Japan, China, and Korea. Most of the epidemiological studies are performed in Japan. The incidence of MMD in Japan is 3-10 per 100 000 persons, whereas the incidence in the United States is 0.086 per 100 000 persons [9, 10]. In Japan, the prevalence rate doubled from 3.16 per 100 000 persons in 1994 to 6.03 per 100 000 persons in 2003 [9]. The incidence of MMD is also increasing in the USA. In 2013, Kainth D found that from 2005 to 2008 in the USA, there were an estimated 7,473 patients diagnosed of MMD. Patients admitted with MMD were most frequently women and Caucasian [11]. In China, an epidemiological study was performed in the area of Nanjing, the capital city of Jiangsu province, showed the prevalence of MMD is 3.92 per 100 000 persons [12]. whereas, the incidence was 1.61 per 100 000 based on 2000-2011 data [13]. The nationwide epidemiological study has not been performed in the mainland China. In Korea, the incidence was increased from 2.7 to 4.3 per 100000 persons from 2005 to 2013 [14]. Previous studies have shown the incidence of MMD increased over time across different regions in the last decade [11-17].

2.2.2 Clinical

There are two peaks of distribution of age at onset and the clinical features differ substantially between children and adults [9]. The age distribution of Asian patients was bimodal with a first peak in childhood between 5 and 10 years of age and a second peak during the fourth decade [18]. However, the onset of syndrome is usually in their third, fourth, and fifth decades in North America and Europe [19-22]. Female preponderance is obvious in the population of the United States, female to male ratio prevalence is 2-4:1; In Japan and Korea,

female to male ratio prevalence is about 2:1, but about a 1:1 ratio in China [15, 23]. Generally, adult patients with MMD usually present with intracranial bleeding, whereas most paediatric cases with MMD develop TIAs or cerebral infarction [24]. Many patients are asymptomatic. Other symptoms are also reported to occur among MMD patients, including headache, epilepsy, hearing loss, cognitive dysfunction, confusion, paresis, visual defect, and involuntary movements etc. Clinical signs are often provoked by periods of hyperventilation, such as after extreme tiredness, crying, laughing, coughing, straining, and having extremely spicy foods.

2.3 Aetiology of Moyamoya disease

2.3.1 Genetic factors

The aetiology of MMD is yet to be fully elucidated, however, ethnic predisposition and familial distributions feature from epidemiological or observation studies revealed that MMD genetic factors might play an important role [25]. Approximately 6–15.4% patients of MMD were reported to have a family history [9, 26, 27], and the concordance rate of MMD in twins is reported to be as high as 80% [28]. Recently, Han et al. [29] found that the proportion of familial MMD patients was as high as 15% by scanning immediate family members of 527 MMD patients [29].

Inoue et al. performed the first genetic study on MMD in 1997, revealing that human leukocyte antigens (HLA) genes, located on chromosome 6p21.3, might be related to MMD [30]. Since then, several loci on Chromosome, including 6p21.3 [30-33], 3p24.2–p26 [34], 6q25 [35], 17q25 [36-39], 8q23 [40], 12p12 [40], 10q23.3 [41], 5q31-q32 [42], and 19q13.1 [42] have been identified to relate to MMD.

Recently, genome-wide association study identified RNF213 as an important susceptibility gene for MMD [43]. Strong associations between polymorphisms of the RNF213 gene and

MMD were observed in Japanese, Korean, Chinese and Caucasian patients with MMD [44-49]. Knockdown of RNF213 in zebra fish caused irregular wall formation in trunk arteries and abnormal sprouting vessels [43, 50]. Angiogenesis was enhanced in genetically engineered mice lacking RNF213 after chronic hind-limb ischemia, which suggested the potential role of RNF213 abnormality in the development of pathological vascular networks in chronic ischemia [51]. The increased vascular expression of MMP-9 and subsequent vascular wall thinning were also found in RNF213 knockout mice [52]. Many mutation genotypes of RNF213, including p.R4810K, p.A1622V, p.V3933M, and p.R4131C, c.14576G > A, p.R4810K (c. 14429G>A, rs112735431) were identified in different populations [46-49, 53-57]. The exact mechanism by which the RNF213 abnormality leads to MMD remains unclear. Which RNF213 variant could serve as a biomarker for early diagnosis should be further studied.

2.3.2 Angiogenesis factors

Many angiogenesis factors have been reported to relate to MMD, including basic fibroblast growth factor (bFGF) [58], smooth-muscle cells (SMCs) [59-62], smooth-muscle progenitor cells (SPCs) [63], endothelial progenitor cells (EPCs) [64, 65], vascular endothelial growth factor [66, 67], and hepatocyte growth factor (HGF) [68]. Reid et al. reported a striking bilateral occlusion of the anterior circulation resulting from intimal proliferation of SMCs in a young girl patient diagnosed of MMD. Most strikingly, the ascending aorta and the superior mesenteric artery demonstrated similar intimal proliferation, along with SMC proliferation in the media. The globally uncontrolled SMC proliferation might play a primary etiologic event leading to MMD [62]. Kang et al. used a novel experimental cell model, firstly cultured and isolated the SPCs from the peripheral blood of patients with MMD [59]. Jung et al. purified SPCs from the peripheral blood of patients with MMD [63]. Yoshimoto et al. reported the level of bFGF is high in cerebrospinal fluid (CSF) taken from patients with MMD and found a

linear correlation between the values of bFGF and cerebral vascular response to acetazolamide [58]. Jung et al. [64] found the characteristics of circulating EPCs reflect mixed conditions of vascular occlusion and abnormal vasculogenesis during the pathogenesis of MMD. EPCs play an important role in vascular homeostasis, which has been shown to be related to endothelial dysfunction, cerebral infarction, coronary artery disease and pathogenesis of stroke. Jung et al. isolated EPCs from the blood of 24 adult MMD patients and found EPCs reflect mixed conditions of vascular occlusion and abnormal vasculogenesis during the pathogenesis of MMD [64]. Nanba et al. reported the CSF level of HGF, was markedly elevated in MMD, suggesting that HGF may be a key protein for pathogenesis of MMD [68].

2.3.3 Immune factors

Immune-related factors also play roles in the pathogenesis of MMD. Lin retrospectively evaluated histopathological and immunohistochemical findings of intracranial vessels from 3 MMD patients and showed the migration of smooth muscle cells in the thickened intima, and aberrant expression of IgG and S100A4 protein in vascular SMCs. The aberrant expression of S100A4 protein was reported to be associated with upregulated SMCs proliferative and migratory activities [69].This study revealed that immune-related factors might be involved in the functional and morphological changes of SMCs, which finally caused the thickened intima [23]. Sharfstein et al., Hsiung et al. reported cases in which MMD might be related to human immunodeficiency virus infection [70, 71]. Tara et al. identified 6 MMD-associated autoantibodies against APP, GPS1, STRA13, CTNNB1, ROR1 and EDIL3 by performing high-throughput analysis of autoantibodies in 56 MMD patients [72]. Furthermore, elevated levels of circulating autoantibodies, including anti-cardiolipin [73], anti-thyroid [63, 74] and anti-α-fodrin [75] were also found in MMD patients. Kim et al. identified 5 proteins in the CSF, including PC326, SRY, and peroxisomal D3, D2-enoyl-CoA isomerase by performing a

SEREX profile of CSF obtained from MMD patients [76]. In addition, many metabolomic studies found the elevation of cellular retinoic acid-binding protein-I in CSF might be related to MMD [77, 78].

2.3.4 Radiation factors

Radiation-induced vasculopathy usually cause changes in large vessels, microscopically displaying intimal thickening and medial necrosis [79]. Radiation therapy might cause progressive intracranial occlusion of the arterial circulation, inducing the development of the Moyamoya vessels [80]. Manion et al. reported radiotherapy treatments in a paediatric patient with astrocytoma could induce MMD [81]. MMD developed following radiation therapy for optic glioma were also reported [82, 83]. In addition, Desai et al. found patients who received radiation therapy to the parasellar region at a young age (<5 years) are the most susceptible to Moyamoya syndrome. Younger children appear to be at a high risk for cerebrovascular morbidity because the vessels are immature structurally. Furthermore, higher dosages of radiation was also related to the increase in probability of developing MMD. The incidence for Moyamoya syndrome continues to increase with time, with half of cases occurring within 4 years of radiation therapy and 95% of cases occurring within 12 years [80]. A case study from Kondoh et al. reported a boy who developed Moyamoya 5 years after prophylactic cranial irradiation for the treatment of acute lymphocytic leukemia [84]. After that, more MMD cases were reported after radiotherapy for leukemia [85, 86]. However, the underlying mechanisms are still unclear. Both vascular walls and the elastic tissue on the inner walls of blood vessels were degraded after radiation, followed by occlusion of the terminal ICA and formation of Moyamoya vessels [87].

2.3.5 Other factors

The typical MMD is bilateral, while Moyamoya-like pathological vessels can also be observed unilaterally, which is defined as Moyamoya syndrome (MMS). MMS is associated with multiple clinical conditions. In addition to the related pathogenesis mechanisms aforementioned, many studies have shown that diseases coexist with MMD, such as multiple neurofibromatosis I [88-94], sickle cell disease [95-100], Down syndrome [101-106], Grave's disease [107], Turner syndrome [108], and glioma. Recently, Manjila et al. reported an adult patient with previously unrecognized mosaic Turner syndrome had acute subarachnoid and intracerebral haemorrhage as the initial manifestation of MMS [109]. Lo et al. reported two cases of individuals with Noonan-like syndrome with loose anagen hair also had MMS and heterozygous germ line mutation in SHOC2 gene was found in both cases [110].

2.4 Pathophysiology of Moyamoya disease

The pathophysiology of MMD has not been elucidated, whereas the intimal hyperplasia and medial thinness in major intracranial arteries are well-known histopathological characteristics of MMD. Hosoda et al. found that distal portions of the major cerebral arteries indicated severe waving of the internal elastic lamina, and the collapse and obstruction of the lumen. The media were atrophic, and a decrease of smooth muscle cells was observed. Stenotic or occlusive segments showed eccentric multi-layered intimal fibrous thickening and sometimes eccentric mural hrombosis [111].These occlusive changes usually involve ICA, ACA and MCA, however, PCA involvement has also been reported [112, 113]. Additionally, PCA stenosis in patients of MMD was regarded to be one of the most significant factors related to poor outcome [114, 115]. The thickened intima increased the number of smooth muscle cells, and then smooth muscle cell proliferation and fibrosis lead to the arterial stenosis [116]. Degradation of the smooth muscle cells in the medial layer and subsequent death of the

vascular smooth muscle cells are regarded to result in the medial thinness at the terminal ICA, as well as the peripheral middle cerebral artery [116].

An irregular-shaped lumen with either intimal wall thickening or thinning consistent with the angiographic appearance of abnormal angioarchitecture was found in the collateral fine vascular networks (Moyamoya vessels) [117]. Furthermore, microaneurysm formation, focal fibrin deposits and marked attenuation of the wall thickness with diminution of the elastic lamina were also observed [111]. Intimal proliferation and recruitment of EPCs might be causative of this process [68, 118, 119]. The intracranial arteries of MMD generally have intrinsic fragility due to the waviness and duplication of the internal elastic lamina [120].

2.5 Diagnosis of Moyamoya disease

2.5.1 Current diagnosis criteria

Conventional digital subtraction angiography (DSA) remains the gold standard in the diagnosis of MMD from the time of its initial description. The Research Committee on Spontaneous Occlusion of the Circle of Willis stated the DSA angiography criteria include: (1) Stenosis or occlusion at the terminal portions of the internal carotid artery or proximal areas of the anterior or middle cerebral arteries; (2) Abnormal vascular networks in the arterial territories near the occlusive or stenotic lesions, as observed during the arterial phase; and (3) Bilateral lesions [18]. With advances of other image techniques, the Committee revised the diagnostic criteria in 2012. It also included MR techniques to diagnose MMD. The present diagnostic MR criteria for MMD is as follows: (1) stenosis or occlusion of the terminal ICA or proximal ACA and/or MCA on magnetic resonance angiography (MRA); (2) abnormal vascular networks in the basal ganglia on MRA including visible flow voids ≥2 in the basal ganglia on magnetic resonance image (MRI) [121-123]. Compared with DSA, the MR techniques are non-invasive, lack of radiation, with high diagnostic yield. However, the

small vessel changes might not be detected by MRA. Additionally, the possibility of overestimating stenosis due to poor image quality should be borne in mind [123, 124]. MRI scanning for diagnosis should be done in 1.5 T MR at least.

2.5.2 Suzuki's Angiographic staging

The angiographic MMD stages were described by Suzuki et al. in 1969 [26]. It has been used widely to determine the stage of disease progression. The grading system is described as follows: I, narrowing of ICA apex; II, initiation of Moyamoya vessels (MMV); III, progressive ICA stenosis with intensification of MMV; IV, development of external carotid artery (ECA) collaterals; V, intensification of ECA collaterals and reduction of MMV; and VI, occlusion of ICA with disappearance of MMV [26]. However, the relationship of angiographic staging with the severity of MMD is still unclear. In 2011, Czabanka et al. proposed a new MMD grading system which included thorough assessments of angiography, MRI, and cerebrovascular reserve capacity. By applying it in 40 MMD patients who underwent bilateral revascularization surgery, their study revealed the new grading system could stratify clinical symptoms [125].

2.5.3 Supportive Diagnosis tools

In addition, leptomeningeal collateral, represented as 'ivy sign' on enhanced T1-weighted images or fluid-attenuated inversion-recovery (FLAIR) images, was a useful finding for suspecting MMD [126]. Recently, Seo et al. tried to use total ivy score to predict severity of disease progression [127]. Sawada et al. suggested that sylvian cistern MMV seen on T2-MRI or MRA could be used to diagnose MMD [128]. Increased conspicuity of deep medullary veins, illustrated as 'Brush sign' on susceptibility-weighted MR images, could be used to indicate the severity of MMD [129]. More recently, Uchino et al. introduced non contrast-enhanced time-resolved four-dimensional magnetic resonance angiography using an

arterial spin labelling technique (ASL-4D MRA) to diagnose MMD [130]. In their study, MMD stages assessed by DSA and ASL-4D MRA were completely matched in 18 hemispheres [130].

2.6 Treatment Options of Moyamoya disease

No curative treatment allowing the reversal of MMD pathogenesis has been proved. The concepts of management of MMD are to reduce the risks of cerebral ischemia by improving cerebral haemodynamics and to prevent intracranial haemorrhage by relieving the haemodynamic stress and reducing the pathological Moyamoya collateral network. Numerous treatment methods have been introduced in the treatment of MMD, and they are mainly divided into three categories: medical, endovascular and surgical treatment.

2.6.1 Medical treatment

To date, there is no available evidence that the use of medicine could prevent the disease progression of MMD. Medical therapy is usually recommended in patients presenting with ischemic Moyamoya angiopathy to prevent further stroke. Medical treatment is also usually used in acute phases of infarction or haemorrhage when interventional therapies are not recommended. Antithrombotic drugs, mostly aspirin can be used for adult MMD patients presenting with cerebral infarction [123, 131]. Recently, Schubert et al. concluded antiplatelet treatment was not associated with an increased risk for haemorrhage or revision, but improved outcome by reviewing 168 direct revascularization procedures of patients with MMD or cerebrovascular atherosclerotic disease [132]. Other drugs, including argatroban, clopidogrel and thienopyridine can also be used when aspirin is intolerable or ineffective [122, 133, 134]. Common supportive medical treatments, including medicines to control headache, fevers, blood pressure, high glucose level, seizure, numbness can be recommended [135]. The short-

term and/or long-term efficacy of different medications in comparison with surgical treatment for MMD should be further studied.

2.6.2 Endovascular treatment

There has been a paucity of reports in which the authors tried to use endovascular approaches to treat MMD [136-140]. Natarajan et al. [141] reported their experiences using endovascular approaches to treat intracranial stenosis in six patients with Moyamoya-type collaterals. After endovascular treatments, two patients remained asymptomatic for 4 years and 6 months, respectively. However, vessel rupture occurring during angioplasty caused severe disability in one patient. And one asymptomatic patient had severe restenosis [141]. Khan et al. reported five adult MMD patients who underwent endovascular treatment with angioplasty and/or Wingspan stenting, all patients remained symptomatic or presented with recurrent symptoms and recurrence of stenosis/occlusion on angiography [137]. Eicker et al. reported a severe intracranial and subarachnoid haemorrhage following intracranial stenting of the ICA in a young patient with MMD [138]. The high recurrence of restenosis or re-occlusion and severe complications reported in these case series indicated against endovascular treatment. However, as aneurysms usually coexist in MMD patients, endovascular treatments could be used to embolize the aneurysm, preventing the risks of haemorrhage [142-151]. Recently, Chen et al. [142] reported a case series of 5 patients with ruptured basilar tip aneurysms associated with MMD treated by stent-assisted coiling technique. All aneurysms were partially or completely occluded. There were no adverse events happening during the procedures. Medium-term follow-up angiographic examinations demonstrated total occlusion without in-stent restenosis in all cases [142].

2.6.3 Surgical treatment

Numerous EC-IC bypass techniques have been introduced for individuals with steno-occlusive cerebrovascular diseases and MMD. These techniques fall into two categories: direct revascularization, in which extracranial artery is directly anastomosed to the intracranial cortical artery for augmenting blood flow to the ischemic brain, and indirect revascularization, in which revascularized tissues are applied to the cortical surface in order to promote angiogenesis and to augment the blood flow over time [152]. The first EC-IC bypass was performed on a patient with a complete occlusion of the MCA by Donaghy and Yasargil in 1968 [153]. Since then, with the development of operating microscopes, microvascular suture material and microsurgical techniques, this surgical procedure has developed dramatically. However, the International EC-IC Bypass Study Group reported failure of EC-IC bypass surgery to prevent stroke in 1985 [154]. This study had various limitations caused by study design: Inclusion criteria for patients were disordered for the ischemia degree was not grouped; Haemodynamic evaluation was not performed in patients prior to the EC-IC bypass; Poor microsurgical technique and unstandardized postoperative therapies. The efficacy of EC-IC bypass surgery to prevent stroke for brain ischemia was re-evaluated. In 2011, the Carotid Occlusion Surgery Study also reported EC-IC bypass surgery plus medical therapy compared with medical therapy alone did not reduce the risk of recurrent ipsilateral ischemic stroke at 2 years [155]. Since then, EC-IC bypass surgery for the treatment of symptomatic cerebral ischemia related to carotid occlusive diseases has been abandoned in most centres. However, EC-IC bypass, including direct bypass, indirect bypass, and combined bypass (combination of direct and indirect procedures) have been a primary treatment for Moyamoya angiopathy for many years. Surgical indications and choices of surgical techniques varied among different neurosurgeons in different centres according to the disease concept and experiences in surgeries and perioperative management [135]. However, clinical, radiographic, metabolic and haemodynamic (cerebral perfusion and/or cerebrovascular

reserve) information must be integrated as indications for surgeries. According to Japanese and US guidelines, indications for revascularization surgery include clinical ischemic symptoms or a decreased regional cerebral blood flow, vascular response and perfusion reserve, retrieved from cerebral circulation and metabolism studies [123, 131, 156]. In our institution, we postulated surgical indications for MMD based on a comprehensive evaluation of the DSA findings, clinical manifestations, and perfusion examinations (including CT perfusion and MR perfusion). The indication criteria has been described in detail [157].

2.7 Surgical Revascularization Techniques

2.7.1 Direct Revascularization

The most common used technique for direct EC-IC bypass technique is the STA–MCA bypass [158]. Besides that, STA-ACA was used for patients with MMD in whom haemodynamic insufficiency was observed in the frontal lobe [159, 160]. Kawashima et al [160] reported the successful use of simultaneous STA-ACA and STA-MCA direct bypasses in 7 patients with MMD in which the revascularization in the ACA territory was needed. Ishikawa et al. [159] underwent simultaneous STA-MCA to and STA-ACA bypass with pan-synangiosis covering both ACA and MCA territories in 26 hemispheres of 16 patients of MMD. After the combined operations, the impaired cerebral haemodynamics in the frontal lobe was normalized and the intellectual deterioration was prevented. However, the direct STA-ACA anastomosis is not always essential in all patients with MMD, the surgical collaterals from STA-MCA bypass or the indirect revascularization procedure to the MCA territory might also provide some blood flow to the ACA territory [161]. There was no report of long-term benefits and the surgical indications for STA-ACA bypass should be further studied.

STA is most commonly used as donor artery, however, occipital artery (OA) [162, 163], the posterior auricular artery (PAA) [164-166] have been also used as donor arteries for EC-IC bypass. Menno et al. [166] reported three cases of MMD in which PAA-MCA bypass was used for EC-IC bypass. After operation, the flow directly from the bypass graft was nearly 30 ml/min after establishment of the PAA-STA bypass and the long-term bypass patency was confirmed, demonstrating that the PAA can be successfully used for EC-IC bypass surgery with good flow velocities and patency. OA-PCA anastomosis with indirect revascularization was effective for postoperative ischemia that showed symptoms in the anterior cerebral artery and PCA territories as a result of progression of a PCA lesion. Hayashi et al. performed OA-PCA bypass with encephalogaleodurosynangiosis and burr holes surgery for 3 patients with MMD who suffered from TIAs and showed disease progression, especially in the PCA after first revascularization surgery. Follow-up MRA scanning showed widening of the OA and development of peripheral collateral vessels. After the surgery, all patients showed clinical, haemodynamic and radiological improvement. One patient showed postoperative cerebral oedema as a result of focal cerebral hyperperfusion [162]. These studies of case reports showed arteries other than STA could be also considered as alternative donor vessels when the STA is not available for bypass surgery, owing to hypoplasia of the artery, division of the artery at previous craniotomy, damage of the artery during dissection, or it is already used for an intracranial bypass [166]. However, more thorough understanding of the anatomies of these arteries should be performed before using such direct revascularization arteries. Another alternative method is to use an interposition graft (vein or radial artery) for connecting ECA with intracranial ICA or MCA. However, it is usually used for high-flow bypass and not commonly used in EC-IC bypass for MMD [167, 168].

2.7.2 Indirect Revascularization

Indirect revascularization techniques differ in different neurosurgical centres and among children and adult patients. There was no standard indirect revascularization technique. The most common indirect procedures include EDAS, EMS, EDMS, EDAMS, encephalo-duro-myo-arterio-pericranial-synangiosis (EDMAPS), encephalo-duro-arterio-galeosynangiosis (EDAGS), omental flap, pial synangiosis and multiple burr hole surgery [157, 161, 169-172]. The optimal indirect revascularization strategy is still under debate [173]. However, the ultimate goal of all revascularization surgical strategies is to form vascular anastomoses between the extracranial tissues and the brain to supply blood flow to the ischemic regions. The underlying mechanisms of various indirect revascularization techniques are still unclarified, however, they were supposed to involve the formation of new vessels which require at least two processes, angiogenesis and arteriogenesis [174-176]. Angiogenesis is induced by hypoxia under pathologic conditions such as ischemic or damaged tissue and results in new capillaries. Arteriogenesis is defined as the remodelling of pre-existing arterioarteriolar anastomoses induced by physical forces, mostly fluid shear stress [174-176]. To date, there is no randomized trial assessing the superiority of any indirect revascularization technique over any other [131]. However, all of these techniques have been reported to result in favourable clinical and angiographic outcomes in patients with MMD by different high-volume MMD centers [157, 169-171, 173, 177-184].

2.7.3 Direct versus Indirect or Combined Revascularization

There is no randomized controlled trial (RCT) study comparing which revascularization technique is superior over the other among direct, indirect or combined bypass. Most research has found no significant difference in long-term outcome between the direct and indirect bypass procedures [185]. In a meta-analysis of 1,156 children with MMD on whom revascularization procedures were performed with various techniques, it was concluded that

direct and combined procedures provide better revascularization based on DSA than solely indirect procedures, but better revascularization was not associated with differences in symptomatic outcome for paediatric patients [186]. In order to investigate the incidence and characteristics of postoperative stroke in combined bypass and compare the differences with that associated with indirect bypass, Kazumata et al. performed a systematic review containing 6203 hemispheres treated, direct/combined bypass was more often associated with excellent revascularization (angiographic opacification greater than two-thirds) than indirect bypass, however, the postoperative stroke rate of the direct/combined procedure was comparable to that for the indirect procedure [187]. Amin-Hanjani et al. observed a reciprocal relationship between direct STA bypass flow and indirect EDAS collaterals after combined procedures. They retrospectively analysed the flow of STA graft by performing quantitative MRA (QMRA) in a small case series of MMD patients who underwent combined direct STA-MCA bypass and EDAS procedures. In 16 hemispheres of 13 patients, 11 (69%) demonstrated a significant (>50%) decline in direct bypass flow at >6 months compared to early post-operation, only 5 (31%) demonstrated stable graft flow over a median of 12 months follow-up period. 8 bypasses with blood flow decline and one bypass without flow decline revealed improved angiographic grading score focused on the extent of filling attributable to the revascularization as a whole [188]. The authors deduced that indirect revascularization is the reason for the favourable long-term clinical outcome and concluded the graft shrinkage over time likely is a response to reduced demand in the setting of developing collaterals. However, bypass occlusion or stenosis might be the primary reason for the flow decrease of the STA graft. In our own experiences (unpublished data), most of the patent bypass flow remained stable at around 3- to 12-month follow-up, accompanying good collateral vascularization of EDMS. Additionally, there are also many other factors leading to the bypass occlusion such as the anastomosis technique, high flow resistance of recipient artery, poor bypass morphology remodelling, high blood coagulation status, and irregular medication taking after surgery. A well-designed prospective cohort study was much more meaningful to

analyse the relationship between the haemodynamic changes of STA graft measured by QMRA and peri-operative short-term complications and/or long-term benefit of direct bypass for MMD patients [188]. According to the recommendation of American Heart Association Stroke Council, indirect revascularization is preferred in children because direct bypass is technically difficult on small-diameter vessels, whereas direct bypass is preferred in adult patients [135, 156]. Combined direct and indirect bypass is recommended for patients when the direct bypass is feasible, in order to obtain immediate increased blood flow through direct bypass and benefit from the neovascularization through indirect revascularization that develops over time [185]. In addition to the controversy about which revascularization technique is best, there are still controversies about the indication and timing of revascularization surgery in asymptomatic patients, or for the asymptomatic contralateral hemisphere in symptomatic patients [185]. Regular and careful monitoring through thorough haemodynamic and clinical evaluations are recommended for these situations. The revascularization methods should be designed based on patient-specific haemodynamic analysis.

2.7.4 Revascularization procedures in Huashan Hospital, Fudan University, China

Incision and skin flap

A modified pterional approach was adopted and to increase the contact area of the temporal muscle, the incision was curved posteriorly as much as possible with the posterior branch of the STA included in the flap. The incision was extended superiorly by 1-1.5 cm above the superior temporal line. The superior incision did not have to avoid the posterior branch of the STA, as this branch served the only purpose of direct anastomosis, and its length in the flap was already sufficient for anastomosis with any of the arteries in the bone window. The

anterior and posterior branches of the STA could be clearly observed on the medial surface of the flap.

Disposal of the temporal muscle, bone flap, and dural mater

The temporal muscle was incised along the posterior margin of the flap. The temporal muscle was dissociated from the temporal bone using a periosteal elevator to expose the entire deep temporal artery network on the deep surface of the temporal muscle. The bone window below the frontal and temporal bones was expanded carefully towards the sphenoidal crest until the site where the middle meningeal artery exited the bone tissue was exposed. Holes were then drilled at the spacing of 2-2.5 cm along the margin of the bone window for later fixation of the dura mater and temporal muscle. The dura mater on both side of the sphenoidal crest residue was suspended and fixed to avoid potential avulsion or rupture of the middle meningeal artery trunk. The middle meningeal artery trunk and its main branches were preserved intact and incised on both sides, resulting in dura mater strips in width of 0.5-1 cm. Radial incisions were made on the dura mater at the other side. After haemostasis, the dura mater was flipped over and spread over the bone window with its cranial surface in close contact with the cerebral tissue surface.

Artery anastomosis

The dissociated anterior and/or posterior branches of the STA were pulled through the temporal muscle to the vicinity of the target arteries for anastomosis. The STA was washed with pressurized normal saline containing heparin to relieve the spasm. The anastomotic end of the STA was then anastomosed with the incision on the wall of the cortical artery in an end-to-side fashion using a single 10-0 nylon atraumatic suture. After the anastomosis, Doppler ultrasound or indocyanine green (ICG) fluorescence angiography was performed to verify the patency of the anastomotic stoma.

Dura mater flip-over and temporal muscle placement

The dura mater strips incised along the middle meningeal artery trunk and branches were flipped over and sutured at the margin of the bone window. Doppler ultrasound was used to

verify the patency of the middle meningeal artery. The flip-over of the dura mater should be given up in the following conditions: (1) detection of preoperative formation of distal spontaneous anastomosis of the middle meningeal artery in stage V or VI patients, and the artery trunk was maintained in its original state without flip-over; (2) identification of diminished blood flow by ultrasound in the middle meningeal artery after the flip-over; (3) Bleeding of the accompanying veins of the middle meningeal artery. In cases with bleeding of the accompanying vein that cannot be controlled by compression with gelatin sponge, the margin of the dura mater could be sutured into the shape of a barrel (with the medial surface outside) containing the middle meningeal artery, the accompanying veins and some gelatin sponge for haemostasis. The margins of the temporal muscle was sutured with the dura mater at the fold of flip-over and fixed to the bone window. The bone flap was trimmed into compatible shape followed by reduction and fixation without compressing the STA. As the bone flap and the temporal muscle exchanged positions in the operation, the inferior of the bone flap needed to be elevated a little to reduce the space-occupying effect of the temporal muscle.

2.8 Advances of Surgical Revascularization

2.8.1 Advances in Direct Revascularization

Recently, nonocclusive anastomosis, meaning that recipient was never occluded during anastomosis creation, can be performed with the excimer laser-assisted nonocclusive anastomosis (ELANA) technique [189, 190]. The conduit vessel is sewn to the recipient vessel along with the excimer laser-associated nonocclusive anastomosis platinum ring and then the laser catheter is used to make the arteriotomy. After the anastomosis is performed between the excimer laserassociated nonocclusive anastomosis platinum ring and the conduit, the ring/graft complex is sewn to the recipient vessel, and then the laser catheter, composed of

a central suction portion and outer circular fiberoptic array, is passed through a side slit in the donor vessel and the arteriotomy is created [163, 191]. This technique has been widely used as high-flow bypass technique in the treatment of giant aneurysms or symptomatic carotid artery occlusion for the advantage of no need for temporary vascular occlusion. Recently, a completely sutureless ELANA (SELANA) bypass has been developed in order to be applied through minimal space [192]. However, this technique can't be used for very small vessels for only 2.8mm and 2.6mm ELANA platinum rings are currently available. The research of downscaling the size of the ring, downsizing the size of the laser system, as well as varying the laser catheter design and energy to allow vessels of any calibre to be effectively anastomosed using ELANA technique is underway [190, 193].

2.8.2 Advances in Indirect Revascularization

During the past decade, there has been a dramatic development in devices and technologies in the field of interventional/endovascular neurosurgery. However, fewer new surgical devices or technologies have been developed for use in the vascular neurosurgery in recent years. Newer indirect revascularization procedures are usually refined and used in combination of previous techniques by placing different tissues to the surface of ischemic brain to increase the efficiency and extent of collateral formation [194].

Seung et al. [195] described the procedures of EDAS combined with bifrontal encephalogaleo (periosteal) synangiosis for the treatment of paediatric MMD to augment revascularization. By retrospectively analysed the data for 159 children (76 boys and 83 girls) who underwent indirect revascularization procedures for the treatment of MMD, they compared the surgical results of simple EDAS (n = 67) and EDAS with bifrontal encephalogaleo (periosteal) synangiosis (n = 92). In the long-term follow-up (more than 22 months for both group), the EDAS with bifrontal encephalogaleo (periosteal) synangiosis proved to be a more effective surgical modality for the treatment of paediatric MMD, compared with simple EDAS, with

respect to the symptoms and haemodynamic changes on single photon emission computed tomography (SPECT). However, the incidences of postoperative infarctions were not significantly different between the two groups [195]. Recently, Navarro et al. [196] refined a laparoscopic method of harvesting an omental flap that preserves its gastroepiploic arterial supply. They successfully applied this technique in three paediatric patients with MMD with previous STA-MCA bypasses and progressive ischemic symptoms. After surgery, the ischemic symptoms of all 3 children resolved within 3 months postoperatively. MRI at 1 year follow-up showed improved perfusion and no new infarcts. Angiography showed excellent revascularization of targeted areas and patency of the donor gastroepiploic artery. Gross et al. [197] applied occipital pial synangiosis to posterior circulation indirect revascularization. More recently, Esposito et al. [198] tried to perform "STA-MCA bypass with EDMS combined with bifrontal encephalo-duro-periosteal-synangiosis (EDPS) as a one-staged revascularization strategy for paediatric Moyamoya vasculopathy. A case series consisting of eight children, in which six children presented with MMD, two with Moyamoya syndrome were successfully treated with this one-staged revascularization of one MCA territory and both frontal areas. However, the surgical time is quite long, the mean duration of the procedure (from incision to closure of the skin) was 6 hours and 54 minutes (range 5:10–9:35). Furthermore, two patients experienced postoperative focal seizures, successfully treated with anti-epileptic medication [198]. The benefits of these complicated methods should be assessed in the further investigations.

2.8.3 Preoperative planning

Preoperative virtual reality planning has been used to perform a reliable and minimally invasive STA-MCA bypass [163]. Kikuta et al. introduced an innovative technique to identify the recipient artery when performing STA-MCA bypass preoperatively via coregistering three-dimensional (3D) images of the arteries (MRA), the anatomic structures of the brain

(MRI), and the distribution of the regional cerebral blood flow, including positron emission tomography (PET), SPECT [199]. This technique was successful in six (STA-MCA) bypass operations, allowing STA-MCA anastomosis through a small craniotomy. However, the efficacy of this technique on clinical outcomes is unclear. Similarly, Nakagawa et al. [200] used three-dimensional DSA to perform minimally invasive virtual surgical planning for STA-MCA bypass. By applying this technique in 28 consecutive patients with various occlusive cerebrovascular diseases (including 6 MMD cases), the localization of the minicraniotomy, the skin incision on the top of STA branch, and the anastomosis point were accurately determined. Recently, Matteo et al. [201] used multiple image series(CTA, MRA) to accurately localize the STA trajectory in eight STA dissections prior to skin incision. Cabrilo et al. [202] introduced an augmented reality-based setup for EC-IC bypass. They applied this technique in a case series of three MMD patients who underwent STA-MCA anastomoses and one patient with vertebral artery aneurysm who underwent an OA-to-posteroinferior cerebellar artery bypass. Many 3D image data sets (DSA, MRA and CTA) are acquired preoperatively to segment patients' heads, skulls, and extracranial and intracranial vessels and were used for intraoperative image guidance via overlaying surgical images onto the surgical field through the operating microscope. The technique was proved to be helpful for each patient in precisely localizing donor and recipient vessels and in tailoring craniotomies [202]. The most appealing feature of this technique is that the exact course of the STA can be projected onto the field, allowing for highly efficient localization and dissection of the artery [203]. The craniotomy and locations of the donor and/or recipient arteries for minimally invasive neurosurgical procedures can be accurately identified though these techniques. However, an important issue to be kept in mind for the use is that the ischemic territory of MMD patients might be large and might widen during the bypass procedures. Whether these virtual reality planning methods translate into better clinical outcome should be further investigated.

2.8.4 Intraoperative monitoring

There are various methods for intraoperative assessment of bypass patency in cerebrovascular revascularization. Simple visual inspection and palpation of pulse is the easiest and most commonly used. However, it is subjective and mainly dependent on the experience of surgeon. Though angiography is considered as 'gold standard' for visualizing vascular anatomy, the use of intraoperative DSA is limited for the need of a specified intraoperative angiography team and the exposure of patient and medical staff to the risks of ionizing radiation.

Doppler ultrasound and ultrasonic perivascular flow probe device can measure blood flow velocity (speed and direction) in the proximal portions of large intracranial arteries. The accuracy of measurements could be influenced by the diameter and thickness of vessels.

ICG emits near-infrared fluorescence when it is excited by near-infrared light. Intraoperative ICG angiography has been applied to EC-IC bypass surgery to evaluate the haemodynamic changes induced by bypass in MMD. Awano et al. evaluated the bypass blood flow in 13 MMD and 21 non-MMD patients during STA-MCA bypass by means of ICG angiography. ICG angiography successfully demonstrated bypass blood flow from the anastomosed STA to the cortical vessels in all patients [204]. Woitzik et al. [205] applied ICG videoangiography for intraoperative confirmation of EC-IC bypass patency. They examined the role of ICG videoangiography after EC-IC bypass in 40 patients, of whom 18 had MMD. After comparing the ICG videoangiography findings with those of postoperative DSA or CTA, they confirmed ICG videoangiography could provide a reliable and rapid intraoperative assessment of bypass patency. Besides that, they identified four non-functioning STA-MCA bypasses during surgeries, which could be revised successfully in all cases, illustrating ICG videoangiography could help reduce the incidence of early bypass graft failure [205]. Schuette et al. also found ICG videoangiography was a rapid, effective, and reliable technique in determining the intraoperative patency of bypass grafts, allowing revision to reduce the incidence of technical

errors that may lead to early graft thrombosis [206]. However, ICG angiography needs special software and hardware equipped with ICG microscope; the targeted vessel should be exposed as much as possible; it is vulnerable to surrounding brain tissues, nerves, vessels and operation instruments. Meanwhile, it requires injection of foreign materials which has severe side effects including hypotension, arrhythmia, and anaphylactic shock.

Near-infrared spectroscopy (NIRS) is a technique that can be used as a noninvasive and continuous monitor of the balance between cerebral oxygen delivery and consumption[207]. It could be used for evaluating bypass function via detecting the changes of cerebral blood oxygenation [208]. However, it is difficult to evaluate bypass patency and local haemodynamics because it only reflects regional changes of CBF. In other words, they are incapable of determining blood flow velocity of targeted vessels. Meanwhile, evoked potentials are affected by the condition of electrical stimulation, the stimulating paradigms, the anaesthetic protocol and errors in electrical stimulation.

Quantitative MR angiography using non-invasive optimal vessel analysis (NOVA) software provides the ability to noninvasively assess bypass patency by measuring the blood flow through the bypass conduit. However, it is mainly used in evaluating EC–IC bypass postoperatively in serial follow up of bypass function. No data was available in the intraoperative monitoring of bypass function yet.

Intraoperative MRI (iMRI), providing real-time images for neuronavigation to compensate for errors caused by brain tissue deformation and brain shift, has been rapidly developed and widely applied in neurosurgery. We have also routinely employed iMRI in the intraoperative assessment of various cerebral neoplasms, such as microsurgical management of pituitary adenoma, cerebral glioma, lymphoma and metastasis [209-212]. Some other centres also reported its use in epilepsy surgery [213], biopsy [214] and needle implantation [215]. The use of iMRI in neurosurgery was mainly in the assessment of tumour residue and functional neuronavigation, especially in glioma, sellar region tumours, frameless stereotactic biopsy and functional neurosurgery. Few studies were reported for neurovascular surgery [216, 217].

Kaibara et al. discussed the potential impact of iMRI on the management of arteriovenous malformations (AVM) resection. Recently, Sakurada et al. reported a case in which the utilization of iMRI helped to confirm the complete removal of a left occipital AVM [216]. Compared with 1.5T iMRI, the 3.0T iMRI shows obvious advantages in the structural and functional imaging of central nervous system including faster imaging, thinner layers and high-resolution vascular images [210, 218]. The 3.0T iMRI system used in this study enabled high-resolution MRA and other multimodal functional MRI studies including diffusion weighted imaging (DWI), PWI, blood oxygenation level-dependent functional MRI and diffusion tensor imaging. High-resolution time of flight (TOF) MRA can depict the morphologic features and the vessels, especially the feeding and recipient artery. DWI demonstrates the presence of severe cytotoxic ischemic injury within minutes, which provides an estimate of the ischemic core [219]. PWI provides an assessment of cerebral haemodynamics with the potential not only to confirm the ischemic nature of DWI hyperintensities but also reveal hyperperfusion [220].

We performed intraoperative functional monitoring of the blood flow and velocity of STA graft during STA-MCA bypass and EDMS surgery in MMD patients by various image series including DWI, PWI and cine phase contrast images. We also performed high-resolution MRA to evaluate the morphological changes of the donor artery by comparing the image series pre- and post- bypass. High-resolution MRA confirmed the structural bypass patency. Neither DWI nor PWI documented the presence of brain ischemia by measuring and comparing the CBF both pre-operatively and post-operatively. By using the cine phase MR angiographic technique, we showed that the blood flow and blood volume flow values of the posterior branch of STA (anastomosed to MCA) increased markedly after the bypass surgery. Because of the possibilities of angiopathy progression and persistent stroke risk, a clinical and imaging follow-up should be continued after surgical treatment, especially for patients with unilateral angiopathy who present a risk of bilateralization [135].

2.9 Outcomes of Treatment for MMD

2.9.1 Treatment outcome classification

Angiographic treatment outcome of surgery are usually assessed by DSA according to the grading system proposed by Matsushima [221]. This grading was the proportion of the MCA area of distribution supplied by the surgical revascularization: (A), more than two thirds of the MCA distribution; (B), between two thirds and one third of the MCA distribution; and (C), less than one third of the MCA distribution. Patency of the bypass, disease progression, relief of various symptoms, disappearances of ischemic and/or haemorrhagic stroke, functional and cognitive outcome, mortality, morbidity, and improvement of haemodynamic impairment should be also included to clarify the surgical treatment outcomes.

2.9.2 Treatment outcomes

Angiographic diminishment of Moyamoya vessels was observed after EC-IC bypass surgery, which was regarded to result in decreased haemodynamic stress to pathological Moyamoya vessels [183, 222, 223]. Many observational studies indicated that direct and/or indirect bypass could reduce the risk of cerebral ischemic stroke by flow augmentation for patients with MMD [224-226]. The role of revascularization procedures to prevent haemorrhage has been controversial. Jiang et al. [183] performed a prospective single-centre cohort study in which a consecutive cohort of 113 patients with haemorrhagic MMD treated by combined direct and indirect bypass were enrolled. They observed that the annual re-bleeding rate was 1.87%/person/year after a total of 114 surgeries were performed. Ipsilateral re-bleeding occurred in 5 patients and no patient suffered ischemic or haemorrhagic stroke through 30 days after surgery. Furthermore, they found the improvement of dilation and branch extension of AChA-PCoA might be correlated with the low re-bleeding rate after detailed assessment of the angiographic changes [183]. Recently, the Japanese Adult Moyamoya (JAM) trial, a

multicenter RCT study, performed by Miyamoto et al. was reported to confirm that direct bypass surgery can reduce the risk of haemorrhage in adult patients presenting with haemorrhage secondary to Moyamoya syndrome with the strongest and best evidence to date [222, 227]. A total of 80 patients were enrolled, including 42 and 38 patients were respectively performed surgical and conservative treatments respectively after randomization. Adverse events causing significant morbidity were observed in 6 patients in the surgical group (14.3%) and 13 patients in the nonsurgical group (34.2%). Recurrent haemorrhage was more frequent in the medical group (12 versus 5) [222]. However, whether surgery contributes to a better functional outcome is unclear from these data. Further studies are required to pursue with strong evidence in this regard [227].

2.10 Treatment Complications of MMD

Postoperative complications following revascularization include cerebral ischemia, intracranial haemorrhage, hematoma, CHS, seizure, headache, infection, skin necrosis, morbidity, and mortality [122].

2.10.1 Stroke, morbidity, and mortality

Guzman et al. retrospectively reviewed a total of 233 adult patients undergoing 389 procedures and 96 paediatric patients undergoing 168 procedures for patients with MMD (In 264 patients undergoing 450 procedures), the surgical morbidity rate was 3.5% and the mortality rate was 0.7% per treated hemisphere. The cumulative 5-year risk of perioperative or subsequent stroke or death was 5.5% [228]. Kazumata et al. observed seventeen instances of postoperative strokes in 16 patients (4.7% per surgery, 95% CI 2.8%–7.5%) among a total of 358 revascularization procedures in 236 patients. Postoperative stroke occurred more frequently (7.9% per surgery) in adults than in paediatric patients (1.7% per surgery, OR 4.07, 95% CI 1.12-14.7; $p < 0.05$) [187]. Hyun et al. [229] reported an ischemic complication rate

of 7.7% in adult MMD patients by reviewing 246 revascularization procedures in 165 patients. Multiple ischemic, presence of a preoperative low density area on CT scanning, and a high signal intensity on diffusion-weighted MRI were regarded significant risk factors for peri-operative ischemic complications. Close monitoring of the perioperative care of patients with these risk factors are highly recommended [229]. Recently, Funaki et al. [230] reported the incidence of postoperative DWI-defined lesions was 9.3% by retrospective reviewing 140 consecutive direct bypass procedures on both paediatric and adult patients with Moyamoya disease. Furthermore, most of the ischemic lesions were observed in the group of "Unstable Moyamoya disease" (incidence rate is 33.3%), defined as either the rapid progression of a steno-occlusive lesion or repeat ischemic stroke, either occurring within 6 months of surgery. The unstable disease, underlying disease, and recent stroke were significant risk factors associated with DWI-detected lesions. Unstable MMD, more prevalent in younger patients and those with underlying disease, was regarded as a possible risk factor for perioperative ischemic complications. Recognition of unstable MMD may be of significant benefit to an improved surgical result through focused perioperative management based on appropriate surgical risk stratification [230].

Funaki et al. [231] reported the incidence of late cerebrovascular events after direct bypass among children with MMD. They found four patients experienced late cerebrovascular events, comprising one with stroke and three with haemorrhages, an average period of 13 years after surgery, one of whom experienced a fatal second haemorrhage. The incidence of late cerebrovascular events was 0.41 % per year; 10-year, 20-year, and 30-year cumulative incidences were 1.8 %, 7.3 %, and 13.1 %, respectively [231].

Mortality after an initial haemorrhage was 7% and increased to 29% after re-bleeding for untreated MMD patients [232]. Ryan et al. [233] performed an extensive review in regards to a future risk of haemorrhage following cerebral revascularization in MMD. They concluded that the published cases and series of MMD treatment showed a risk of haemorrhage after treatment with either direct or indirect bypass both in the immediate as well as in the long-

term future. There is Class III evidence for the predictive effect of multiple microbleeds on preoperative imaging. Recently, Miyamoto et al. [222] proved EC-IC bypass reduces the risk for recurrent haemorrhage in adult patients presenting with haemorrhage secondary to Moyamoya syndrome in a multi-center RCT study. However, among 84 surgical procedures for 42 patients in the surgical group, perioperative complications were observed in 8 cases (9.5%). Hyperperfusion symptoms were observed in 3 cases (7.1%).Other perioperative events which consisted of TIAs, seizure, local vasogenic oedema, scalp bedsore, and tear of a subcutaneous drainage tube were also observed [222].

Schubert et al. [132] retrospectively reviewes158 consecutive cases consisted of 59 MMD (37.3%) patients and 99 (62.7%) patients of cerebrovascular atherosclerotic disease undergoing 168 direct revascularization procedures. Early morbidity was 10.7% with no mortality, with evidence of ischemia in 6.9% of patients. Soft-tissue swelling (35.4% vs. 12%), any evidence of hyperdensity (63.1% vs. 12.6%) and haemorrhage (24.6% vs. 1.9%) were significantly more frequent in MMD cases, but the percentage of good/equal outcome was comparable (89.2% vs. 89.3%, mortality: 0%). They found antiplatelet treatment was not associated with an increased risk of haemorrhage or revision, but improved outcome [132].

Lee et al. reviewed a large series 292 patients with Moyamoya disease, representing 496 revascularization procedures. 7 (2.4%) patients in 7 procedures (1.8% of direct bypasses) developed a new ischemic stroke, 7 (2.4%) patients in 8 procedures (2.1% of direct bypasses) developed a postoperative haemorrhage, and 10 (3.4%) patients in 10 (2.7% of direct bypasses) procedures developed a transient neurologic deficit. All transient neurologic deficits resolved between a few hours to 14 days. High postanastomotic MCA flow was significantly correlated with perioperative ischemia, haemorrhage, and transient neurological deficits [234]. Cho et al. reviewed the long-term outcomes of combined revascularization surgery in patients with adult Moyamoya disease. 77 hemispheres in 60 patients were included. Combined STA-MCA bypass and EDAS surgery resulted in satisfactory long-term improvement in clinical, angiographic, and haemodynamic states and prevention of recurrent

stroke. The annual risks of symptomatic haemorrhage and infarction were 0.4% and 0.2%, respectively, in the operated hemispheres [235].

2.10.2 Hematoma, Seizure, and Headache

Andoh et al. reported three cases developing postoperative chronic subdural hematoma after STA-MCA bypass, in which two patients with stroke were treated with STA-MCA bypass and one patient with MMD was treated with STA-MCA bypass and EMS [236]. Seizure as a rare complication after revascularization for MMD and the underlying mechanism is still unclear. Narisawa et al. [237] investigated the relationship between seizure attack and postoperative alteration in CBF. CBF was measured by SPECT 1 and 7 days after STA-MCA anastomosis on 64 sides of the 44 consecutive patients with MMD. Three patients suffered from seizure attack at 1 to 10 days after bypass surgery. Postoperative SPECT revealed significant increase in CBF at the sites of the anastomosis in all three patients. So hyperperfusion might be the causative factor for seizure after bypass surgery with MMD. Headache is one of the major clinical presentations in MMD, especially in paediatric patients. The disturbed cerebral haemodynamics might play key roles in developing severe headache in MMD. This symptom can be completely resolved after improving the supplying collateral blood flow to the impaired hemispheres by effective revascularization surgery [238]. Hayashi et al. [239] reported headache occurred after double anastomosis and indirect bypass in a case of MMD presenting as left homonymous hemianopsia. A severe ipsilateral headache and focal seizure regardless of the blood pressure control was observed after surgery. She complained of the headache for >2 weeks. Follow-up MRI showed a small subcortical haemorrhage in the right frontal lobe. SPECT revealed that the hyperperfusion relapsed 9 days after surgery. So close monitoring of haemodynamic changes and suitable perioperative management are recommended for MMD patients.

2.10.3 Scalp complications

Scalp complications, such as alopecia or scalp necrosis, infection have been reported. Scalp necrosis and delayed wound healing have been reported as the most serious complications after STA-MCA bypass for MMD [240, 241]. Scalp necrosis is an infrequent complications of revascularization surgery for MMD patients when scalp vascularity is severely compromised. It is more prevalent in the parietotemporal area. Kwon et al. used occipital pedicle V-Y advancement flaps in 7 patients who had scalp necrosis of the parietotemporal area and a mean defect size of 8.7 cm. There were no complications such as flap necrosis, infection, or recurrence of defect in all patients during 9-month follow-up [240]. Scar widening and hair loss after craniotomy were also reported. Recently, Sanada et al. [242] designed the zigzag scalp incision for vascular reconstruction surgeries in six hemispheres of five MMD patients. All patients underwent STA-MCA bypass with EMS. Five of six hemispheres underwent simultaneous STA-ACA bypass. The scalp incision was designed not parallel to the hair stream, and the bevelled incision was conducted not to jeopardize the hair follicles. The scar and hair loss were effectively camouflaged throughout the postoperative period in all cases [242].

2.10.4 Cerebral hyperperfusion syndrome

CHS is a group of symptoms after revascularisation with headache, epilepsy, disturbance of consciousness, focal neurological deficits and intracranial bleeding as the main clinical manifestations, of which the metabolism or perfusion images may display obviously elevated regional perfusion. The definition of postoperative CHS is complicated. It is judged on radiological changes or clinical presentations. The risk factors for CHS included pre-operative CBV increases and surgery on the dominant hemisphere [243, 244]. Traditionally, the definition of radiological postoperative hyperperfusion is >100% increase over preoperative CBF values based on PET or SPECT [245]. Kim et al. [246] described a definition of post-

operative HPS as follows: (i) new post-operative neurologic deficits that were not detected in the pre-operative period; (ii) delayed post-operative neurologic deficits that were not observed immediately after the operation; (iii) reversible neurologic deficits resolved within 15 days; and (iv) the absence of other possible causes for neurologic deficits such as definite hematoma on a CT scan or acute infarction on diffusion MR images.

Although the mechanism of CHS are unknown, some studies suggested that the blood-brain barrier destruction and reactive oxide species damage led by chronic hypoxia were associated with CHS [245]. Clinically, it often occurs after carotid endarterectomy or carotid stent angioplasty [247]. Though STA-MCA bypass is traditionally regarded as the low-flow vascular anastomosis, recent studies showed that it can cause postoperative symptomatic CHS, with an incidence of 15% -50% [245, 248, 249].

2.11 Quantitative Haemodynamic studies in MMD

There are a number of ways to evaluate cerebral haemodynamics in clinic, such as PET, SPECT, XeCT. PET was considered to be the 'gold standard' image technique to accurately and quantitatively reflect the metabolism information of brain tissue; SPECT, XeCT are considered as semi-quantitative methods to measure the brain perfusion [250]. These technologies have been applied in the haemodynamic analysis of occlusive cerebrovascular disease, however, each technique has drawbacks such as high cost and unavailability for real-time monitoring. Kawamata et al. [251] performed a prospective study using intraoperative laser Doppler flowmetry and/or thermography to predict the postoperative hyperperfusion in 27 MMD patients (39 hemispheres) who underwent STA-MCA bypass surgery. During surgery, regional cerebral blood flow (rCBF) was measured with a laser Doppler flowmeter and the temperature of the cortical surface was measured with an infrared thermograph. A significant correlation was observed between intraoperative rCBF changes and postoperative rCBF increase. Furthermore, the rCBF changes measured by laser Doppler flowmetry were

significantly greater in patients with postoperative hyperperfusion. The study suggested intraoperative rCBF measurement using laser Doppler flowmetry may predict a risk of post-EC-IC bypass CHS in MMD. Recently, Fujimura et al. [252] quantitatively evaluated regional CBF at the site of the anastomosis in 23 MMD patients before and 1 day after STA-MCA bypass by an auto-radiographic method using N-isopropyl-p-[123I] iodoamphetamine SPECT, demonstrating the regional CBF value 1 day after surgery and operating on the left hemisphere significantly correlated with hyperperfusion syndrome. The cut-off value of pathological postoperative CBF increase was 46.1 ml/100 g/minutes [252]. The use of PWI and CFD in MMD will be discussed in Chapter 3.

Chapter 3

Quantitative Haemodynamic Analysis Techniques

3.1 Perfusion Weighted Image

3.1.1 The use of perfusion weighted image in MMD

PWI techniques, including computed tomography perfusion (CTP), and MR perfusion (MRP), are able to give insights into the perfusion information of tissues by blood. CTP is a technique for measuring cerebral that uses first-pass tracer methodology after bolus infusion of intravenous iodinated contrast material [253]. CBF, CBV, MTT can be measured to reflect the perfusion status of the brain. The great advantages of the technique include wide availability, high speed of the examination, and lack of significant contraindications. Disadvantages include radiation exposure to the patient and the some patients cannot endure iodinated contrast material. Zhang et al. have applied CTP to evaluate cerebral haemodynamic changes in MMD patients before and after surgery [254] .

Compared with CTP, MRP has many advantages, especially lack of radiation exposure and good repeatability. However, the arterial times through collateral pathways in Moyamoya patients can be delayed and thus underestimate the CBF values [250]. Among various MRP techniques, dynamic susceptibility contrast imaging (DSC) was used to derive various perfusion values: CBF, CBV, MTT and TTP; Dynamic contrast enhanced imaging mainly provides transfer constants and ASL imaging usually only provides CBF [255]. MRP has been increasingly applied in the diagnosis and treatment of MMD, as well as the prevention of postoperative hyperperfusion syndrome [256-264].

3.1.2 Intraoperative MRI scanning

Intraoperative MRI studies were performed with a mobile MRI system (IMRIS, Innovative Magnetic Resonance Imaging Systems, Inc., Winnipeg, MB, Canada) interfaced to a 3.0-T MR Systems console (Verio, Siemens Medical Systems, Erlangen, Germany). Besides

intraoperative use, the equipment is also used for conventional diagnostic imaging when it is not required in the operation room (OR) [265, 266]. When the system is required for intraoperative evaluation, the magnet can move from the radiological suite adjacent to the OR. All the OR equipment are MRI-compatible. MRI sequences were obtained by using an IMRIS 8 channel head coil. The following sequences were evaluated: 1) T1W TSE dark-fluid sagittal images (16 slices; TR, 2000ms; flip angle, 150; TE, 9ms; Slice-selective Inversion Recovery, TI 860ms ; matrix size, 214×320; slice thickness 5mm; field of view 224×230 mm2) were obtained in 1:28 minutes; 2) TOF MRA scans (4 slabs , 40 slices per slab; TR, 22 ms; TE, 4.2ms; flip angle, 18; matrix size, 365*384; slice thickness 0.5mm; field of view 181*200 mm2) were obtained in 8:32 minutes; 3) Diffusion Weighted Imaging (16 slices; TR 6000ms; TE 100ms; matrix size, 162*162; slice thickness 6mm; field of view 240*240 mm; fat saturation; b value=0 and 1000 s/mm2; scan time 1:08 minutes); 4) PWI was performed based on enhanced fat-suppressed T2 single-shot echo-planar imaging sequence with the following acquisition parameters: TR: 1500ms; TE: 30ms; FOV: 230×230mm^2; matrix 128×128; number of layers: 19; slice thickness: 4mm; interval: 1.2mm; flip angle: 90°. The use of intraoperative MRI for MMD is illustrated in Figure 3.1.

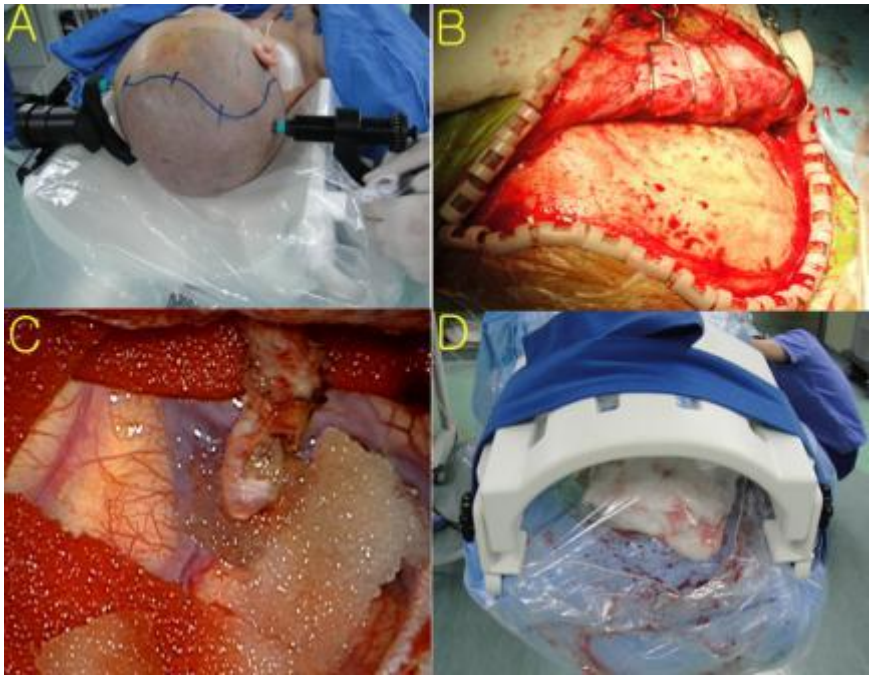

Figure 3.1 The use of intraoperative MRI for Moyamoya disease

A, The patient was fixed with a three-pin, MRI-compatible headholder for surgery and MRI scanning. B, The posterior branch of the STA (donor artery) was dissociated, the terminal part of the artery was deligated waiting for anastomosis. C, Check out the surgical field and patient body was covered with sterile envelope, the head coil was connected and fixed when intraoperative scanning was performed. D, The dissociated posterior branch of the STA was pulled through the temporal muscle and anastomosed with cortical branch of the MCA.

3.1.3 Post-processing of perfusion weighted imaging (PWI)

PWIs were post-processed by a software called Perfusion Mismatch Analyzer (PMA) (Ver.3.4.0.6, ASIST, Japan). The software computes CBF, CBV, MTT and TTP by estimating the contrast concentration using deconvolution by numerical method. The concentration of the contrast at a particular voxel in the brain, $C_v(t)$ is obtained by the time series PWI. $C_v(t)$ is related to the tissue flow, F, the fraction of contrast remaining in that voxel, or the residue function, $R(t)$, and the arterial blood supply function, $AIF(t)$, by the equation [267]:

$$C_v(t) = F \int_0^t AIF(u)R(t-u)du \quad (1)$$

$C_v(t)$ was obtained by measurement of contrast concentration from PWI. AIF(t) was evaluated by reference points automatically chosen by the software and assumption on F as a constant value was made.

In each voxel, PMA calculated R(t) by deconvolution using singular value decomposition (SVD) [268]. It was done by discretizing Eq.(1):

$$C_v(t_j) = F \sum_{i=0}^{j} AIF(t_j)R(t_j - t_i)\Delta t \quad (2)$$

where Δt is the sampling time interval. Then, Eq.(2) could be further formulated as an inverse matrix problem:

$$\begin{pmatrix} C_v(t_0) \\ C_v(t_1) \\ \vdots \\ C_v(t_{N-1}) \end{pmatrix} = F \begin{pmatrix} AIF(t_0) & 0 & \cdots & 0 \\ AIF(t_1) & AIF(t_0) & & 0 \\ \vdots & & \ddots & \vdots \\ AIF(t_{N-1}) & AIF(t_{N-2}) & \cdots & AIF(t_0) \end{pmatrix} \begin{pmatrix} R(t_0) \\ R(t_1) \\ \vdots \\ R(t_{N-1}) \end{pmatrix} \Delta t \quad (3)$$

The second matrix on the right side of Eq.(3) could be solved by SVD to obtain R(t) scaled by F. Practically, AIF(t) can lag $C_v(t)$ by a time delay in diseased regions which leads to errors in R(t) estimation. It could be tackled by replacing discretized AIF(t) with a block-circulant matrix which has been shown being equivalent to linear convolution with time aliasing [269].

The values of R(t) obtained was then plotted against time and the four perfusion parameters were calculated. In each voxel, CBF was evaluated by the peak of R(t) and CBV was determined by the area under the curve of R(t). By the central volume principle [270], MTT was calculated as the ratio of CBV to CBF. TTP was the time to the peak of $C_v(t)$.

3.2 Computational Fluid Dynamics

3.2.1 The use of computational fluid dynamics in MMD

CFD is one of the branches of mechanical engineering for analyzing fluid flow, heat transfer, and associated phenomena, using computer-based simulation [271]. With the advances in imaging and computer technology, CFD has been widely adopted in the field of biomedical engineering. In cerebrovascular disease, CFD was usually used to characterize the haemodynamic features of the formation, growth and rupture of aneurysm [272-276]. Besides that, it was also used to simulate the stent implantation for intracranial stenosis [277]. Alnaes et al. used CFD technique to analyse the haemodynamic features of complete circle of Willis, indicating high wall shear stress (WSS) was associated with an increased risk for aneurysm development [278]. More recently, Amin-Hanjani et al. applied the CFD in the treatment of cerebral AVM, demonstrating that WSS is high in the cerebral AVM arterial feeders which might result from high blood flows and insufficient compensation with feeder enlargement. The decreases of WSS might be regarded as a potential biomechanical factor for efficient AVM treatment [279][280].

There are a few studies investigating the haemodynamic characters of MMD. Seol et al. simulated the haemodynamics in the circle of Willis using computational models of 2D geometries of the distal ICA and PCA. CFD results demonstrated that shear stress was relatively low at the ICA region. The distribution of shear stress was related to the predisposing area of MMD. A continuous low shear stress level might promote the migration of smooth muscle cells and thus initiate progression of MMD [281]. Charbel et al. used computerized model to analyse the flow distribution of one Moyamoya disease and simulate cerebral blood flow following various treatment options and tried to decide which treatment option would be the best for a particular patient [282]. Karunanithi et al. [283] carried out CFD analysis on eight patients with MMD treated by indirect bypass surgery, observing

haemodynamic changes of ICA after bypass surgery. The percentage flow change and pressure drop increased at follow up for improved patients who did not develop any complications after surgery, however, the inverse changes were observed in patients who were clinically classified as no change and retrogressed [283]. More recently, Kim et al. investigated the morphology and haemodynamic characters of MMD. The vascular length and tortuosity of ICA was significantly small in Moyamoya patients showing lower curvature angles in the petrous and intra-cavernous segments compared with normal ICA. Faster blood flow and higher wall shear stress in the ICA bifurcation were verified using CFD technique [284].

3.2.2 Blood Flow Model

Governing Equations

The governing equation for fluid dynamics is the Navier-Stokes equations, which are a mathematical description of conservation of mass, momentum and energy. Since the temperature in blood is almost constant, the flow is considered to be isothermal when modeling haemodynamics. Therefore, the energy equation is omitted here.

The Continuity Equation (mass conservation) is given by:

$$\frac{\partial \rho}{\partial t} + \nabla \cdot (\rho \boldsymbol{U}) = 0 \quad (4)$$

Where ρ is the density of the fluid and $\boldsymbol{U}$ is the velocity vector.

The Momentum Equation (momentum conservation) is given by:

$$\frac{\partial (\rho \boldsymbol{U})}{\partial x} + \nabla \cdot (\rho \boldsymbol{U}\boldsymbol{U}) = -\nabla p + \nabla \cdot \tau + \rho f \quad (5)$$

Where p is the fluid pressure and f is external body force exerted on the fluid. Since in the case of modelling haemodynamics, the influence of gravitational force or buoyant force is insignificant, f is assume to be zero. τ is the stress tensor which can be expressed as:

$$\tau = \mu(\nabla \boldsymbol{U} + (\nabla \boldsymbol{U})^{\boldsymbol{T}} - \frac{2}{3}\delta \nabla \cdot \boldsymbol{U} \quad (6)$$

Where μ is the dynamic viscosity.

Under the assumption of incompressible flow and Newtonian fluid, the above equations can be simplified into the form as:

$$\frac{\partial \boldsymbol{U}}{\partial x} + (\boldsymbol{U} \cdot \nabla)\boldsymbol{U} = -\frac{1}{\rho}\nabla p + \nu \nabla^2 \boldsymbol{U} \quad (7)$$

Where ν is the kinematic viscosity defined as μ/ρ.

Discretization

The finite volume method is widely used in the field of computational fluid dynamics. The method is based on the discretization of the integral form of the conservation equations into surface integral, which are then evaluated as fluxes at each surface of the finite volume. One salient advantage of the finite volume method is that it can be applied to both structured and unstructured grid, therefore capable of solving fluid in domain with complex geometry. The commercial package ANSYS CFX (Ansys Inc., Canonsburg, PA, USA), used in our study employs the finite volume method.

3.2.3 Vessel geometry reconstruction

The patient-specific vessel models were acquired from Huashan Hospital, Fudan University with ethical approval from Huashan Hospital, Fudan University and Macquarie University. Images were obtained from MRA. Based on the images, the 3D geometries of ICA were reconstructed and segmented by using a commercial software package - MIMICS (Materialise' Interactive Medical Image Control System, Belgium) to create domains for CFD computation. Instead of using "global smoothing", manual "local smoothing" was used to preserve the 3D geometry as realistic as possible. The reconstructed geometries were then exported into ICEM CFD^{R} for mesh generation.

3.2.4 Grid generation

The quality of the mesh has great influence on the accuracy of the simulation and the speed of convergence. There are generally three types of mesh element, tetrahedral, prism and hexahedral. The mesh quality is determined by the choice of element type and their sizes. A fine mesh can usually give more accurate result than a coarse mesh, but at the cost of increasing computational time and memory use. Generally, structured mesh (hexahedral element) is preferred since it gives better result under the same cost of time and memory. However, the use of structured mesh is limited to relatively simple geometry. In contrast, tetrahedral element, though not the most efficient one, can adapt well with complex geometry. Since the ICAs in our model are generally torturous with bends, side branches and bifurcation, tetrahedral elements were chosen to mesh the domain. Element seeding size was set to be 0.3mm based on our previous mesh sensitivity analysis. In order to better capture the near-wall fluid motion and to accurately evaluate the wall shear stress, four layers of prism elements were added to the ICA wall boundary. The thickness of the first layer was set to be

0.01mm with growth ratio 1.3 based on our previous work. The total number of elements in the computational domain for each model ranges from 0.8-1.4 million.

3.2.5 Definition of fluid properties

Blood is a suspension of plasma and blood cells. It is considered to be incompressible with a constant density of 1050kg/m^3. Due to the interaction of cells, blood is a non-Newtonian fluid whose viscosity is dependent on the shear rate. The viscosity of blood decreases with the increase of shear rate, while keeping almost constant when shear rate is greater than 100s^{-1}. Therefore, the non-Newtonian effect of blood is only evident in small vessel (<0.1mm) where the shear rate is low [285]. Blood flow in arteries are treated as Newtonian fluid in many researches [286-289]. Valencia et al. studied the haemodynamics of a carotid artery model with aneurysm using both Newtonian and non-Newtonian blood model and found no significant difference between the two [290]. Therefore in our model, blood is simply considered as a Newtonian fluid having a viscosity of μ=0.0032[Pa s].

3.2.6 Assigning Boundary Conditions

Inlet boundary condition

There are generally two types of boundary conditions available for modeling blood flow. They are the Dirichlet boundary condition which prescribes a value for the variable and the Neumann boundary condition which prescribes a gradient normal for the variable. In our case, the Dirichlet boundary condition fitted best with our measurement of velocity at the proximal end of artery and was therefore chosen. Quantitative MRA, which was implemented with NOVA software (VasSol Inc., Chicago, Illinois, USA), and/or duplex ultrasonography were performed to measure the blood flow of the artery [291, 292][293].

(1) Duplex ultrasonography

Duplex ultrasonography was performed to measure the blood flow of ICA using an L9-3 linear probe (bandwidth, 3-9 MHz) (bandwidth, 1-5 MHz) on a high-end ultrasound device (Philips Healthcare, Andover, MA) [293].

(2) Quantitative MRA

Phase-contrast MRI (PC-MRI) is a noninvasive technique which can be used to accurately measure flow with flexible spatial and temporal resolution [294]. PC-MRI has a variety of established applications in quantifying the flow of cerebrospinal fluid and blood in the brain [295, 296].

However, the accuracy of PC-MRI can be affected by many factors: breathing, velocity encoding (Venc) direction, Venc value, partial volume effect, imaging temporal-resolution. Among them, the imaging plane error, the velocity encoding value and the encoding direction might significantly influence the measurement accuracy. Charbel et al. innovated to develop non-invasive optimized vascular analysis system based on PC-MRI technology [297]. The commercial NOVA software uses TOF-MRA technique to formulate 3D vascular anatomy, and allows users to define regions of interest around a vessel lumen by automatically putting the scanning plane perpendicular to the targeted vessel in the 3D space. PC-MRI scans were then performed to determine the flow direction and quantitatively measure the blood flow of the target vessels. Animal experiments and phantom study has verified that NOVA can accurately and quantitatively measure the blood flow [298-300]. In our study, the Non-invasive NOVA system was integrated into 3.0T high-field iMRI system. TOF-MRA was used to obtain the vessel geometries: TR: 22 ms; TE: 4.2 ms; flip angle: 18°; matrix: 365×384; thickness: 0.5 mm; FOV: 181×200 mm^2. The MIP value of the MRA data was

adjusted to well delineate cerebral vasculature. At the MR TECH PC workstation, the vessel of interest was selected to perform PC-MRI scanning (Figure 3.2). Scanning commands are sent to 3.0T MRI scanner to perform PC-MRI scan, and the latter information was also sent to the MR TECH PC system. After standard post-processing, the blood flow velocity of the targeted artery can be measured (Figure 3.3).

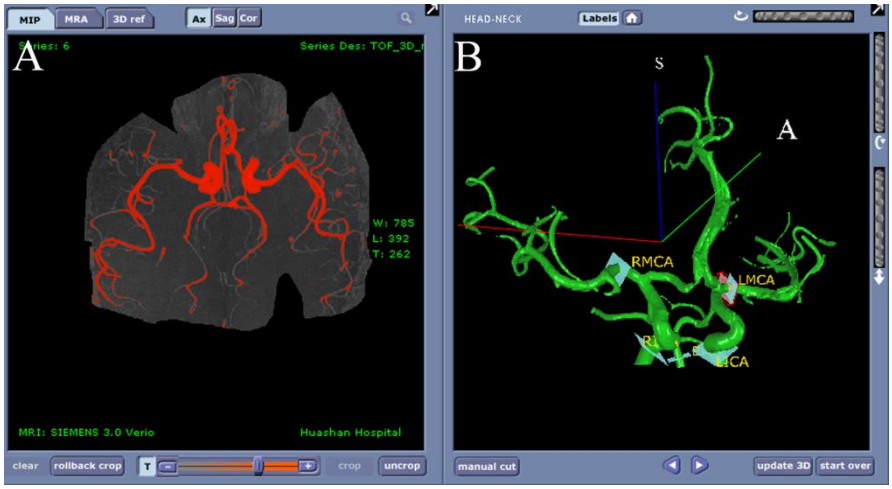

Figure 3.2 Screenshots of 3D vascular model at MR TECH PC workstation

The MIP value of the MRA data (A) can be adjusted to best delineate the 3D cerebral vasculature (B)

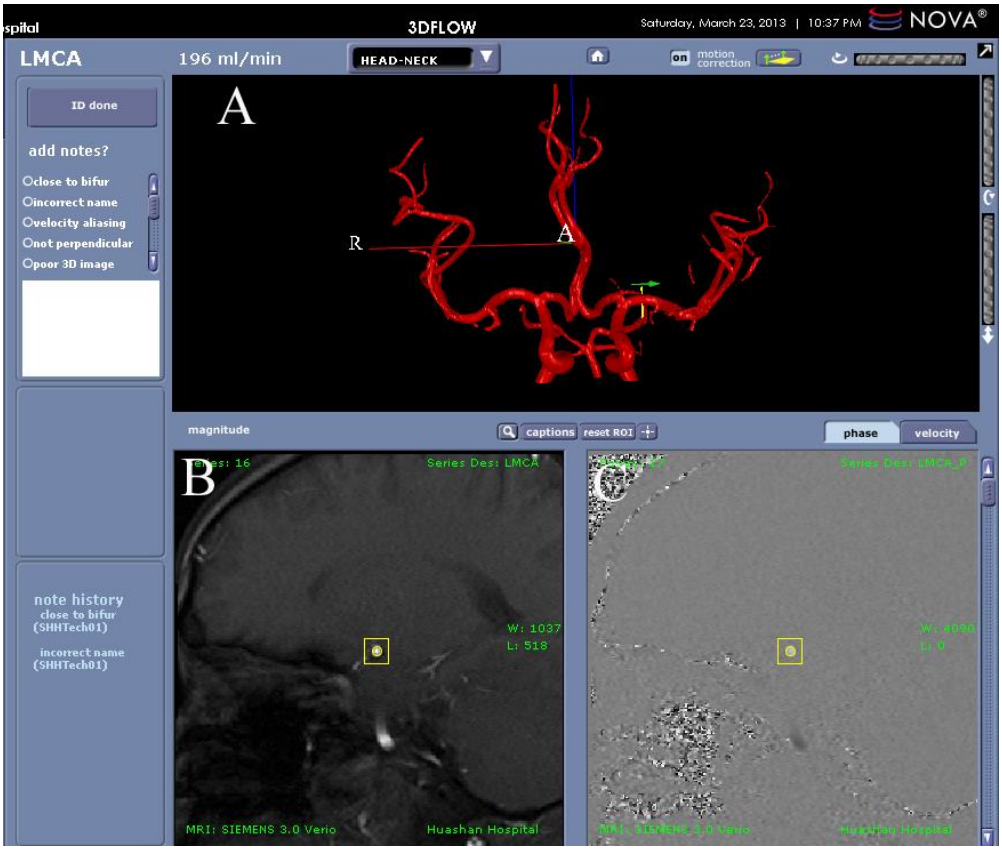

Figure 3.3 Screenshots of 3D flow at MR TECH PC workstation, illustrating the blood flow measurement information after post-processing using PC-MRI

A, The 3D vessel geometry of the cerebral vasculature. The yellow line indicated the scanning plane of PC-MRI; the green arrow indicated the flow direction. B and C, structural and phase images of PC-MRI sequence.

In reality, the velocity of blood flow passing through a certain cross section of a lumen is not evenly distributed. They usually assume a parabolic profile with maximum velocity at the centre of the lumen. Marzo et al. investigated the effect of Womersley and uniform inlet velocity profile on the haemodynamics and found that both assumptions yielded similar results. Therefore a uniform velocity profile was used at the inlet in our study [301].

Outlet boundary condition

Zero static pressure boundary condition was assigned to the outlet of the extended artery with the assumption that the blood pressure drop across a short section of the arteries is negligibly small.

Arterial Wall

Arterial walls in human bodies are compliant and will deform under pressure pulse. However, the lack of information of the arterial wall thickness and elasticity in a patient-specific manner makes it difficult to model the actual arterial wall deformation with flow. If wall thickness and elasticity are known, the arterial wall deformation can be modelled using fluid-structure interaction technique at a cost of increasing memory usage and computational time. However, it has been found out that realistic modelling of carotid arterial bifurcations with rigid and compliant walls yielded no significant difference in the wall shear stress distribution between the two [302]. Given insignificant influence on results, the rigid wall assumption was applied, which means the arterial wall is fixed with no deformation.

No-slip boundary condition was also applied to the artery, which means the fluid will have zero velocity at the wall. This is a valid assumption with laminar flow, as it is used extensively in CFD study of haemodynamics.

3.2.7 Simulation settings and convergence criteria

Laminar model was selected for blood flow since the Reynolds number evaluated at the inlet of the ICA is in the range of 400-800, which stays below the transition region and turbulent region. As it has been established that steady state simulation may provide similar time-averaged results for pulsatile calculations over a cardiac cycle [303], steady state simulation was preferred over pulsatile simulation in consideration of computational resources. The

Navier-Stokes equations were solved using a commercial package (ANSYS CFX-14.0). High resolution convection scheme was used to capture the steep gradient of velocity at the bifurcation point. Auto timescale was selected for the time step control and the solver will determine the time step based on the boundary condition, flow condition, physics and domain geometry. Convergence were achieved with maximum residual of mass and momentum kept below 10^{-5}.

3.2.8 Post-processing

Wall shear stress and pressure distribution on the ICA arterial wall were analysed in contour plots. To better estimate the remodelling characteristics of MMD, different haemodynamic parameters were defined and evaluated based on CFD simulation in different sections of this study.

3.2.9 CFD validation

Computational fluid dynamics has gained increasing interest in the use as a tool to investigate the haemodynamics inside aneurysms, diseased arteries and pre- post treatment evaluation. It has proved its power in providing detail insight into the haemodynamics that would otherwise be impossible to obtain with conventional experiment methods. The validity of CFD results depend on the image segmentation, geometry reconstruction, mesh generation and physical model applied in the simulation. Most of CFD validation work were done for the case of aneurysms, which feature more complicated flow than arteries and is therefore more difficult to obtain an accurate result from simulation. Ford et al. have shown that the virtual angiographic images derived from an image-based CFD model of a giant aneurysm agreed well with the corresponding clinical images when the contrast agent injections are properly chosen[304]. Acevedo et al. have also validated the CFD result by comparing against in-vitro

and in-vivo phase contrast MR imaging [305]. Detail of the flow field predicted by CFD has also been validated by comparing result to PIV measurement [306].

Chapter 4

Predicting Cerebral Hyperperfusion Syndrome Following STA-MCA Bypass based on Intraoperative Perfusion-Weighted Magnetic Resonance Imaging

Published as

Defeng Wang*, **Fengping Zhu* (Co-first Author)**, Kaming Fung, Wei Zhu, Yishan Luo, Winnie Chu, Vincent Mok, Jinsong Wu, Lin Shi, Anil Ahuja, Ying Mao. Predicting Cerebral Hyperperfusion Syndrome Following Superficial Temporal Artery to Middle Cerebral Artery Bypass based on Intraoperative Perfusion-Weighted Magnetic Resonance Imaging. Scientific Reports. 2015; 5: 14140.

4.1 Abstract

Moyamoya disease leads to the formation of stenosis in the cerebrovasculature. A superficial temporal artery to middle cerebral artery (STA-MCA) bypass is an effective treatment for the disease, yet it is usually associated with postoperative CHS. This study aimed to evaluate cerebral haemodynamic changes immediately after surgery and assess whether a semiquantitative analysis of an intraoperative PWI is useful for predicting postoperative CHS. Fourteen patients who underwent the STA-MCA bypass surgery were included in this study. An atlas-based registration method was employed for studying haemodynamics in different cerebral regions. Pre- versus intraoperative and group-wise comparisons were conducted to evaluate the haemodynamic changes. A postoperative increase in relative CBF at the terminal MCA territory ($P = 0.035$) and drop in relative mean-time-transit at the central MCA territory ($P = 0.012$) were observed in all patients. However, a significant raise in the increasing ratio of relative-CBF at the terminal MCA territory was only found in CHS patients ($P = 0.023$). The cerebrovascular changes of the patients after revascularization treatment were confirmed. Intraoperative PWI might be helpful in predicting the change in relative-CBF at MCA terminal territory which might indicate a risk of CHS.

4.2 Introduction

MMD leads to stenosis or occlusion at the terminal portions of ICA or proximal areas of ACA or MCA [307]. It is accompanied by formation of fine vascular network at the base of brain which looks like “puff of smoke” in angiogram. Although RCTs have not been performed, there are strong indications from observational studies that direct superficial temporal artery - middle cerebral artery (STA-MCA) bypass combined with or without indirect revascularization can reduce the risk of cerebral ischemic or haemorrhagic stroke by flow augmentation and collateralization reduction for patients with MMD.

CHS is a group of symptoms after revascularization with severe headache, epilepsy, disturbance of consciousness, focal neurological deficits and intracranial bleeding as the main clinical manifestations [308]. The mechanism of CHS is unknown. Some studies suggested that blood-brain barrier destruction and reactive oxide species damage led by chronic hypoxia were associated with CHS [309, 310]. STA-MCA anastomosis was traditionally regarded as low-flow bypass, however, it could also cause symptomatic CHS with a high incidence of 16.7%-71.4%, which might lead to severe neurological deficits [311, 312]. Detailed investigation of cerebral haemodynamic changes following STA-MCA bypass is important to predict and avoid occurrence of postoperative CHS because treatment is with strict blood pressure control.

PWI is known to strongly correlate with PET in studying cerebral haemodynamics by noninvasively measuring parameters of cerebral dynamics, including CBF, CBV and MTT. Therefore, this technique theoretically appears to be a helpful tool in assessing the surgical effect and predicting postoperative CHS following cerebral revascularization surgery. To the best of our knowledge, intraoperative PWI has not been reported in the usage of monitoring STA-MCA bypass surgery. Thus, the aim of this study is to demonstrate the usage of

intraoperative PWI in bypass surgery and to determine its role in predicting surgical effect and postoperative CHS.

4.3 Materials and Methods

4.3.1 Subjects

This study included 14 patients who underwent STA-MCA anastomosis and EDMS surgery due to ischemic cerebrovascular disease in the 3.0T iMRI operating suits at our hospital. There were six males and eight females diagnosed of MMD with a mean age of 35.3 ± 5.1 years, ranging from 25 to 46 years. The study was approved by the local ethical committee of Huashan Hospital. Written informed consent was got from each patient.

4.3.2 Surgical procedures and diagnosis of postoperative CHS

In each patient, standard STA-MCA anastomosis were performed as previously described. Briefly, a modified pterional approach was adopted. The frontal and/or parietal branch of STA was carefully dissociated from scalp and then pulled through the temporal muscle to reach the surface MCA. STA was anastomosed with the cortical branch of MCA in an end-to-side fashion using a single 10-0 nylon atraumatic suture. Pressurized normal saline containing heparin was used to relieve spasm of the artery. In this study, CHS was defined as the postoperative development of a severe headache, new neurological deficits without cerebral infarction or intracerebral haemorrhage.

4.3.3 MRI scanning parameters

Intraoperative MRI studies were performed with a mobile MRI system (IMRIS, Innovative Magnetic Resonance Imaging Systems, Inc., Winnipeg, MB, Canada) interfaced to a 3.0T MR Systems console (Verio, Siemens Medical Systems, Erlangen, Germany).

TOF MRA scans (4 slabs, 40 slices/slab; TR, 22ms; TE, 4.2ms; flip angle, 18; matrix size, 365×384; slice thickness, 0.5mm; field of view, 181×200mm^2) were obtained to reconstruct the 3D brain template.

PWI was performed based on enhanced fat-suppressed T2 single-shot echo-planar imaging sequence with the following acquisition parameters: TR: 1500ms; TE: 30ms; FOV: 230×230mm^2; matrix 128×128; number of layers: 19; slice thickness: 4mm; interval: 1.2mm; flip angle: 90°. The contrast agent Gadolinium-diethylenetriamine pentaacetic acid (Gd-DTPA) (Magnevist,Bayer, Berlin, Germany) was administered into an antecubital vein by using a power injector (the OptiStar LE Mallinckrodt, Liebel-Flarsheim Company, USA) with a dosage of 0.2mmol/kg and an injection rate of 4 ml/s.

4.3.4 PWI post-processing

The post-processing procedures of PWI have been described in detail in the chapter 3.

4.3.5 Definition of atlas

Using the MRA data, a template for the cohort was constructed using group-wise registration in ANTs toolbox [313]. With an existing Chinese MRI brain template and atlas for arterial territories of human brain proposed by Tatu et al. [314], we can construct the atlas for the template in this study using registration-based segmentation techniques. The atlas indicates

various arterial regions separated for left and right sides, including terminal and central regions of ACA, MCA and PCA, anterior choroidal artery, superior cerebellar artery, anterior and posterior inferior cerebellar artery territories. Since MMD mainly affects the blood supply areas of ACA, MCA and PCA, central and terminal areas of ACA & MCA and terminal areas of PCA were focused in the analysis (Figure 4.1).

After the brain template space and its atlas were created, all pre- and intra-operative PWIs were mapped onto the template space. This process was done by the coregister function of SPM8 (Wellcome Department of Imaging Neuroscience, London, United Kingdom). In each brain segment, the statistical values of the four perfusion parameters were computed for further analysis.

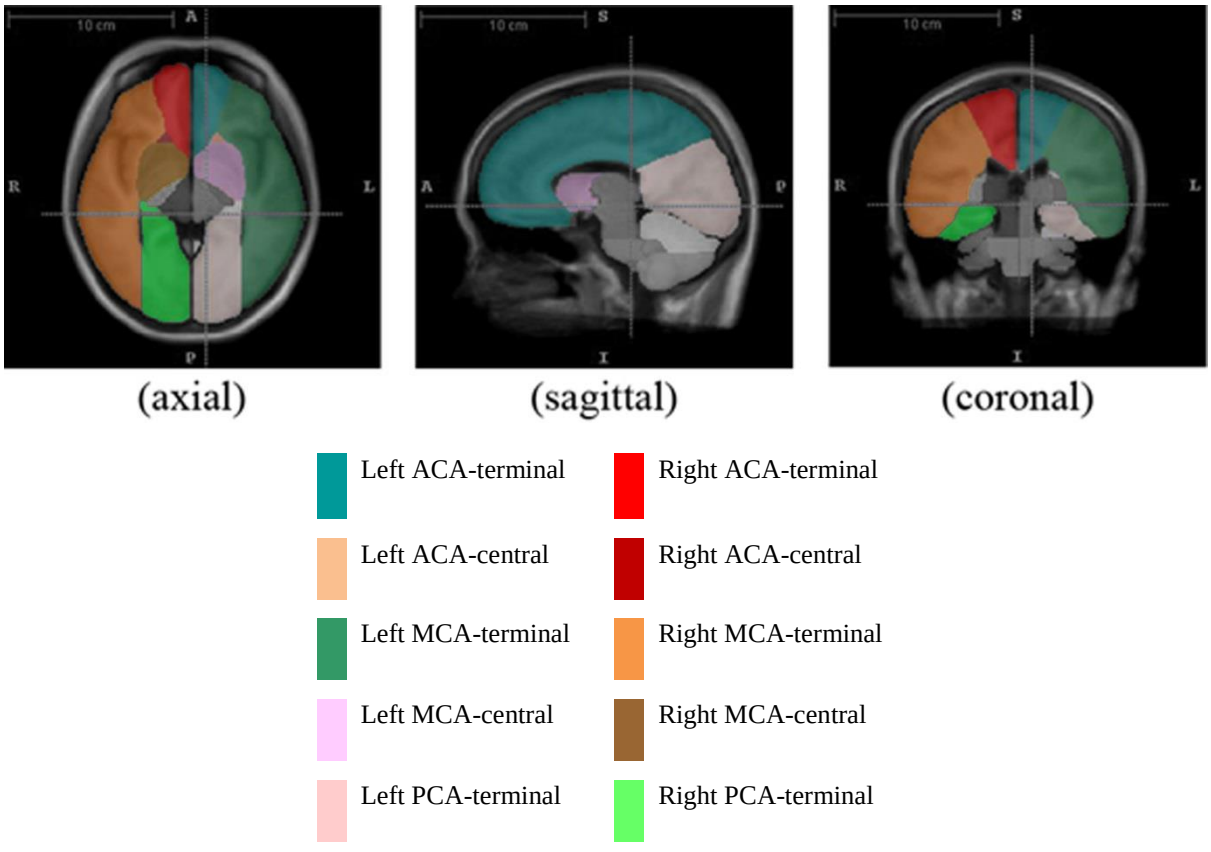

Figure 4.1 Screenshots showing the axial, sagittal and coronal views and of the brain template and atlas used in this study

4.3.6 Statistical analysis

With the averaged parameters, two-tailed paired Student's t-test was used to compare the pre- and intra-operative perfusion parameters in the areas of ACA, MCA and PCA. To minimize symmetric error of left and right hemispheres, we used relative perfusion parameter values for comparison, which were calculated by the ratio of parameter value on the surgical side to that on the contralateral side [254]. A significant level of 0.05 was chosen for the test to verify if the changes in the perfusion parameters were statistical significant. Pre- and intra-operative comparisons were conducted for all patients and repeated for CHS and non-CHS groups separately.

4.4 Results

4.4.1 Patients and clinical outcome

Intraoperative MRA and PWI were successfully conducted in each patient. The patency of bypass graft was evaluated during surgery, using intraoperative MRA and Doppler flowmeter. Postoperative DSA, MRA and/or CTA also confirmed the patency of bypass graft in all 14 patients. There was no haemorrhagic or ischemic infarction after the operation.

Five cases (35.7%) suffered from postoperative complications which is suspected CHS, including seizure attacks in two cases, severe headache in one case, aphasia in one case, transient motor deficit in one case. All patients recovered well without neurological deficits within two weeks. For further PWI parameters analysis, the case series were divided into two groups, which are CHS group in which patients have postoperative complications caused by suspected CHS after surgery (5 cases), and non-CHS group in which patients had no complications after surgery (9 cases).

4.4.2 Preoperative versus intraoperative comparisons for all patients

STA-MCA bypass surgeries effectively improved cerebral blood flow at the surgical side. The mean relative-CBF at the terminal MCA territory increased from 0.98 ± 0.10 to 1.03 ± 0.14 after bypass on the surgical side of all patients (P = 0.035, versus preoperative data, insignificant after correction). No significant increase was observed for relative-CBF at the central territory of ACA, PCA and MCA. Relative-MTT values at all other regions were insignificant (P > 0.05 for all, versus preoperative data). For all patients, the changes of relative-CBV were insignificant at all regions. Preoperative and intraoperative mean relative-CBF, CBV and MTT values are listed in Table 4.1, Table 4.2 and Table 4.3 respectively.

4.4.3 In-group preoperative versus intraoperative comparisons

For the CHS group, the average relative-CBF rose from 1.03 ± 0.14 to 1.17 ± 0.13 at the terminal MCA territory (P = 0.011). However, no significant difference for relative-CBF at other regions was observed. There were trends showing increases in relative-MTT at the terminal MCA and PCA territories, but the p-values were insignificant. At PCA, the CHS group had an elevated mean relative-CBV from 0.84 ± 0.10 to 1.00 ± 0.12 (P = 0.005), while there were no significant changes at the other territories. For those without CHS, there were no significant changes to both relative-CBF and relative-MTT in all regions. The relative-CBV for this group changed from 1.04 ± 0.10 to 0.95 ± 0.17 (P = 0.015) at PCA and was without changes in other regions.

4.4.4 Across-group preoperative versus intraoperative comparisons

At the MCA-terminal region, the intraoperative relative-CBF values of patients with CHS and those without CHS were significantly different (1.17 versus 0.95 respectively, P = 0.016)

(Figure 4.2). The percentage increase of intraoperative relative-CBF of the CHS group was also significantly larger than that for the non-CHS group (14.3% versus 0.0% respectively, *P* = 0.023). At the PCA territory, the preoperative value and percentage change of intraoperative relative-CBV for the CHS group were significantly different from that of the non-CHS group (0.84 vs 1.04 with *P* = 0.010 and 19.8% vs -8.9% with *P* = 0.001 respectively). No other significant difference between the two groups was observed in our results.

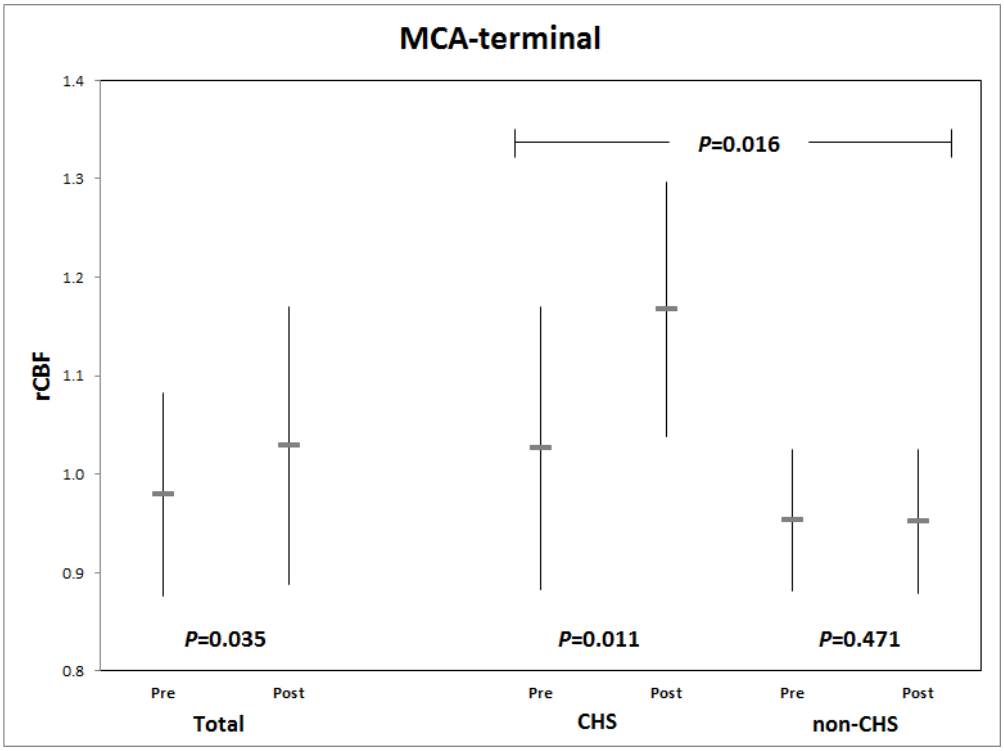

Figure 4.2 Graph showing mean ± SD of pre- and intra-operative rCBF values in MCA-terminal regions of CHS and non-CHS patients

Table 4.1 Summary of mean relative cerebral blood flow (relative-CBF)

Table 4.1. Summary of mean relative cerebral blood flow (relative-CBF) *significant P-values after multiple comparison correction

	All Patients (n = 14)	CHS Group (n = 5)	Non-CHS Group (n = 9)	P-value (CHS vs non-CHS)
ACA-terminal				
- Pre	0.93	0.90	0.95	0.590
- Intra	0.92	0.93	0.91	0.818
- %increase	-0.2%	5.0%	-3.2%	0.162
P-value (Pre vs Intra)	0.338	0.210	0.110	
ACA-central				
- Pre	0.85	0.77	0.90	0.567
- IntraIntra	1.01	0.99	1.03	0.862
- %increase	32.7%	58.6%	18.4%	0.518
P-value (Pre vs Intra)	0.047	0.169	0.098	
MCA-terminal				
- Pre	0.98	1.03	0.95	0.333
- Intra	1.03	1.17	0.95	0.016*
- %increase	5.1%	14.3%	0.0%	0.023*
P-value (Pre vs Intra)	0.035	0.011*	0.471	
MCA-central				
- Pre	0.96	1.07	0.90	0.386
- Intra	0.98	1.10	0.91	0.357
- %increase	2.3%	4.3%	1.2%	0.721
P-value (Pre vs Intra)	0.266	0.347	0.326	
PCA-terminal				
- Pre	1.01	0.92	1.06	0.268
- Intra	0.99	0.92	1.02	0.303
- %increase	-1.2%	3.4%	-3.8%	0.338
P-value (Pre vs Intra)	0.241	0.452	0.146	

*significant P-values after multiple comparison correction

Table 4.2 Summary of mean relative cerebral blood volume (relative-CBV)

Table 4.2. Summary of mean relative cerebral blood volume (relative-CBV) *significant P-values after multiple comparison correction

	All Patients (n = 14)	CHS Group (n = 5)	Non-CHS Group (n = 9)	P-value (CHS vs non-CHS)
ACA-terminal				
- Pre	0.97	0.98	0.97	0.893
- Intra	0.94	0.94	0.94	0.986
- %increase	-2.3%	-3.3%	-1.8%	0.863
P-value (Pre vs Intra)	0.240	0.296	0.336	
ACA-central				
- Pre	0.88	0.88	0.88	0.998
- Intra	1.06	1.02	1.09	0.777
- %increase	33.2%	41.7%	28.5%	0.802
P-value (Pre vs Intra)	0.152	0.293	0.206	
MCA-terminal				
- Pre	1.04	1.12	0.99	0.503
- Intra	1.05	1.32	0.90	0.152
- %increase	0.7%	17.7%	-8.8%	0.083
P-value (Pre vs Intra)	0.436	0.085	0.127	
MCA-central				
- Pre	0.99	1.09	0.93	0.417
- Intra	0.99	1.15	0.90	0.275
- %increase	1.5%	8.1%	-2.2%	0.460
P-value (Pre vs Intra)	0.493	0.308	0.318	
PCA-terminal				
- Pre	0.97	0.84	1.04	0.010*
- Intra	0.97	1.00	0.95	0.472
- %increase	1.4%	19.8%	-8.9%	0.001*
P-value (Pre vs Intra)	0.484	0.005*	0.015*	

*significant P-values after multiple comparison correction

Table 4.3 Summary of mean relative mean transit time (relative-MTT)

Table 4.3. Summary of mean relative mean transit time (relative-MTT) *significant P-values after multiple comparison correction

	All Patients (n = 14)	CHS Group (n = 5)	Non-CHS Group (n = 9)	P-value (CHS vs non-CHS)
ACA-terminal				
- Pre	1.09	1.19	1.04	0.534
- Intra	1.03	1.03	1.04	0.954
- %increase	-2.2%	-8.2%	1.1%	0.347
P-value (Pre vs Intra)	0.190	0.190	0.479	
ACA-central				
- Pre	1.04	1.24	0.93	0.088
- Intra	0.98	1.02	0.96	0.612
- %increase	-3.9%	-14.7%	2.1%	0.226
P-value (Pre vs Intra)	0.202	0.103	0.366	
MCA-terminal				
- Pre	1.03	1.06	1.01	0.703
- Intra	1.00	1.07	0.97	0.428
- %increase	-2.0%	2.1%	-4.3%	0.520
P-value (Pre vs Intra)	0.244	0.476	0.104	
MCA-central				
- Pre	1.07	1.05	1.08	0.563
- Intra	0.97	0.99	0.96	0.583
- %increase	-8.9%	-4.8%	-11.1%	0.340
P-value (Pre vs Intra)	0.012	0.107	0.030	
PCA-terminal				
- Pre	1.00	1.05	0.97	0.690
- Intra	1.05	1.20	0.97	0.312
- %increase	9.1%	24.5%	0.6%	0.332
P-value (Pre vs Intra)	0.112	0.115	0.459	

*significant P-values after multiple comparison correction

4.4.5 Illustrative case

A 36-year-old man presented transient weakness of the right extremities, and was diagnosed as having MMD. Preoperative PWI revealed decreased CBF and increased MTT in the left MCA and ACA territory, suggesting severe haemodynamic compromise. Left STA-MCA anastomosis plus EDMS surgery was successfully performed. Intraoperative MRA confirmed the patency of the bypass graft. Intraoperative PWI revealed the rCBF at MCA-terminal area markedly increased from 0.95 to 1.18 at the rate of 24.30%, however, rMTT at MCA-terminal area just decreased from 0.97 to 0.96 at the rate of 1.10% (Figure 4.3). The patient developed with focal seizure attacks (2-3 times per day) 1 day after surgery. After strict blood pressure control, seizure attacks were well controlled 4 days later. He developed no neurological dysfunction during the perioperative period.

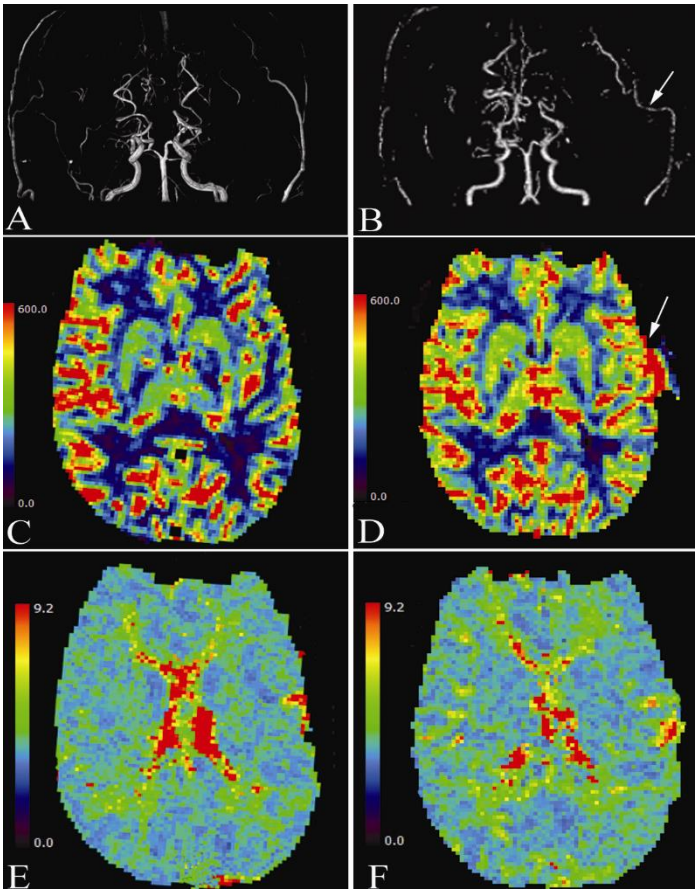

Figure 4.3 Illustrative case of diagnosis for CHS using interopative MRI

A, Pre-operative MRA showing bilateral occlusion of the proximal ICA and Moyamoya change of intracranial vessels. B, Intra-operative MRA showing the patency of left STA-MCA bypass graft (arrow). C, Pre-operative PWI demonstrating diminished CBF of the left hemisphere. D, Intra-operative PWI demonstrating CBF of the left hemisphere markedly increased, mainly at the MCA-termina area (arrow). E, Pre-operative PWI demonstrating prolonged MTT of the left hemisphere, especially at the MCA-terminal area. F, Intra-operative PWI indicating the prolonged MTT of the left hemisphere didn't change obviously.

4.5 Discussion

Detailed cerebral haemodynamic information allows doctors to assess the severity of brain ischemia, determine the indication for surgery, design surgical procedure, predict the outcome and avoid complications. There is a list of imaging modalities to evaluate brain perfusion or

metabolism, including CTP, PET, SPECT and Xenon-enhanced Computed Tomography (XeCT). These technologies have been applied in clinic, however, each technique has drawbacks, such as high cost, radiation exposure, low spatial resolution and unavailability for real-time monitoring.

Bolus PWI, by intravenous bolus injection of paramagnetic contrast agents, used fast echo-planar imaging sequence with high time-resolution to process continuous multi-temporal brain tissue scan and detect the tissue signal intensity changes over time caused by blood flow with the contrast agent flowing through the inspected tissue. It reflects haemodynamic information of the brain tissue and subsequently obtains quantitative information through calculation of the mathematical model. Compared with other types of imaging technologies, PWI has many advantages including low price, no radiation, high spatial resolution and simple image acquisition. It can effectively evaluate perfusion information in the brain tissue and its results were revealed to be consistent with PET studies.

Scholars analysed perfusion parameters mainly by two approaches, which are atlas-based method and region of interest (ROI) analysis. ROI analysis was mainly carried by manual selection of region in the brain images at which the Moyamoya syndrome presents [315, 316]. Atlas-based method considered the brain in several sections according to some well-established brain template [317-320]. This study proposed to use the atlas-based method as this method minimized potential selective errors contributed by choosing ROIs. Atlas-based method provides a holistic picture of the whole brain for assessing development of cerebral vascular network in the MMD patients before and after revascularization. Before segmentation, a brain template space was built from MRA data and a brain atlas with main arterial territories. All PWI images were registered to the template space and segmented according to predefined segments. Averaged values of perfusion parameters in each segment

were calculated for further analysis. By comparing pre- and post-operative perfusion parameters of each patient, changes in cerebrovasculature of the patients were studied.

Intraoperative MRI was widely used to provide real-time images for neuronavigation in brain tumor surgery, however, it is rarely reported to be used in the neurovascular surgery. It was proven to be helpful in preventing insidious or early complications during operation, such as cerebral ischemia and haemorrhage [321]. To our best knowledge, this is the first study on semiquantitative analysis of intraoperative PWI to quantify cerebral haemodynamic changes in bypass surgeries.

With the atlas-based registration method, information of blood circulation in different cerebral regions was obtained during operation. By studying the relative perfusion parameters (surgical side versus contralateral side), an objective assessment of the effectiveness of STA-MCA bypass was conducted. The feasibility of semiquantitative analysis of PWI in predicting postoperative CHS after STA-MCA bypass was also evaluated.

When analyzing data in whole case series, statistically significant increases in rCBF at MCA - terminal regions after surgery were found, suggesting blood flow of the surgical cortex was immediately augmented after bypass procedures and the intraoperative rCBF value at MCA-termial area might be a sensitive parameter to reflect the bypass effect. However, rCBF values at other areas of arterial territories revealed no significant changes. It indicates that bypss approach is important to surgical effect and the decision on specific surgical procedure should be based on detailed haemodynamic analysis. More importantly, for patients with CHS, increases in rCBF at MCA-terminal regions have been found. rCBF at MCA-terminal area increased about 25% of the preoperative values in five patients who developed postoperative CHS on PWI scans immediately after surgery. However, the value increased only about 1% of the preoperative values in nine patients who did not develop CHS. There was a significant

raise in the ratio of rCBF at MCA-terminal area in patients with postoperative CHS compared against those without CHS. So the immediate great increases of rCBF at MCA-terminal region might be the prognostic factor for postoperative CHS. The cut-off value of the variation rate of the rCBF at MCA-terminal area for predicting postoperative CHS might be made in the future.

Among the fourteen patients, nine of them were found no complication after revascularization surgery. Referring to previous similar studies, it was expected that there would be significant increases in CBF and CBV and delays in MTT [254, 320, 322, 323]. The possible causes of the discrepancies could be the short time interval for capturing the intraoperative images after bypass surgeries. Cerebral vascular networks may not have been fully developed in such a short time.

Another sources of error in the perfusion parameters change were that the image quality and the deconvolution method used by PMA. Deconvolution is highly sensitive to image noise which could lead to great error for determination of the residue function and thus the perfusion parameters. Besides, selection of the arterial input function was automatically performed by the software. It might potentially affect the accuracy of the calculated haemodynamic changes after surgery.

The number of subjects is limited in the present study. Further research with a larger set of cases is required to confirm the result. Furthermore, follow-up should be performed to estimate the clinical effectiveness of surgery in the long-term run.

4.6 Conclusion

This study demonstrates that semiquantitative analysis of atlas-based intraoperative PWI is an effective method for assessing surgical effectiveness and predicting postoperative CHS after STA-MCA anastomosis. The changes in cerebrovasculature for MMD patients after revascularization treatments were confirmed. Intraoperative immediate great increases of rCBF at MCA-terminal area might be regarded as a sensitive parameter for predicting postoperative CHS.

Chapter 5

Haemodynamic Analysis of Vessel Remodelling in STA-MCA Bypass for Moyamoya Disease and Its Impact on Bypass Patency

Published as

Fengping Zhu, Yu Zhang, Yi Qian, Masakazu Higurashi, Bin Xu, Yuxiang Gu, Ying Mao, Michael Kerin Morgan. Haemodynamic analysis of vessel remodelling in STA-MCA bypass for Moyamoya disease and its impact on bypass patency. Journal of biomechanics. 2014; 47(8):1800-1805.

5.1 Abstract

The purpose of this study is to estimate the remodelling characteristics of STA-MCA bypass and its influence on patency via the use of CFD technology. The reconstructed three-dimensional geometries from MRA were segmented to create computational domains for CFD simulations. Eleven patients, who underwent regular MRA both immediately following surgery and at the six months follow-up, were studied. The flow velocities at STA were measured via the use of QMRA to validate simulation results. STA-MCA bypass patency was confirmed for each patient immediately following surgery. The simulation indicated that the remodelling of the arterial pedicle in nine patients was associated with a reduction in the resistance to flow of the bypass. For these cases, the modelling of a driving pressure of 10 mmHg through the bypass at 6 months post-surgery resulted in a 50% greater blood flow than those found immediately following surgery. However, two patients were found to exhibit contradictory patterns of remodelling, in which a highly curved bending at the bypass immediately post-surgery underwent progression, with increased resistance to flow through the bypass at 6 months follow-up, thereby resulting in a modelled flow rate reduction of 50% and 25% respectively. This study revealed that STA-MCA bypass has a characteristic remodelling that usually reduces the flow resistance. The initial morphology of the bypass may have had a significant effect on the outcome of vessel remodelling.

5.2 Introduction

Moyamoya disease, first reported in 1957 by Takeuchi and Shimizu, is a chronic cerebrovascular disorder characterized by progressive occlusion of arteries around the internal carotid artery bifurcation [324]. This occlusion results in the formation of collaterals from a fine vascular network at the base of the brain called Moyamoya vessels responsible for the "puff of smoke" appearance on angiography, from which the name is derived [325, 326]. Despite extensive collateralisation, the clinical manifestation of infarction and haemorrhage may ensue. In order to ameliorate these complications, bypass surgery is often indicated [327]. Though there is still some argument about whether bypass surgery is useful for the treatment of occluded cerebrovascular disease due to atherosclerosis, direct STA-MCA bypass combined with or without indirect revascularization is often performed for Moyamoya patients to reduce the risk of cerebral ischemic or haemorrhagic stroke by flow augmentation and collateralisation reduction [327, 328]. However, spontaneous changes to the bypass from the time that the STA-MCA bypass is established, are expected in the first few weeks and even months following surgery. Such auto-remodelling may modify the final outcome of the treatment.

The objective of this paper is to estimate the vessel auto-remodelling after STA-MCA bypass surgery using CFD. We carried out CFD analysis on eleven patients with Moyamoya disease treated by STA-MCA anastomosis, with subsequent follow-up by MRA to capture auto-remodelling and observed flow resistance modifications due to its effect on the bypass flow rate. The change in the WSS occurring at the bypass due to auto-remodelling was also calculated.

5.3 Materials and Methods

5.3.1 Subjects

Eleven consecutive adult patients with ages ranging from 24 to 47 years were examined by MRA after undergoing STA-MCA bypass surgery and at 6 months following surgery. All patients were diagnosed with Moyamoya disease and treated with combined STA-MCA bypass and EDMS at Huashan Hospital from 2010 to 2012 [157]. Anterior and/or posterior branch of STA were anastomosed to the cortical branch of MCA in end-to-side fashion. The demographic features of patient's details are listed in Table 5.1. All protocol was approved by the Institutional Research and Ethics Committee of Huashan hospital. Each participant provided written informed consent.

3D geometries of bypasses were reconstructed and segmented via use of commercial software package - MIMICS (Materialise' Interactive Medical Image Control System) to create domain for CFD computation.

QMRA, which was implemented with NOVA) software (VasSol Inc., Chicago, Illinois, USA), was performed to measure the blood flow of the STA [291, 292]. In this study, the inflow rate of the STA immediately following surgery was measured to be at an average of 37.7 ml/min.

5.3.2 Surgical procedures

A modified pterional approach was adopted. The branches of the STA could be observed on the medial surface of the flap, with the dissociated anterior and/or posterior branches of the STA (donor artery) pulled through the temporal muscle to the vicinity of the target arteries for anastomosis. The STA was washed with pressurized normal saline containing heparin to

relieve spasms, and then anastomosed with the cortical branch of MCA in an end-to-side fashion using a single 10-0 nylon atraumatic suture. Additional EDMS and dural pedicle insertion were performed as described in previous papers [157].

5.3.3 CFD modelling

Three-dimensional (3-D) geometry bypass was built via generation of two-dimensional contours from grey scales of pixels, and by subsequent interpolation in a normal direction. This method prevents the intrusion of surface noise. Rather than utilising "global smoothing", we used manual "local smoothing" to keep 3-D geometries as realistic as possible. This method exhibited an average error of approximately one-third of a pixel in size [329].

Conservation equations for 3-D steady flow with rigid walls were solved via use of the CFX finite-volume-based CFD solver in the ANSYS 14.0 package (Ansys Inc., Canonsburg, PA, USA), with flow considered under steady state conditions. It has been established that steady state simulation may provide similar time-averaged results for pulsatile calculations over a cardiac cycle [303].

Grid independence validations have been carried out in our previous work [330, 331]. In order to accurately measure WSS at near-wall-regions, the body-fitted prism layers were generated near the vessel walls to improve the resolution of relevant scales in fluid motion.

5.3.4 Bypass flow resistance

It is known that under the same pressure drop, the conduit with lower flow resistance will have a higher blood flow rate; i.e. better patency. The bypass conduit from STA to MCA is irregular in geometry, with vessel auto-remodelling modifying the morphology of the bypass and thereby flow resistance as well. By measuring bypass flow resistance, the effect of auto-

remodelling to the bypass patency may potentially be estimated. Based on pipe flow theory [332], pressure drop within a vessel can be expressed as having the following relationship with flow:

$$\Delta p = A\dot{m}^2 + B\dot{m} \quad (8)$$

Where, $\dot{m}$ is the mass flow rate passing through the vessel. A is the quadratic flow resistance coefficient representing the effect of elbows and other bends on the pressure drop and B is the linear flow resistance coefficient determined by the length and diameter of the vessel. Greater pressure drops will occur with the same amount of mass flow rate through arteries with greater values of A and B.

It has already been demonstrated that blood flows obey pipe flow theory [333]. Thus, the quantitative relationship between blood flow rates and pressure drops can be obtained via the determination of A and B. In our current study, the mass flow rate of the STA was adjusted to lie in the range of 20-100 ml/min, in order to allow for calculations of various pressure drops via CFD simulation. Based on the results of the pressure drop regression curve, obtained via the least square method, flow resistance coefficients (A and B) were determined.

5.3.5 Statistical analysis

Statistical analyses were performed via use of the commercial statistical software package SPSS (version 17.0), with the results presented as mean ± standard deviation (SD) .

Differences between the values estimated immediately following surgery and at the follow-up stages, were assessed with an independent-samples *t* test. Pearson correlation tests were used to estimate the correlations between flow resistance, WSS and volumetric flows. Throughout analyses, a significance level of 0.05 was assumed.

5.4 Results

5.4.1 Observation of bypass morphological change in 6 months follow-up

The average bypass diameter increased from 1.35 ± 0.47 mm immediately following surgery, to 1.60 ± 0.36 mm at follow-up. Despite this, however, no statistical significance was achieved ($P > 0.05$). The quantitative changes of the narrowest diameter in bypass for eleven cases are listed in Table 5.1. These changes were not uniform. This is exemplified by cases A and J. Changes in morphology of the bypass for case A are shown in Figure 5.1A. At 6 months follow-up, the stenosis present in the middle cerebral recipient vessel immediately following surgery resolved. Figure 5.1. depicts the morphological change of the bypass for case J, in which the pre-existing curvature of the STA trunk (marked by circle) had further increased and the bypass underwent shrinkage at follow-up; reducing the diameter of the bypass as a result.

Table 5.1 Clinical characteristics of the patients and the bypass diameter and flow results

Case	Sex, Age	Clinical onset	Surgical side	Immediate post-surgery		Follow up	
				Bypass diameter (mm)	Bypass diameter (mm)	Bypass diameter (mm)	Bypass flow (ml/min)
A	F, 30	Ischemic stroke	Rt	0.44	22	1.35	33
B	M, 44	TIAs	Lt	1.08	30	1.97	100
C	M, 46	Ischemic stroke	Rt	1.23	43	2.19	75
D	M, 45	Ischemic stroke	Lt	1.66	40	1.50	55
E	F, 24	Ischemic stroke	Lt	2.10	42	1.60	100
F	M, 34	TIAs	Lt	1.54	39	1.92	85
G	M, 38	Hemorrhagic stroke	Rt	1.77	44	1.73	65
H	M, 35	Hemorrhagic stroke	Lt	1.00	15	1.69	35
I	F, 43	Ischemic stroke	Lt	1.14	35	1.00	80
J	M, 45	TIAs	Lt	1.78	35	1.60	15
K	F, 47	Ischemic stroke	Rt	1.11	70	1.09	45

F: Female; M: Male; TIAs: Transient ischemic attacks; Rt: Right; Lt: Left.

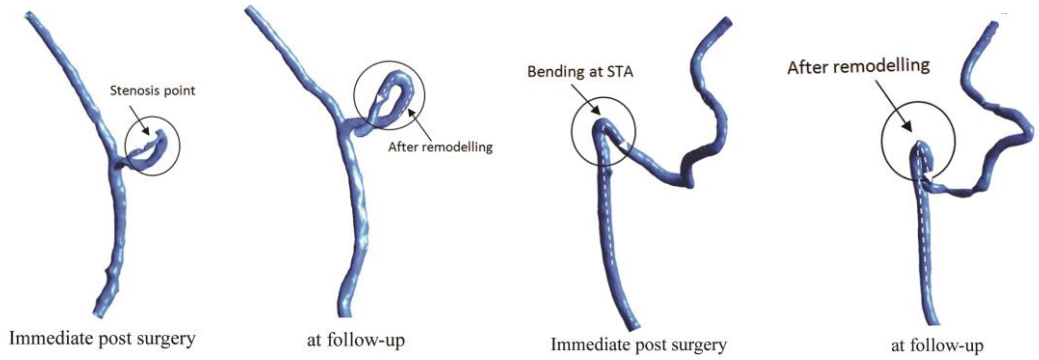

Figure 5.1 Morphological change of patient A and J due to vessel remodelling

1A: For patient A there was a stenosed part. At follow-up, the pre-existed stenosis was opened up due to the vessel auto-remodelling. The configuration of the bypass vessel was smoothend by the auto-remodelling.

1B: For patient J, there was an obvious bending at the STA trunk immediate after surgery. Blood flow changes in the opposite direction after this bending. It should be noted that the local bending at the STA trunk will greatly affect the blood perfusion in the downstream. At follow-up, the whole bypass shrunk.

5.4.2 Flow resistance estimation during the 6 months follow-up

The flow resistances of case A-I were reduced at follow-up (Table 5.1), whilst the average quadratic resistance value of *A* and linear resistance value of *B* at the bypass immediately following surgery in nine cases (A-I), was found to be 0.0033 ± 0.0035 Pa/(ml/min)^2 and 0.1816 ± 0.1358 Pa/(ml/min), respectively. At 6 months follow-up, *A* and *B* were reduced to 0.0015 ± 0.0016 Pa/(ml/min)^2 and 0.0844 ± 0.0483 Pa/(ml/min), respectively. The statistical study indicated a significant difference between the values measured immediately following surgery and at 6 months follow-up ($P < 0.01$ for flow resistance values). The reduction in flow resistance at follow-up is shown in Figure 5.2. Variations within the patients' group are illustrated by cases A and J. Figure 5.3A indicates that the flow resistance at the bypass of

case A decreased greatly due to the reduction of the stenosis at 6 months follow-up. With a flow condition of 37.7 ml/min, the pressure drop was calculated to be around 10 mmHg. On the other hand, we found an increase in resistances at follow-up analysis, for both case J and case K, an increase attributed to the curvature of the vessel (Figure 5.3B, case J). Under the assumed flow condition of 37.7 ml/min, the pressure drop was observed to increase from 9 mmHg to a physiologically improbable 30 mmHg, i.e. the real-flow rate of this bypass must be less than the measured average flow (37.7 ml/min). The results indicated that both vessel curvature and bending will cause high flow resistances in STA bypass.

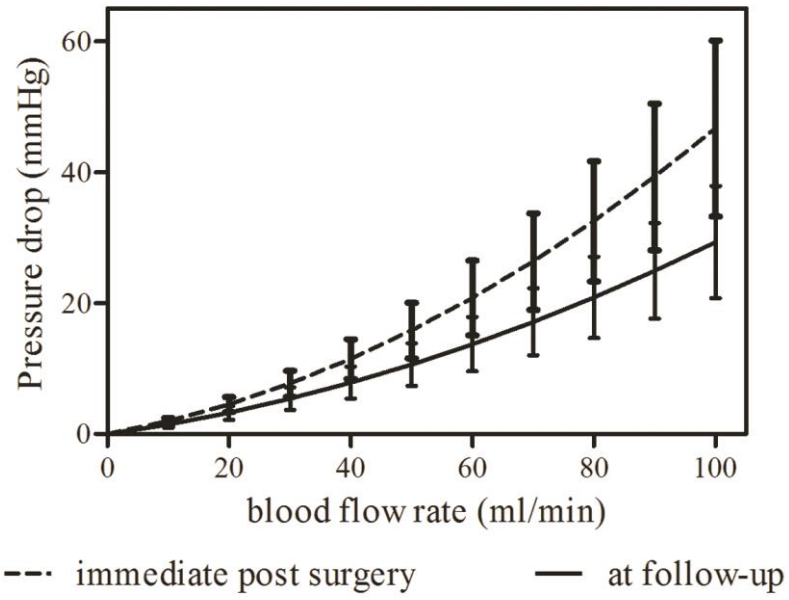

Figure 5.2 Statistic flow resistance change due to vessel remodelling

The statistic flow resistance at follow-up decreased compared with that at immediate post-surgery. This is in consistent with the expanding of the bypass in diameter.

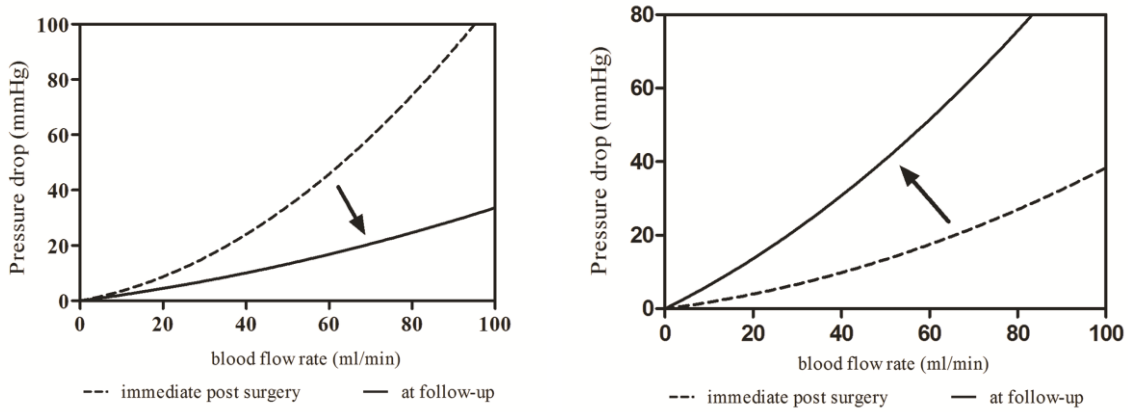

Figure 5.3 Flow resistance modulation for patient A and J

5.3A: For patient A, as the opening of the pre-existed stenosis, the flow resistance of the bypass was greatly reduced at follow up. The pressure drop decreased at the same flow rate, as the arrow indicated.

5.3B: For patient J, due to the shrink of the bypass, the flow resistances increased at follow-up. The pressure drop increased at the same flow rate, as the arrow indicated.

5.4.3 Bypass patency examination

We compared the flow rates at the averaged pressure drop from the origin of the STA to the point of bypass anastomosis. Based upon the average mass flow and flow resistances immediately following surgery, we estimated this pressure drop to be at a value of around 10 mmHg. Table 5.1 reports the flow rates of the bypass immediately following surgery and at follow-up. The mass flow rates of the bypass measured by QMRA increased significantly from 37.72 ± 14.04 ml/min immediately following surgery to 62.55 ± 28.34 ml/min at follow-up (P<0.05). As a result of auto-remodelling (e.g. reduction of stenosis, dilation in diameter, vessel wall smoothening), the flow rate in the bypass increased by about 50% for cases A-I, whilst for cases J and K, the blood flow was reduced by 50% and 25%, respectively. The average resistance coefficients; A and B, as well as shear stress; WSS, were calculated to

significantly correlate with STA blood flows. The correlation coefficients found were -0.722, -0.847 and -0.800 respectively ($P < 0.01$).

5.4.4 WSS analysis

Analysis revealed a reduction in WSS at the bypass due to vessel remodelling. The maximum WSS within the bypass was found to be 22.82 ± 5.02 Pa, falling to 16.91 ± 5.59 Pa at follow-up and thereby achieving statistical significance ($P < 0.05$). These reductions in WSS are illustrated in Figure 5.4.

Variations within the patient group can be seen throughout cases A and J. As a result of flow-resistance reduction, the maximum WSS occurring at the bypass for case A was likewise reduced. Figure 5.5A indicates that the maximum WSS immediately following surgery was approximately 30 Pa, whilst at follow-up, it had reduced to approximately 20 Pa. On the contrary, for case J, the maximum WSS was increased from 17 Pa immediately following surgery, to 28 Pa at follow-up (Figure 5.5B).

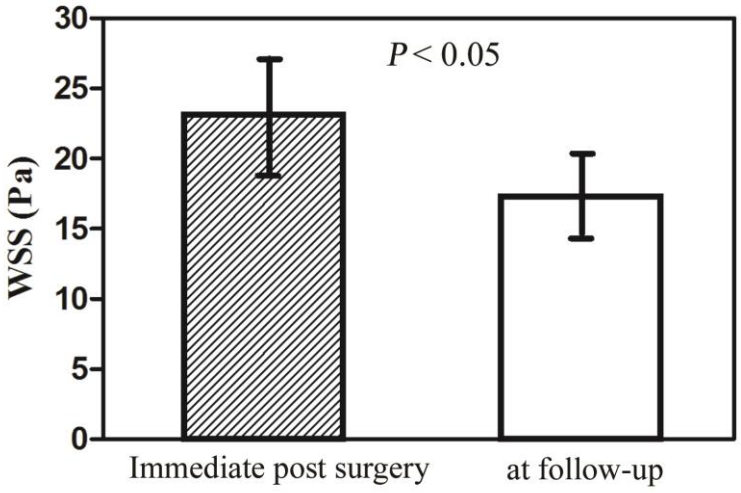

Figure 5.4 Statistic WSS change due to vessel remodelling

The statistic WSS at follow-up decreased compared with that at immediate post-surgery. The decrease of WSS confirmed that vessel remodelling reduces the impedance of the bypass.

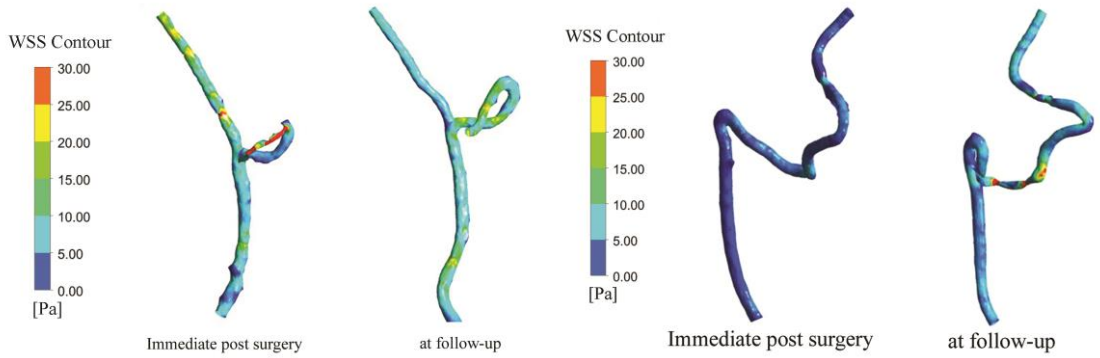

Figure 5.5 WSS distribution of patient A and J due to vessel remodelling

5.5A: For patient A, as the opening of the stenosis, the blood flows more smoothly at follow-up that causes uniform distribution of WSS.

5.5B: For patient J, as the shrink of the bypass WSS increased at follow-up.

5.5 Discussion

5.5.1 Bypass patency and vessel auto-remodelling

Goldman and colleagues reported that the original bypass morphology and graft position significantly modified during the 10 years following coronary bypass surgery [334]. Lajos and colleagues followed 83 patients who underwent isolated coronary artery bypass surgery with valvular and valveless vein graft and found that venous valves had considerable effect upon the long-term patency of the bypass. As a consequence, they suggested using valveless vein segments whenever possible [335]. In cerebrovascular procedure, remodelling of EC-IC bypass has also been reported. Eguchi et al. found that the EC-IC bypass diameter alternated within the first 6 months following surgery [336]. Amin-Hanjani et al. moreover observed a complementary and inverse relationship between the direct bypass graft and indirect revascularization, suggesting that the bypass graft remodels in response to blood demand over time [292]. Even today, the evaluation of intracranial bypass surgery and its patency at

follow-up remains empirical. Sia and colleagues found that 178 STA-MCA bypasses had excellent long-term patency over many years [337]. Likewise, Gu and colleagues demonstrated the occlusion of one of 96 bypasses at the one-year follow-up assessment stage in 53 cases who received combined STA-MCA bypass and EDMS surgery[338]. Though bypass flow is excellent immediately following STA-MCA bypass operations, occlusions may still occur during late follow-up stages. Although this may be related to a number of patient factors, vessel auto-remodelling may play a significant part amongst these causes.

Amid the many physiological mechanisms contributing to this remodelling, the actions of matrix metalloproteinases (MMPs) are considered to have a critical role [339, 340]. Inflammatory cells, such as macrophages, release MMPs in response to blood flow change within vessels. This contributes to the morphological changes of vascular remodelling, characterized by an increase in luminal diameter with relative small changes in wall thickness [340]. Haemodynamic research has indicated that the morphological changes occurring within the bypass is highly dependent upon flow resistance [341]. Our results confirm that vessel auto-remodelling, flow resistance, and blood flow rate are interdependent on each other.

5.5.2 STA-MCA bypass flow modulation due to vessel auto-remodelling

In order to further understand the effect of STA-MCA bypass remodelling to adult Moyamoya patients, we have studied STA-MCA bypasses with haemodynamic methodology to measure the flow resistance of coefficients (A and B) at the bypass and test the modifications of bypass patency over a 6-month period. In most cases, the flow resistance of the bypass decreased. Previous studies have shown that the volume of WSS is considered to be an important indicator of vessel remodelling [342, 343]. Our data illustrates that WSS immediately following surgery tended to be high. This is due to a sudden change in the vascular environment of the STA after incorporation into the bypass. As a consequence of auto-remodelling with time, WSS underwent a reduction. Figure 5.5A confirms that for

successful cases, WSS tends to be uniform due to the influence of remodelling, a finding that is consistent with previous physiological studies [344].

In our last 2 cases (case J and case K), WSS and flow resistance increased at follow-up, although patients have yet to exhibit any abnormalities of symptoms during current clinical observations. We speculate that this unexpected remodelling is most likely due to the marked degree of STA curvature at the time of STA-MCA bypass surgery. As discussed above, the initial morphology of the bypass may affect flow distribution inside the vessel, which will further result in differences in vessel remodelling. Our results suggest that bypass with a marked curvature of the STA trunk should be avoided.

5.5.3 Limitations of the current study

This research analysed STA-MCA bypass mainly in terms of haemodynamics, rather than clinical outcome. Other factors may also affect long-term bypass patency in spite of vessel auto-remodelling; e.g. the actual demand of blood flow, collateral development from indirect revascularization, blood coagulation status and medication protocol. We were not able to distinguish the impacts of these factors in this study. Another limitation of this study is that the number of cases is small. To fully elucidate the nature of auto-remodelling, further investigation is required.

5.6 Conclusion

This research investigates STA-MCA bypass auto-remodelling for adult Moyamoya patients. For most STA-MCA bypasses, vessel auto-remodelling reduced stenoses present within the recipient artery immediately after surgery and increased the uniformity of internal diameter with time. As a result, the flow resistance of the bypass is reduced, with increased flow rate and increasingly uniform WSS. Our results also highlight the significance of the initial bypass morphology in the auto-remodelling process. If the STA trunk possesses marked curvature,

the auto-remodelling may be associated with a worsening of the pre-existing curvature, increasing flow resistance and, potentially, vessel occlusion. To ensure optimal STA-MCA bypass at follow-up, both the curvature and lie of the bypass vessel must be carefully considered.

Chapter 6

Assessing Surgical Treatment Outcome Following STA-MCA Bypass Based on Computational Haemodynamic Analysis

Published as

Fengping Zhu, Kaavya Karunanithi, Yi Qian, Ying Mao, Bin Xu, Yuxiang Gu, Wei Zhu, Liang Chen, Yong Wang, Huiwen Pan, Yujun Liao, and Michael Morgan. Assessing Surgical Treatment Outcome Following Superficial Temporal Artery to Middle Cerebral Artery Bypass based on Computational Haemodynamic Analysis. Journal of biomechanics. 2015; 48(15): 4053-4058.

6.1 Abstract

To estimate haemodynamic modification of ICA after bypass surgery using CFD technology and thereby aid in our understanding of the influence of haemodynamic parameters on the outcomes of bypass operations. 18 patients who underwent superficial temporal artery to middle cerebral artery bypass and EDMS surgery were included. Reconstructed three-dimensional vessel geometries from MRA were segmented to create computational domains for CFD simulations. All cases were classified as three groups according to the proportion of the MCA area of distribution supplied by revascularization: A, more than two thirds; B, between two-thirds and one-third; and C, less than one-third of the MCA distribution. Pre-operative and follow-up haemodynamic parameters, especially volume flow rate and pressure drop index (PDI) in ICA were compared. For all cases, PDI and volume flow rate in the surgical-side ICA decreased significantly at follow-up ($P < 0.05$). For the cases of group A, volume flow rate in surgical-side ICA decreased by average 24.2%, whilst for the cases of group B and C, flow rate reduced by 10.5% and 3.7%, respectively. An average PDI for cases in group A was -1.67mmHg, conversely average PDI values of group B and C were -0.53 and 0.82mmHg, respectively. The remodelling of ICA after bypass was associated with reduction in the volume flow rate and pressure drop. Good correlation with angiographic grading suggested that CFD might play a critical role as a quantitative haemodynamic technique for predicting treatment outcome during the follow-up of MMD patients.

6.2 Introduction

Prevalent in Asia, MMD leads to stenosis or occlusion of the main intracranial arteries, including terminal ICA, proximal portions of ACA and MCA. Subsequently, a fine vascular network forms at the base of brain [345]. Arterial stenosis around the circle of Willis induces

blood flow reduction in the brain and formation of fragile Moyamoya vessels [346]. There exist two peaks of distribution of age at onset and the clinical features differ substantially between children and adults. Generally, adult patients with MMD usually present with intracranial haemorrhage, whereas most paediatric cases have cerebral ischemia.

Surgical revascularization, including direct superficial temporal artery – middle cerebral artery (STA-MCA) bypass, and indirect revascularization methods are common treatments for reconstructing cerebral blood flow of MMD patients. Recently, EC-IC bypass surgery was reported to help decreasing the rate of recurrent bleeding in the haemorrhagic type of Moyamoya disease in one RCT study [347]. Angiographic diminishment of Moyamoya vessels was observed after EC-IC bypass surgery, which was regarded to result in decreased haemodynamic stress to pathological Moyamoya vessels [183, 223, 347].

CFD technology has been applied widely in many cerebrovascular diseases for quantitative haemodynamic analysis, especially for aneurysms and intracranial artery stenosis[348-350]. In the past, CFD techniques have been employed to look into maintaining the patency of high flow bypass [351]. Our previous study revealed STA-MCA bypass has a characteristic auto-remodelling after surgery using CFD [352]. The decrease of ICA PDI was also observed at follow-up after indirect bypass surgery [353]. In this study, we are trying to estimate the haemodynamic modification of ICA after combined STA-MCA bypass and EDMS surgery by using CFD technology and to verify whether haemodynamic parameters correlate with treatment outcome.

6.3 Materials and Methods

6.3.1 Subjects

18 patients were diagnosed with MMD and treated with combined STA-MCA bypass and EDMS in Huashan Hospital from 2010 to 2013. MMD was diagnosed according to the criteria of the Research Committee on Spontaneous Occlusion of the Circle of Willis (Moyamoya Disease) of the Ministry of Health and Welfare, Japan [18]. The circle of Willis was incomplete and bypass surgery was performed on one hemisphere for each patient. All patients were routinely examined by MRA and duplex ultrasonography preoperatively and at follow-up. The study was approved by ethical committees of Huashan Hospital, Fudan University and Macquarie University. Written informed consent was obtained from each patient.

6.3.2 Surgical procedures

Surgical intervention for MMD was indicated after comprehensively evaluating the DSA, clinical manifestations and brain perfusion or metabolic findings in our department, detailed surgical indications were described before [157, 183]. Anterior and/or posterior branch of STA were anastomosed to the cortical branch of MCA in end-to-side fashion using a single 10-0 nylon suture. EDMS, the indirect bypass procedure has been described in our previous study [157]. Fifteen cases were operated by Professor B Xu, and three cases were operated by Professor YX Gu.

6.3.3 MRI scanning and Ultrasonography

MRA scans (4 slabs , 40 slices per slab; TR, 22 ms; TE, 4.2ms; flip angle, 18; matrix size, 365×384; slice thickness 0.5mm; field of view 181×200 mm^2) were obtained with 3.0 T MR Systems console (Verio, Siemens Medical Systems, Erlangen, Germany).

Duplex ultrasonography was performed to measure the blood flow of ICA using an L9-3 linear probe (bandwidth, 3-9 MHz) (bandwidth, 1-5 MHz) on a high-end ultrasound device (Philips Healthcare, Andover, MA) [293].

6.3.4 CFD modelling

3D geometries of ICA were reconstructed and segmented by using a commercial software package - MIMICS (Materialise' Interactive Medical Image Control System, Belgium) to create domains for CFD computation. Instead of using "global smoothing", we used manual "local smoothing" to keep the 3-D geometry as realistic as possible. Mesh generation yielded elements ranging from 0.8 to 1.4 million. The conservation equations for 3D steady flow with rigid walls were solved by using the ANSYS CFX 15.0, a finite-volume-based CFD solver (ANSYS Inc., Canonsburg, PA, USA). Patient specific inflow boundary conditions of blood flow were measured by duplex ultrasonography. A zero static pressure was specified as outlet boundary condition. Blood flow was modelled as a laminar Newtonian fluid with a density and dynamic viscosity of 1050 kg m^{-3} and 0.0032 Pas, respectively.

6.3.5 Pressure drop index

PDI was calculated as the difference in pressure reduction along the ICA at pre-operation and follow-up. PDI can be calculated using the formula

$$PDI = \Delta P_f - \Delta P_p = [(P_{if} - P_{of}) - (P_{ip} - P_{op})] \quad (9)$$

Where, ΔP_f and ΔP_p are the calculated pressure reduction at follow-up and pre-operation respectively.

P_{if} and P_{of} are the follow-up pressure values calculated at the inlet and outlet sections, respectively, and P_{ip} and P_{op} are the pre-operative pressure values calculated at the ICA inlet and outlet, respectively as shown in Figure 6.1. The positions of proximal (inlet) and distal (outlet) planes where we measured the pressure values are the same between pre-operative and follow-up models. All units are in mmHg.

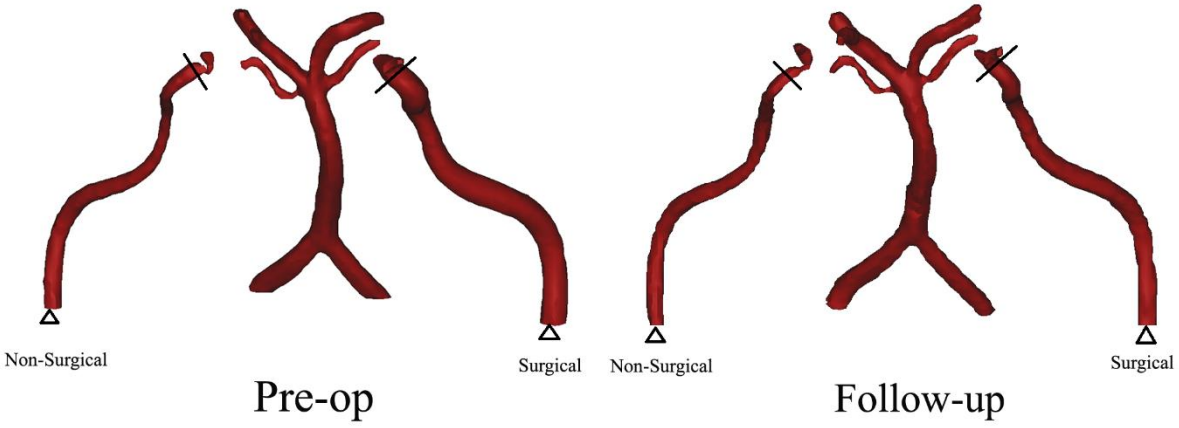

Figure 6.1 Illustration of planes for pressure measurement in the pre-operative and follow-up CFD models

Inlet measurement plane is marked with triangle, outlet measurement plane is labelled using black line

6.3.6 Inflow conditions and volume flow rate change

Velocities were measured at the proximal end of ICA by ultrasonography and were used as inflow conditions in CFD simulation. The volume flow rate of ICA was measured by utilising the mass flow from CFD. The percentage of volume flow rate change was calculated by using the formula.

$$\text{Percentage of volume flow change} = \left(F_f - F_p\right)/F_p * 100\% \quad (10)$$

Where, F_p and F_f are the measured mass flow of ICA at pre-operation and follow-up respectively.

6.3.7 Angiographic treatment outcome

All cases are classified as three groups according to angiographic outcomes from surgery by the criteria proposed by Matsushima [221]. This grading was the proportion of the MCA area of distribution supplied by the surgical revascularization: A, more than two thirds of the MCA distribution; B, between two thirds and one third of the MCA distribution; and C, less than one third of the MCA distribution. The angiographic treatment outcome was evaluated by 2 independent neurosurgeons who were blinded to this study.

6.3.8 Statistical Analysis

The normality of haemodynamic parameter distributions was checked. Mean and standard deviation were calculated to represent the normal variable, and non-normal distribution variables were represented as median and quartile. Two-tailed paired Student's t-test was applied to compare the results of pre-operative and follow-up parameters both in the surgical side and non-surgical (contralateral) side of ICA. Nonparametric analysis was used among

non-normal variables. A significance level of 0.05 (*P*-value) was selected for the test to verify if the changes in the haemodynamic parameters were statistically significant. Statistical analyses were performed using SPSS 17.0 software (IBM Corp, USA).

6.4 Results

6.4.1 Surgical outcome

There were seven males and eleven females diagnosed of MMD with a mean age of 34.8 ± 8.38 years, ranging from 18 to 50 years. Demographic features of patients' details are listed in Table 6.1. The 18 patients were followed up for 3-13 months, an average of 6.2 months. Preoperative symptoms were improved in all cases. There was no new cerebral infarction or bleeding during the follow-up observation. Eleven, four, and three cases were classified as group A, B and C respectively.

Table 6.1 Demographic and clinical characteristics of the patients

Age (Years)	
Mean ± SD	34.8 ± 8.38
Range	18-50
Gender	
Male	7 (38.9%)
Female	11 (61.1%)
Surgical Side	
Right	10 (55.6%)
Left	8 (44.4%)
Clinical presentation	
Cerebral infarct	8 (44.4%)
Transient Ischemic Attack	5 (27.8%)
Haemorrhage	5 (27.8%)

6.4.2 Volume flow rate change

In this study, the volume flow rate in ICA at pre-operation and follow-up were compared, and the percentage of volume flow rate change in both sides of surgical and non-surgical ICA were calculated. At the follow-up observation, the volume flow rate of surgical ICA significantly decreased from 157.77 ± 50.14 ml/min to 131.28 ± 51.78 ml/min ($P < 0.01$) (Figure 6.2). While, in the non-surgical ICA, the volume flow rate insignificantly increased (157.18 ± 55.74 ml/min at pre-operation, 175.58 ± 106.51 ml/min at follow-up, $P > 0.05$). The changes of volume flow rate in the surgical and non-surgical ICA appeared significantly different ($P < 0.05$). Table 6.2 summarizes the change of volume flow rates at the conditions of pre-operation and follow-up. For cases classified in group A, as a result of the good auto-remodelling of ICA (e.g. stenosis progression of terminal ICA, reduction in diameter), the flow rate in the surgical ICA was decreased by 24.2%, whilst for cases of group B and C, blood flow reduced by 10.5% and 3.7%, respectively.

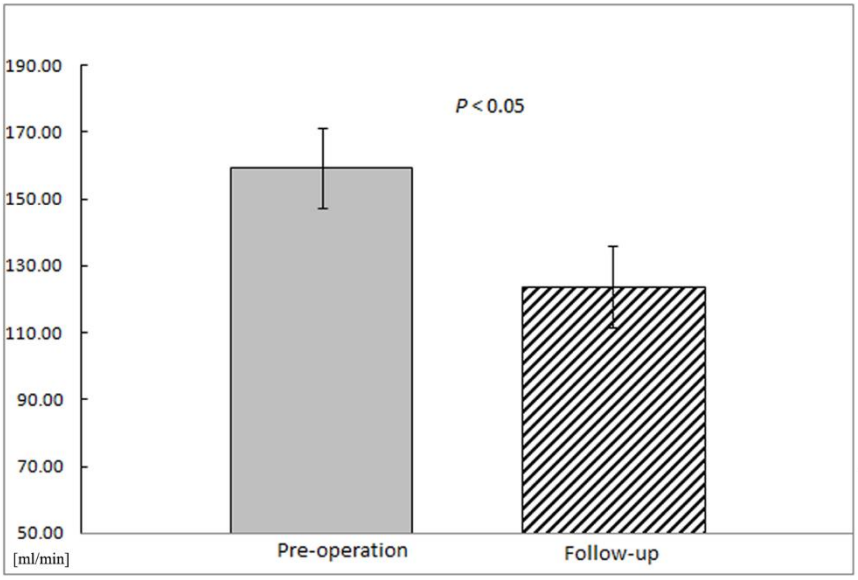

Figure 6.2 Volume flow rate of surgical ICA at pre-operation and follow-up

Table 6.2 Mean volume flow rate, Percentage volume flow rate change of surgical and non-surgical ICA in Pressure drop index

Grading	No	Surgical ICA			Non-surgical ICA		
		Pre-operation (ml/min)	Follow-up (ml/min)	Percentage change	Pre-operation (ml/min)	Follow-up (ml/min)	Percentage change
A	11	159.33	123.75	-24.2%	158.76	184.18	6.2%
B	4	155.12	138.91	-10.5%	154.59	166.28	2.2%
C	3	155.55	148.71	-3.7%	154.84	156.43	2.5%

The difference in pressure drop between pre-operation and follow-up, named as PDI, was calculated for all cases. For all cases, pressure drop in the surgical ICA was significantly decreased from 4.41 (2.37-5.95) mmHg to 3.23 (1.89-4.73) mmHg ($P < 0.01$). While, in the non-surgical ICA, pressure drop shows insignificant change from 3.09 (2.29-4.21) mmHg at pre-operation to 3.29 (2.12-4.61) mmHg at follow-up ($P > 0.05$). An average PDI of surgical ICA and non-surgical ICA for all cases was -1.00 and 0.51 respectively, and the change of PDI in the surgical ICA was significantly different from that in the non-surgical ICA ($P < 0.01$) (Figure 6.3). Table 6.3 summarizes the change of pressure drop and PDI at pre-operation and follow-up. An average PDI of the surgical ICA for cases in group A was -1.67 mmHg. The result indicated that the pressure difference at the terminal ICA was significantly decreased during the follow-up period. This is expected owing to the decrease in flow ratio during the follow-up period. By observing the structural and haemodynamic changes of the surgical ICA, we found diameter and vascular tortuosity of the ICA trunk were decreased. On the other hand, however, the WSS didn't change (illustrated by case 13 in group A, Figure 6.4). In comparison, the average PDI values for the cases of group B and C were -0.53mmHg and 0.82mmHg, respectively. The pressure difference at the terminal ICA was increased for the cases of group C. Following the observation of ICA changes in cases of group C between pre-operation and follow-up, we found that the diameter of ICA did not change. However,

there was a new and severe stenosis in the ICA trunk and the WSS at the terminal and stenotic portions of the ICA were quite different (illustrated by case 11 in group C, Figure 6.5).

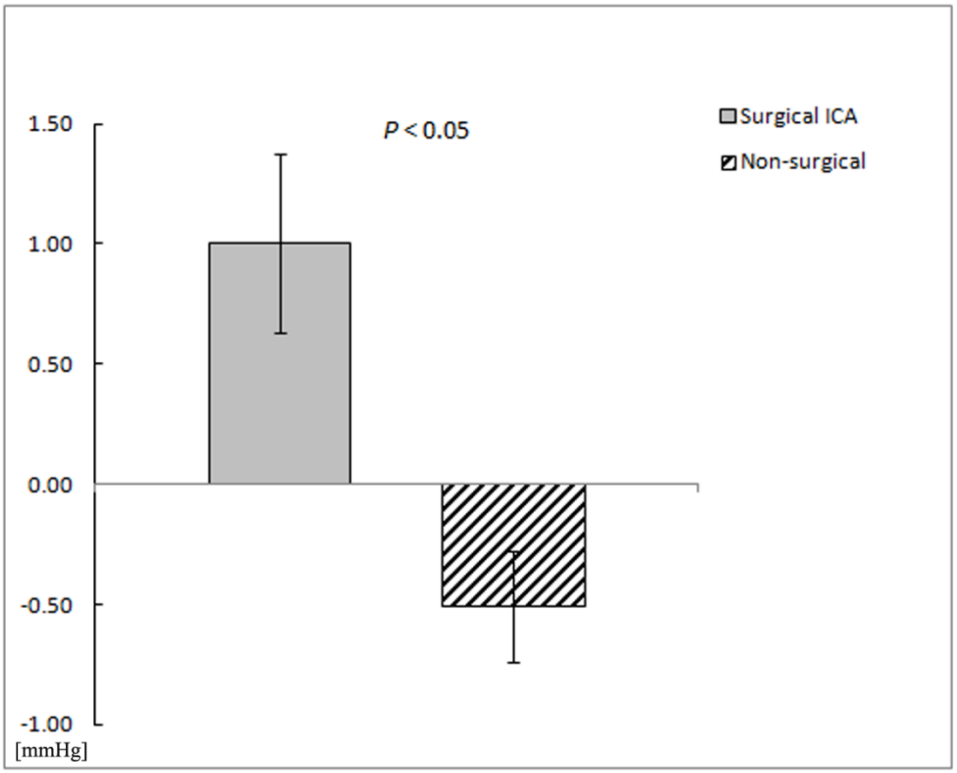

Figure 6.3 PDI of surgical and non-surgical ICA

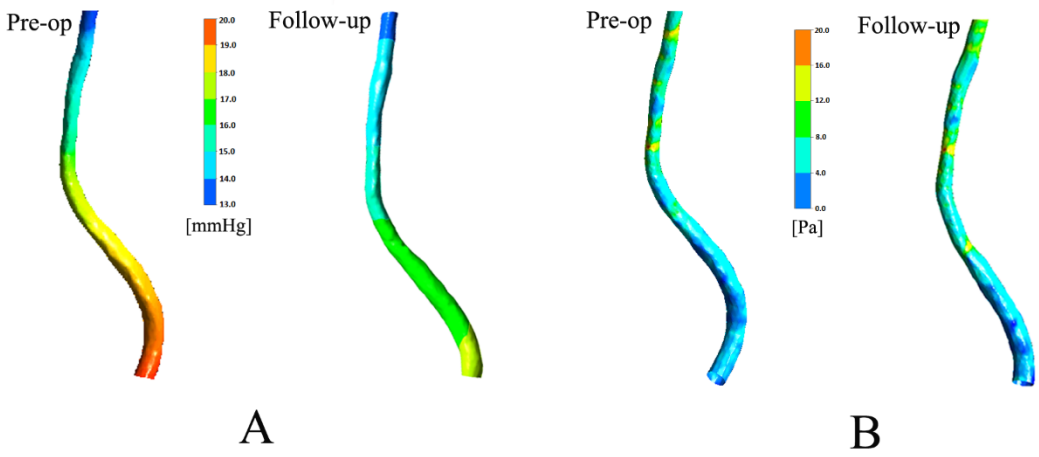

Figure 6.4 Pressure and wall shear stress (WSS) distribution of illustrative case in group A and B

A, Pressure contours and B, Wall shear stress contours of surgical ICA for case 13 in group A at pre-operation and follow-up, representing the characteristic vessel remodelling of ICA. ICA shrunk, the diameter and vascular tortuosity of ICA trunk decreased. WSS of ICA trunk didn't change obviously

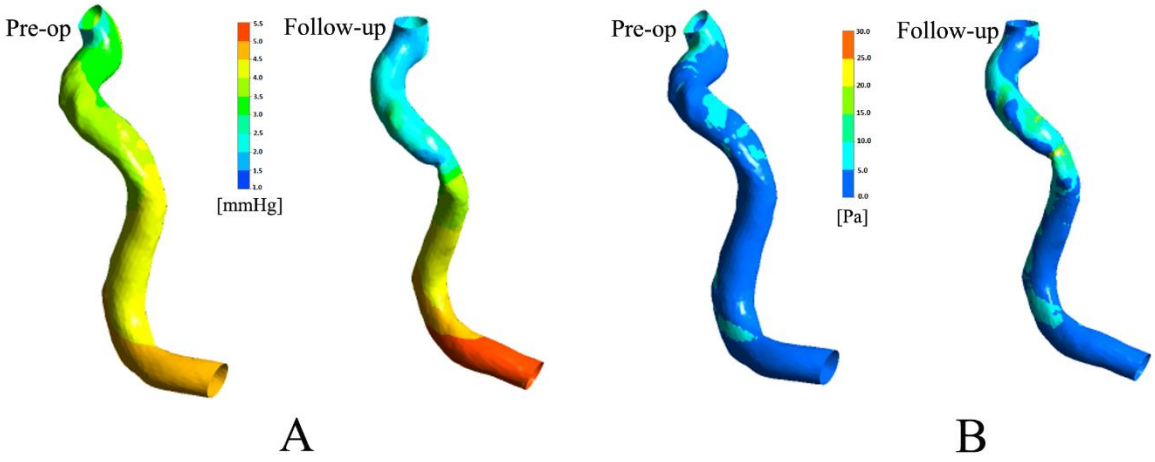

Figure 6.5 Pressure and wall shear stress (WSS) distribution of illustrative case in group C

A, Pressure contours and B, Wall shear stress contours of surgical ICA for one case in group C at pre-operation and follow-up. The pressure drop increased, and the diameter of ICA did not change obviously, however, there was new and severe stenosis in the ICA trunk. WSS at the stenotic portion of ICA were higher than the pre-operative model

6.5 Discussion

MMD is a rare cerebrovascular disease characterized by multiple steno-occlusive changes around the circle of Willis, leading to ischemic and haemorrhagic stroke. Although more prevalent in Asian countries, studies have shown that MMD also occurs amongst patients of no-Asian backgrounds [135].

There is still debate on the best treatment for occluded cerebrovascular disease; however, direct STA-MCA bypass with or without indirect revascularization is routinely performed for Moyamoya patients for the potential benefit of flow augmentation, haemodynamic stress relief, and relatively low surgical complications [183, 345]. Development of collaterals circulation, reduction in Moyamoya leptomeningeal collateral vessels, improvement of dilation and branch extension of the anterior choroidal and posterior communicating arteries can be observed among ischemic and haemorrhagic Moyamoya patients after bypass surgery, leading to surgical benefit and decreased risk of recurrent infarction and bleeding [183, 223, 354].

A few studies have been performed to investigate the vascular morphology associated with MMD. Narrowing of the outer diameter of the ICA bifurcation, high wall shear stress of the ICA bifurcation, progressive stenosis of PCA all have been identified in MMD [284, 345, 355]. However, no computational quantitative methodologies were used to analyse the haemodynamic benefit after bypass surgery of MMD patients. Our previous study, using CFD technique, revealed that bypass graft has a characteristic remodelling after combined direct and indirect bypass surgery that usually reduces flow resistance. The initial morphology of bypass has a significant effect on the outcome of vessel remodelling and bypass patency [352]. To the best of our knowledge, there is no study of vessel remodelling of ICA after combined direct and indirect bypass.

This is a pilot cohort study using CFD technique for haemodynamic quantification analysis of MMD patients, with an incomplete Circle of Willis, treated using combined direct and indirect bypass. For all cases, the pressure drop and volume flow rate of the surgical ICA decreased significantly at follow-up ($P < 0.05$). Whereas in the non-surgical ICA, both pressure drop and volume flow rate showed insignificant changes ($P > 0.05$). Our data illustrates that the ICA has a characteristic vessel remodelling after bypass surgery that

usually decreases pressure drop and volume flow rate. The inverse haemodynamic changes of the surgical and non-surgical side of ICA might be owing to the fact that MMD usually affects bilateral sides of the brain. Further study on the haemodynamic changes after bypass surgery for MMD cases in which the circle of Willis is complete is currently being conducted.

Since the preoperative symptoms varied, it was difficult to quantify the clinical functional treatment outcome with uniform standard. This research classified cases into three groups according to angiographic findings rather than functional outcome of patients. In group A, the pressure drop decreased significantly and average PDI was -1.67 mmHg. This shows that pressure drop at follow up is much greater than the pressure drop at pre-operation. This might be expected owing to the structural shrinkage of ICA as a whole, decrease in diameter of ICA and reduction in flow rates at follow-up. Though the numbers of cases in groups B and C are small, the PDI value is shown to correlate with the angiographic treatment outcome. The average PDI values for cases in groups B and C were – 0.53 and 0.82 mmHg, respectively. These results suggest that the reconstructed flow from direct and indirect bypass can influence the haemodynamic state of the ICA and lessen its haemodynamic stress. PDI might be potentially used as a haemodynamic indicator for treatment outcome classification [353]. The result is corresponding with our previous study, in which we identify PDI correlated with treatment classification after indirect bypass surgery.

In this study, MRA was used to create 3D vessel geometry for creation of CFD computational domains. It is much less invasive and more suitable for follow-up compared with DSA for the absence of radiation exposure to patients and complications induced by catheter angiography procedures. Although the number of cases in this study is limited, haemodynamic analysis based on MRA might be a potential non-invasive quantitative method for follow-up of MMD patients after bypass surgery.

In this study, treatment outcome was classified by angiography. However, functional benefit was still regarded as the crucial standard to judge medical treatment outcome. The computational haemodynamic analysis of ICA is an adjunct tool rather than replacement of careful and thorough assessment of patients' neurological function in the follow-up of MMD patients after bypass surgery. The angiographic changes observed could not be determined as cause or a result of the ICA vessel remodelling through this study. The main limitation of this study is that the small number of cases. However, to the best of our knowledge, this is currently the largest case series study of haemodynamic analysis of bypass surgery for MMD patients using CFD technology. Furthermore, follow-up is short for a disease that is chronic and gradually progressive. To elucidate the nature of auto-remodelling, further investigations of more cases with a longer follow-up will be required in the future.

6.6 Conclusion

The ICA has a characteristic vessel remodelling after combined direct and indirect bypass surgery that usually decreases both pressure drop and volume flow rate. Detailed analysis of haemodynamic changes in the ICA using CFD technology might prove to be a potential non-invasive quantitative method of treatment outcome classification for the follow-up of MMD patients after bypass surgery.

Chapter 7

Haemodynamic Assessment of Surgical Treatment Outcome on Moyamoya Disease Patients with Complete Circle of Willis Following Revascularization Surgery

Submitted as

Kaavya Karunanithi*, **Fengping Zhu* (Co-first Author)**, Bin Xu, Yuxiang Gu, Yong Wang, Liang Chen, Wei Zhu, Ying Mao, Yi Qian. Characterization of Pressure Drop Index (PDI) in MMD patients treated with combined direct and indirect revascularization surgery. Medical Engineering & Physics, Submitted.

7.1 Abstract

Surgical revascularization is the stand-alone treatment for Moyamoya disease. PDI defined as the difference in head loss between post and pre-operation indicates a suggestive correlation with angiographic treatment outcome of MMD patients in our previous research. In the current investigation, we aim to further elucidate the link by analysing the haemodynamic parameters of eight haemorrhagic MMD patients (4-Male and 4-Female) who were treated unilaterally by combined direct STA-MCA bypass and EDMS. Four of them were clinically classified significant improvement and the rest as limited improvement based on MRA findings at post-operation. PDI and percentage flow decrease were calculated for all eight cases and compared against the clinical outcome. The results indicate that an inverse correlation exists between PDI and treatment outcome.

7.2 Introduction

Moyamoya disease refers to progressive luminal stenosis or occlusion of the main branches of the circle of Willis, accompanied by a fine network of collateral vasculature [1, 356]. The aetiology is believed to be genetic as it predominantly appears in Asian population with an incidence rate of 0.94 and 5.2 people per 100,000 in Japan and Korea respectively as compared to the 0.086 people per 100,000 in the US [9, 357]. The disease progression is cogitated to be different in children and adults as Moyamoya clinically presents with cerebral infarction/ischemia in children whereas in adults it usually results in intracerebral haemorrhage due to increased CBF in the collateral vessels [163].

There are various types of revascularization procedures, all of which involve in combating high blood flow to the relatively smaller collaterals [358]. Based on the clinical characterization, the recommended method of revascularization treatment varies. Despite the lack of large-scale clinical trials, there have been various studies that have established direct EC-IC bypass revascularization procedure to be effective for adult patients presenting with intracerebral haemorrhage [359, 360]. Alternatively, paediatric MMD patients who undergo indirect revascularization are believed to have better prognosis with almost 100% rate of change in Moyamoya vessels [361, 362]. Indirect revascularization is an umbrella term that includes multiple techniques such as EDAS, EDMS, Omental Transposition and Multiple burr holes [169]. In adults, recurring haemorrhage poses significant problems post revascularization and severe morbidity and mortality rates have been reported due to re-bleeding and CHS [232, 363]. To combat recurrent intracranial haemorrhage, a united approach consisting of both direct and indirect revascularization procedure have been proven effective in recent times [364]. STA-MCA bypass combined with EDMS has been reported to reduce the risk of re-bleeding by up to 15% [365]. The EDMS is an indirect bypass combining the encephalo-duro- and encephalo-myo-synangioses. The combination treatment

works well for adults as the middle meningeal artery, temporal muscles and STA are dominant blood suppliers thereby reducing the blood flow throughput to the cerebral vessels and any remaining cerebral ischemia if present becomes a driving factor for neovascularization via indirect method [366].

Although the underlying mechanism by which direct revascularization surgery proves effective for adult MMD patients has not been documented through randomized large scale clinical trials, a recent initiative by Japan to conduct a large scale, randomized, multi-centre adult Moyamoya trial to review the long-term efficaciousness of EC-IC bypass in underway [367]. The primary causative of re-bleeding is the rupture of micro-aneurysms that develop in the compensatory vasculature due to increased haemodynamic load [365]. Hence we propose CFD technology to determine if there occurs a decrease in blood flow, thereby loss of energy, in the Moyamoya vessels. CFD simulations of treated MMD patient geometry will help us analyse haemodynamic patterns in the Circle of Willis pre- and post-operatively. In our previous research, we identified a new haemodynamic parameter; PDI (pressure drop index) to analyse the treatment outcome of MMD patients treated with EDAS [368]. This research paved way to our current study where we aim to standardize PDI as an indicator of treatment outcome for MMD patients treated via combined revascularization approach.

7.3 Materials and Methods

7.3.1 Subjects

Eight adult patients (four-Female and four-Male) aged 14-47 years were selected from the patient database. Inclusion criteria were as follows, MMD patients with complete Circle of Willis who presented with haemorrhage as initial symptoms and treated unilaterally with combined direct (STA-MCA Bypass) and indirect EDMS procedures at the Huashan Hospital,

Shanghai, China between 2010 and 2012 [157]. The treatment procedure combined STA-MCA direct bypass and EDMS method in unilateral hemisphere (Table 7.1). We specifically selected the patients who possessed the complete Circle of Willis, in order to analyse the haemodynamic alternation during the artery remodelling after MMD treatment. All patients were examined by MRA, a potential non-invasive quantitative method, and Doppler Ultrasound both at pre- and post-operation. Treatment outcome was clinically classified into A- Significant Improvement, B-Limited Improvement from the MRA measurements by two independent neurosurgeons blind to the study [184]: Significant Improvement- the postsurgical collateral vessels presented revascularization of two thirds or more of the MCA distribution and Limited Improvement- the postsurgical collateral vessels presented from no/ little to two thirds revascularization of the MCA distribution. All participants provided written informed consent. All surgical protocols were approved by the Institutional Research and Ethics Committee prior to the treatment. 3D reconstruction and segmentation of patient geometries was done via use of commercial software package - MIMICS (Materialise, Belgium) for computational meshing in preparation for CFD calculation.

7.3.2 CFD modelling

3D geometry of Circle of Willis including Left, Right ICA and BA of all eight patients were reconstructed via generation of two-dimensional contours from grey scales of pixels, and by subsequent interpolation in a normal direction. This method prevents the intrusion of surface noise. Surface smoothing was kept to a minimum to avoid distortion and limited to few localised areas to keep the surface roughness as close to the real vessel surface as possible. This method has been proven to display an average error of one-third of a pixel in size approximately [369].

Navier-Stokes equations for 3D flow with rigid walls were solved using ANSYS CFX 14 (Ansys Inc., Canonsburg, PA, USA), under steady state flow conditions. Steady state

simulations have been proven to adequately provide similar time-averaged results for pulsatile calculations over a cardiac cycle, which justified the use of steady state flow condition rather than pulsatile condition [303]. The inflow boundary conditions at pre- and post- operation was measured individually for each patient using Trans-Cranial Doppler Ultrasound (TCD). Blood flow was modelled as a laminar Newtonian flow with a density and dynamic viscosity of 1050 kg m^{-3} and 0.0032 Pa s, respectively.

To mimic venous capacitance and to allow sufficient recovery of the blood pressure the vessel outlet was extruded distally in a direction normal to the blood flow downstream to 100 mesh layers [370, 371]. Patient specific inlet boundaries, based on Ultrasonography flow measurements were set and zero pressure condition was applied at all the outlets. Fully developed velocity profiles aping the measured flow rates should be achieved at the proximal inlet boundary layer and for this reason the domains were extruded in the upstream direction to 100 mesh layers. Corresponding grid independence validations have been carried out in our previous work [371, 372]. The total number of elements ranged between 1000,000 and 1400,000. The grid size for the inlet/outlet interfaces were fixed at 0.01 mm and the rest of the computational domain had a maximum size of 0.02 mm.

7.3.3 PDI and Percentage Flow change

In our pilot study, we identified a new haemodynamic parameter, named as PDI, which indicated a suggestive correlation with EDAS treatment outcome in MMD patients [368]. Ideally, decreased haemodynamic stress through Moyamoya vasculopathy post-surgery should lead to significant head loss and thereby pressure reduction; PDI was calculated as the difference between pressure reduction at pre- operation, post-operation and follow-up can help us establish the treatment consequence on an MMD patient. According to Bernoulli's equation, the pressure reduction is calculated as the difference between the total pressure at

the inlet and outlet, at pre-operation as well as at post-operation. PDI is then calculated by the following equation:

$$PDI=\Delta P_{post}-\Delta P_{pre}=\left[(P_{in}-P_{out})_{post}-(P_{in}-P_{out})_{pre}\right] \quad (11)$$

Where PDI is a difference of pressure reduction/ head loss measured at post-operation and pre-operation, ΔP_{post} and ΔP_{pre} are the calculated pressure reductions at post-operation and pre-operation respectively. P_{in} and P_{out} are the total pressure values calculated at the inlet and both the outlet planes, at Pre and post-operation. In this report, we calculate the difference in pressure at the inlet and outlet of the carotid arteries for all eight patients computationally. In order to eliminate human error owing to segmentation, the pressure reduction in the left and right ICA were calculated between fixed co-ordinates at the inlet interface and the proximal end of the outlet, in both pre-operative and post-operative geometries in all patients (Figure 7.1). The difference between the pressure reduction at pre-operation and post-operation was calculated as PDI which was then compared to the clinical classification (based on DSA and MRA measurements). Percentage flow change is calculated by utilising the Ultrasound inflow rate measurements at the pre-operative and post-operative model. The rate of flow change at post-operation and the calculated PDI values were analysed.

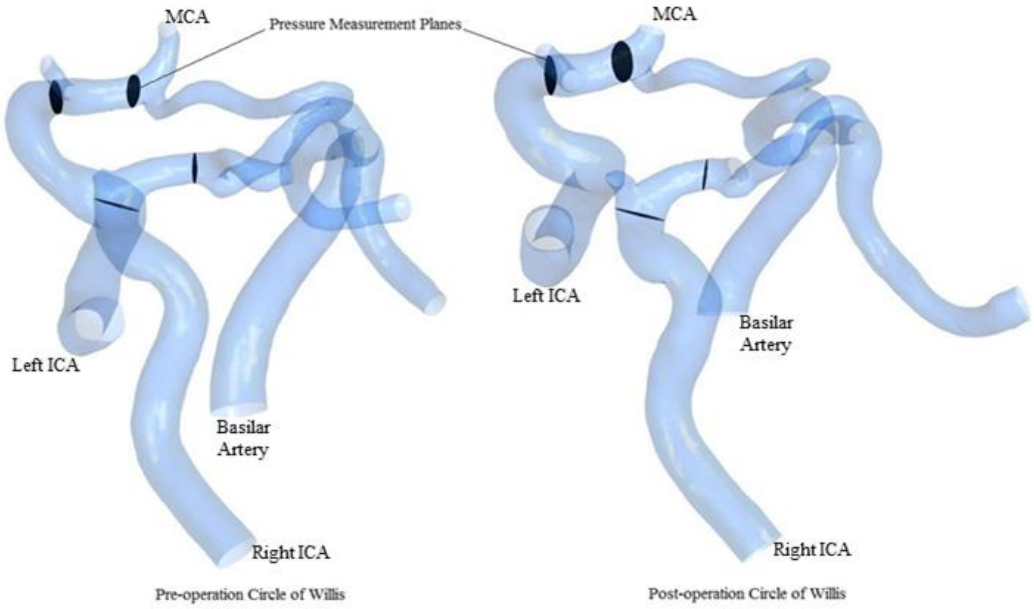

Figure 7.1 Pressure measurement planes at the Circle of Willis for PDI calculation

7.4 Results

7.4.1 Percentage Flow change analysis

Patients' demographic is listed in Table 7.1. Flow measurements were done both at pre- and post-operation in all patients using TCD. The flow rate changes were documented and percentage decrease in flow rate was calculated. The results for the surgical and contralateral ICA are tabulated below. As observed from TCD and CFD results; the flow rate of the surgical ICA decreased by an average of 21% ± 9.4% for all patients classified clinically A-Significant Improvement at post-operation. In contrast, the patients termed B-Limited Improvement had an average increase of 10% ± 13% in flow rate at post-operation ($P < 0.05$). This trend is in accordance with the objectives of combined STA-MCA bypass and EDMS approach, as blood flow through the ICA needs to be reduced to lower the haemodynamic

load through the peripheral Moyamoya vessels. This is shown to successfully reduce the risk of re-bleeding in adult haemorrhagic MMD patients. An intriguing aspect noted here is an insignificant albeit complementary increase in flow through contralateral ICA in A (approximately 7% ± 13% increase) and vice versa: a 3 % ± 3.7% decrease in flow through contralateral ICA for limited improvement patients (Figure 7.2).

Table 7.1 Patient Demographic and treatment outcome

Case	Sex/Age	Surgical side (Left/Right ICA)	Treatment Classification
1	Female/47	Right	A
2	Male/45	Left	A
3	Female/14	Left	A
4	Female/26	Right	A
5	Male/35	Left	B
6	Male/46	Right	B
7	Male/37	Left	B
8	Male/36	Left	B

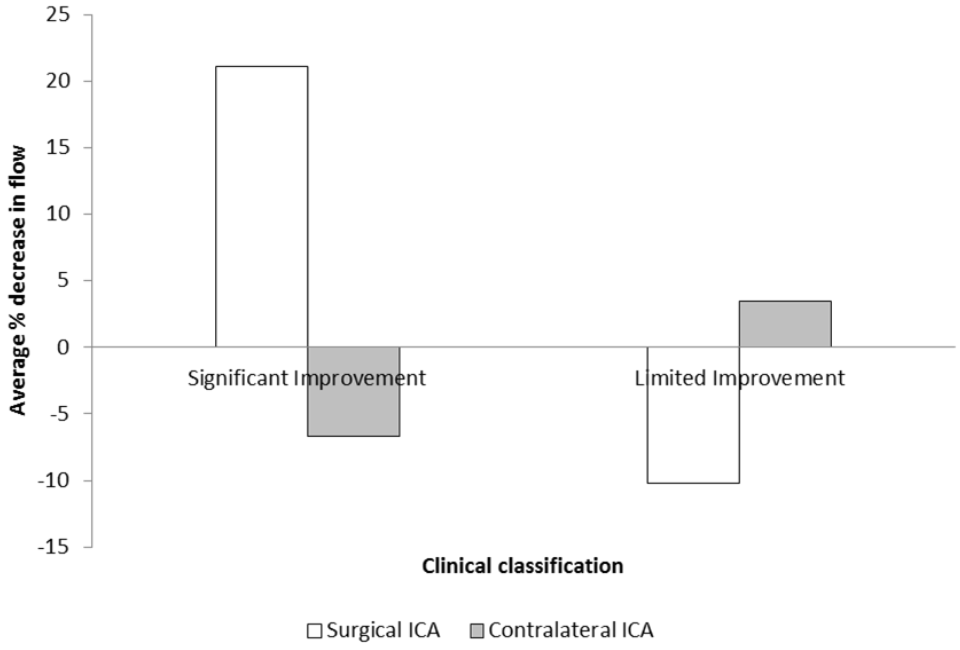

Figure 7.2 Average % decrease in flow rate in Surgical and Contralateral ICA of 8 patients (4-A, 4-B)

7.4.2 Pressure Drop Index

Preceding research into PDI has established it as an indicator of treatment outcome of MMD patients bilaterally treated with indirect EDAS method. Pressure drop index is calculated as the difference between pressure reduction or head loss of the ICA between pre-operation and post-operation. Table 7.2 gives us the PDI values for surgical and contralateral ICA for eight patients.

The average PDI for A-Significant improvement cases was -352 Pa ± 107.8 for the surgical side, average PDI for B-Limited Improvement cases was computed as 13 Pa ±81.6 ($P<0.05$). The contralateral ICA had a reversed display of PDI values; the average PDI for A and B category cases were 105 ± 65.1 and -81 Pa ± 220.1 respectively (Figure 7.3).

Table 7.2 Calculated PDI values for 8 patients

Case	Surgical Side	Status	Surgical ICA PDI (Pa)	Contralateral ICA PDI (Pa)
1	Right	A	-548.2	296.1
2	Left	A	-141.9	71.4
3	Left	A	-189.7	8.6
4	Right	A	-526.3	42.4
5	Left	B	-99.2	378.4
6	Right	B	-82.6	-356.6
7	Left	B	252.18	198.41
8	Left	B	-17.179	-546.04

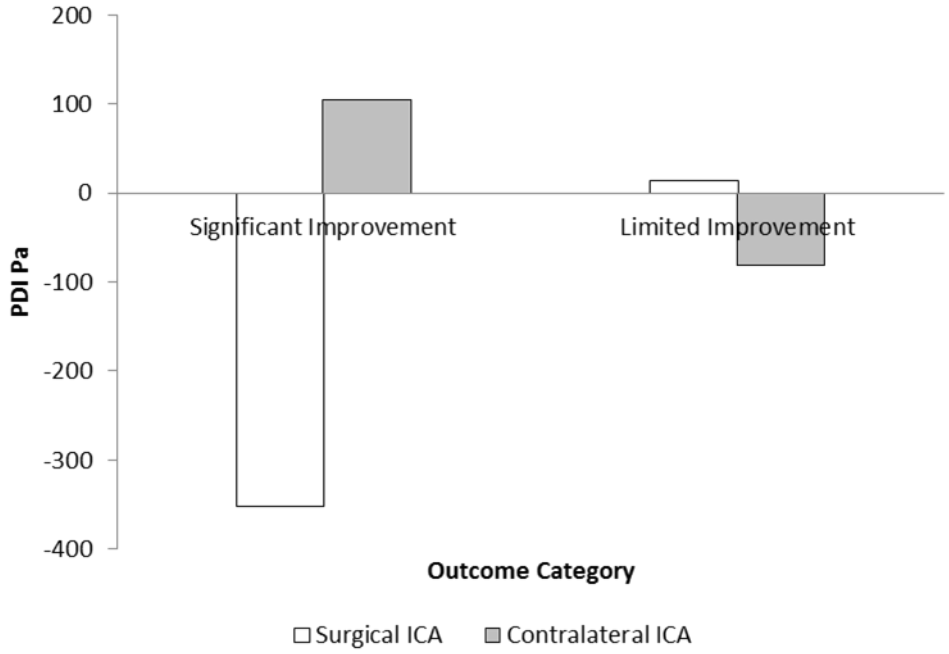

Figure 7.3 Average PDI values for Surgical and Contralateral ICA in 8 patients (4-A, 4-B)

As the surgery is unilateral, a negative PDI for the surgical ICA of patients in category A is expected due to a higher percentage decrease in flow at post-operation than before surgery.

The contralateral ICA shows a counteractive increase in PDI to balance the pressure loop, as the Circle of Willis was complete in all 8 patients selected according to the inclusion criteria from the database. The converse of this theory is evident for the category B cases in which an increase at the flow rate at post-op lead to an increase PDI across the surgical ICA; the contralateral hemisphere in this case has an offset reduction in PDI.

The calculated trend in PDI is further verified by the pressure contours captured from CFD results. Illustrated below are the pressure contours of the Circle of Willis of two patients (category A and B). The pressure contour of the surgical hemisphere for the patient A has a sharp reduction at post-operation in comparison to pre-operation due to successful vessel remodelling. The surgical ICA of patient B has increased pressure values at post-operation (Figure 7.4). An overall increase in pressure is present in the contralateral hemisphere of both A and B patients treated with combined revascularization technique.

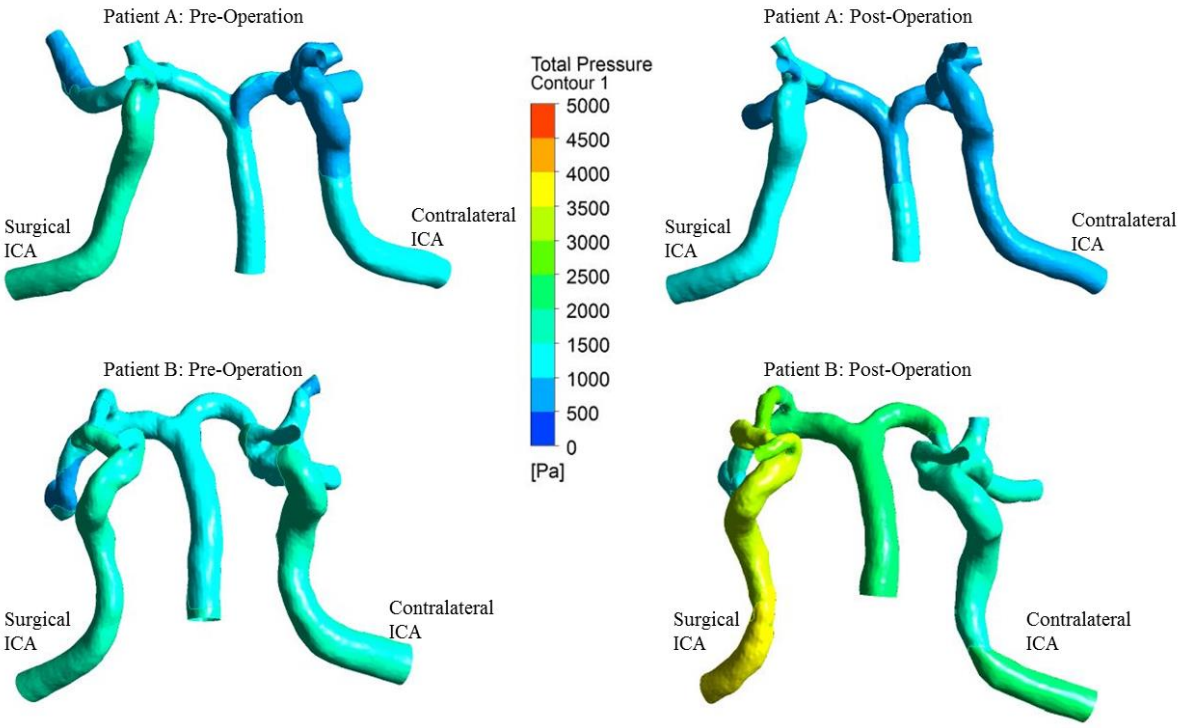

Figure 7.4 Pressure Contour of Patient A-Significant Improvement and Patient B-Limited Improvement

7.5 Discussion

Asymptomatic MMD patients with no traces of ischemia or haemorrhage are recommended conservative treatment as there is inherent risk in revascularization surgery [232]. Yet, Kuroda et al. reported that in 34 asymptomatic MMD patients treated conservatively, 4 patients suffered of haemorrhage and 3 patients had cerebral infarction [373]. This emphasizes the chronic nature of MMD with minimal or no response to treatments. Hence, surgical management to best control the momentum of the disorder is the only option for patients diagnosed with MMD [345]. Revascularization surgery has its own inherent risk of re-bleeding and ischemic attacks. Guzman et al. reported a 5 year cumulative risk of perioperative or subsequent stroke or death to be 5.5% in 450 adult and paediatric cases treated with revascularization surgery (both direct and indirect revascularization) [228].

Understanding the haemodynamics of MMD will enable us to gain insight into the intra- and perioperative complications that are associated with direct and indirect revascularization surgery. Quantitative MRI and MRA along with other imaging methods such as SPECT and PET have been indispensible in acquiring quantitative CBF data in MMD geometry with reasonable spatial resolution [124, 374].

In addition to diagnostic imaging techniques, CFD Technology has been used to haemodynamically quantify various cerebrovascular disorders such as aneurysms in the past [375, 376]. CFD technology can aid in calculating haemodynamic parameters besides just flow velocity such as total and relative pressure, wall shear, volume flow etc. Deployment of CFD technology in MMD has been attempted recently as these haemodynamic parameters have been proven to help clinicians in unravelling the disease pathogenesis and to plan surgical intervention in MMD patients [377]. A study done in 2007 showed that shear stress distribution (WSS) in the distal ICA region; a site for MMD genesis, was relatively low in comparison to the other portions of ICA[377]. Low WSS is believed to augment constriction of the lumen/narrowing of blood vessels which contributes to haemorrhagic episodes [378]. Zhu et al. investigated the patency of bypass in STA-MCA surgery using CFD; the results proved that factors such as initial morphology of the bypass influenced the characteristic remodelling of the vessel by lowering the flow resistance [352]. In our previous work, we identified a novel haemodynamic parameter; PDI for assessing EDAS (indirect revascularization) treatment outcome. We showed for clinically successful patients the calculated PDI was negative. This implies greater pressure reduction across the vessel at post-operation than the follow up [368]. The aim of this paper is to validate PDI as a reliable haemodynamic parameter for assessing MMD patients treated unilaterally with combined direct STA-MCA bypass and indirect EDMS method. Of the eight patients (4-Male, 4-Female) we analysed PDI was found to be negative in the surgical ICA for all four cases classified clinically as having significant improvement (A). The results were in agreement

with our previous research with positive or near negative PDI values calculated in the surgical ICA of the four patients classified having limited improvement (B). However, being unilaterally treated, the contralateral PDIs were found to be complementary to that of the surgical hemispheres. The PDI values of contralateral ICA in group A were in the positive bands, the vice versa was found for the category B. This compensatory loop is also found in percentage decrease of blood flow through the surgical and contralateral ICA. The percentage decrease in blood flow was higher in category A than the B group cases for the treated hemispheres. It is of prime importance to emphasize that our study included patients with complete Circle of Willis. The right and left ICA along with Basilar Artery (BA) and Anterior Communicating artery have been known to play an important role in maintaining the CBF output through the Circle of Willis [379]. Nevertheless, this counterbalance in flow and pressure reduction across the Circle of Willis warrantees further research. Decrease in CBF and its associated negative PDI, post-operation, points to physiologically stable blood flow through the ICA denoting lower haemodynamic stress on the Moyamoya vessels [379]. Lower haemodynamic stress through the vessel is proven to significantly reduce the risk of rupture and thereby advent of peri-operative complications [378].

Our results substantiate our claims that PDI can be used as a reliable parameter in assessing treatment outcomes for prediction of peri-operative complications. Characterization of MMD cases was done solely on the basis of computational haemodynamics and any clinical factors that arise from vessel remodelling were not discernable in our results. Despite the modest patient size, PDI has proved to be consistent in evaluating the treatment outcomes for both stand-alone EDAS and combined bypass surgery. A scaled up study design, consisting of comprehensive haemodynamic profiling of a larger cohort of patients, with long-term follow up is currently underway. If established as an industry standard, PDI can assist clinicians in surgical planning and long-term prognosis of MMD patients in addition to image-based classification.

7.6 Conclusion

This study is a follow-up endeavour to our maiden research wherein PDI showed promising results as an indicator of treatment success in MMD patients. Our findings suggest that there is an unambiguous relationship between treatment outcome and PDI. An analysis of PDI in two groups of eight patients each treated with EDAS and combined STA-MCA bypass and EDMS respectively, confirmed that negative PDI is associated with improved clinical outcomes and positive/near negative PDI represents a risk of re-bleeding. A follow-up study incorporating larger patient cohorts with sample sizes from other indirect surgical techniques is underway to establish PDI as an unfailing haemodynamic tool to assist surgeons in clinical decision-making.

Chapter 8

Conclusions and Future Directions

8.1 Conclusions

The aetiology of MMD remains unknown. Nowadays, there are many diagnostic techniques which facilitate the diagnosis and monitoring of MMD. Among them, DSA has been regarded as the 'gold standard' in the diagnosis for clearly demonstrating the vascular structures. However, there are many disadvantages of DSA, especially the radiation exposure and procedure complications. New emerging diagnostic techniques, including CTA and MRA have overcome these problems, whereas these techniques are mainly focused on the vascular morphology and relied on the experiences of doctors. Quantitative techniques to assess haemodynamic features of cerebral vasculature in MMD patients are rare in the clinic.

Bolus PWI by intravenous bolus injection of paramagnetic contrast agents, used fast echo-planar imaging sequence with high temporal-resolution to process continuous brain scans and detect the tissue signal intensity changes over time caused by blood with the contrast agent flowing through the inspected tissue for the first time. It can reflect haemodynamic information of the brain tissue, and subsequently obtain semi-quantitative information through calculation of the mathematical model, such as tissue blood volume, blood flow and MTT. Compared with other imaging techniques, it has many advantages, including relatively low cost, no radiation exposure, high spatial-resolution and simple image acquisitions. Researches applying PWI to assess cerebral perfusion information revealed the results were consistent with PET evaluation, demonstrating PWI can effectively be used to evaluate the haemodynamic changes of the brain. Intraoperative MRI was widely used to provide real-time images for neuronavigation in brain tumour surgery, however, it is rarely reported to be used in the neurovascular surgery. It has been proven to be helpful in preventing insidious or early complications after operation, such as cerebral ischemia and haemorrhage [321]. Integration of intraoperative MRI and the quantitative PWI technique has potential for assessing the haemodynamic changes after bypass surgery at the earliest time.

Thanks to the dramatic development of imaging and computer technology, CFD application in the field of biomedical engineering has rapidly increased. A key advantage of CFD technique is that it is a very compelling, non-intrusive, virtual modelling technique with powerful visualization capabilities. Furthermore, the outcomes can be evaluated using advanced technology to investigate a wide range of vascular configurations using a high-speed computer more quickly with lower cost [380]. It has been widely applied in the cardiovascular surgeries including the estimation of aortic stenosis [381] and design of arterial anastomosis and stent implantation [382]. In the field of cerebrovascular surgery, it is widely applied in the estimation of aneurysm growth, rupture, as well as intracranial stenosis [272, 273, 383-385]. CFD technology has been applied to analyse the haemodynamic remodelling of EC–IC vein bypass for the treatment of giant aneurysms, showing that flow resistances of the bypass graft play an important role in the long-term patency [351, 386]. However, the bypass procedure used was common carotid–to–intracranial arterial brain bypass with interposition of the saphenous vein, which was regarded as high-flow bypass, of which the haemodynamic character might be quite different from the low-flow bypass, known as STA-MCA bypass. STA-MCA bypass combined with or without indirect bypass surgery is the mainstay treatment for MMD, however, the exact mechanisms of vessel remodelling are still unknown. To elucidate the vessel remodelling characteristics of the cerebral vasculature for MMD after bypass surgery and discuss the potential use of CFD as an assistive tool to predict the treatment outcome, CFD technology has been employed in this study.

The following conclusions and limitations are derived from these studies:

(I) Intraoperative MRA and PWI are used to assess haemodynamic changes following STA-MCA bypass surgery as described in Chapter 4. Intraoperative MRA can be used to intraoperatively assess whether the STA-MCA bypass is patent with high-resolution. Semiquantitative analysis of atlas-based intraoperative PWI is an effective method for

predicting postoperative hyperperfusion syndrome immediately after STA-MCA bypass. Immediate intraoperative great increases of rCBF at MCA-terminal territory might be a sensitive parameter for predicting postoperative CHS. However, the cut-off value for early diagnosis of hyperperfusion syndrome using intraoperative PWI has not been managed for the limited cases.

(II) CFD has been applied to predict the outcome of bypass surgery regarding the bypass patency in Chapter 5. Flow resistance might be regarded as a predictive parameter. Vessel auto-remodelling of STA-MCA bypass graft in the long-term follow-up was observed. For the cases in which STA-MCA bypass is patent at the long-term follow-up observations, the flow resistance of the bypass is reduced, with increased flow rate and increasingly uniform wall shear stress. This study highlights the significance of the initial bypass morphology in the vessel-remodelling process. If the STA trunk possesses marked curvature, the auto-remodelling may be associated with a worsening of the pre-existing curvature, increasing flow resistance and, potentially, vessel occlusion. To ensure optimal STA-MCA bypass at follow-up, both the curvature and position of the bypass graft must be carefully considered. This study is limited due to the small number of cases.

(III) CFD technology has been employed to simulate the haemodynamic changes at ICA in Chapter 6. The ICA has a characteristic vessel remodelling that usually decreases both pressure drop and volume flow rate. The percentage changes of pressure drop and volume flow rate of ICA were correlated with angiographic grading which is used to classify the treatment outcome of revascularization surgery for MMD. In the non-surgical side, ICA exhibits inverse haemodynamic changes for unknown reasons. Detailed analysis of haemodynamic changes in the ICA using CFD technology can be used to predict treatment outcome for the follow-up of MMD patients. The main limitation of this study is that the

follow-up is relatively short to assess the vessel remodelling of ICA. Long-term follow-up is required as MMD is a chronic and gradually progressive disorder.

(IV) To effectively reduce the occurrence of brain ischemia, Circle of Willis is an important structure in creating redundancies or collaterals in the cerebral circulation. CFD technology was applied to assess the haemodynamic changes at ICA of haemorrhagic MMD with complete circle of Willis after bypass surgery in Chapter 7. Pressure drop and volume flow rate were used for computational haemodynamic analysis. The decrease of pressure drop and flow at ICA on the surgical side is thought to be associated with lowering haemodynamic burden and reducing re-bleeding risks, thus improving clinical outcomes. Whereas the contralateral ICA shows a counteractive increase of pressure drop through the circle of Willis.

8.2 Future directions

A number of key questions arise from the studies in this thesis. These include:

(I) Further well-designed prospective study is needed to confirm the utility of intraoperative perfusion weighted imaging in predicting the risks of postoperative CHS. The sensitivity and specificity of intraoperative PWI for early diagnosing CHS should be estimated in comparison with the PET or SPECT studies which were regarded as the ‘gold standard’ at present. The cut-off value of intraoperative regional cerebral blood flow to predict CHS could be determined for the potential clinical use. The cost-effectiveness of the use of intraoperative MRI in bypass surgery for MMD should also be studied in consideration of the extremely high cost.

(II) To elucidate the nature of vessel-remodelling of both ICA and the bypass graft, further investigations of a larger case series with a longer follow-up will be required in the future.

The detailed analysis of blood flow patterns at anastomotic junctions, including blood flow, pressure distribution, wall shear stress and flow resistance should be analysed to avoid graft failure of bypass. The correlation of vessel remodelling features with angiographic assessment as well as neurological outcome will provide more evidence of surgical efficacy. The interaction between the bypass graft and ICA, as well as the combined mass effect of bypass and ICA after surgery should also be investigated.

(III) Haemodynamic monitoring in the circle of Willis is vital to ameliorate the progression of MMD. Detailed haemodynamic characters of the arteries within the circle of Willis could aid in exploring the mechanisms of the revascularization surgery for treating MMD. In addition, sub-group haemodynamic analysis should be performed according to different configurations of circle of Willis (with or without intact arterial circle), as well as different clinical presentations (either ischemic or haemorrhagic type).

(IV) The revascularization surgery should be planned via the virtual simulation by using patient-specific CFD models before surgery in order to enable the design of a more optimal graft anastomotic geometry and the best treatment in a particular case. Automatic segmentation and post-processing of PWI and CFD analysis which is less operator dependent will facilitate their use in clinic, particularly in the follow-up observation.

References

[1] Suzuki J, Takaku A. Cerebrovascular "moyamoya" disease. Disease showing abnormal net-like vessels in base of brain. Arch Neurol. 1969 Mar;20(3):288-99.

[2] Mai JK, Paxinos G. The Human Nervous System 2012.

[3] Bergman R, Afifi A, Miyauchi R. Illustrated Encyclopedia of Human Anatomic Variation: Opus II: Cardiovascular System: Arteries: Head, Neck, and Thorax 2005.

[4] Suzuki J, Kodama N. Moyamoya disease--a review. Stroke. 1983 Jan-Feb;14(1):104-9.

[5] Janda PH, Bellew JG, Veerappan V. Moyamoya disease: case report and literature review. J Am Osteopath Assoc. 2009 Oct;109(10):547-53.

[6] Lee JY, Kim SK, Cheon JE, Choi JW, Phi JH, Kim IO, et al. Posterior cerebral artery involvement in moyamoya disease: initial infarction and angle between PCA and basilar artery. Childs Nerv Syst. 2013 Dec;29(12):2263-9.

[7] Funaki T, Takahashi JC, Takagi Y, Yoshida K, Araki Y, Kikuchi T, et al. Impact of posterior cerebral artery involvement on long-term clinical and social outcome of pediatric moyamoya disease. J Neurosurg Pediatr. 2013 Dec;12(6):626-32.

[8] Kaku Y, Morioka M, Ohmori Y, Kawano T, Kai Y, Fukuoka H, et al. Outer-diameter narrowing of the internal carotid and middle cerebral arteries in moyamoya disease detected on 3D constructive interference in steady-state MR image: is arterial constrictive remodeling a major pathogenesis? Acta Neurochir (Wien). 2012 Dec;154(12):2151-7.

[9] Kuriyama S, Kusaka Y, Fujimura M, Wakai K, Tamakoshi A, Hashimoto S, et al. Prevalence and clinicoepidemiological features of moyamoya disease in Japan: findings from a nationwide epidemiological survey. Stroke; a journal of cerebral circulation. 2008 Jan;39(1):42-7.

[10] Uchino K, Johnston SC, Becker KJ, Tirschwell DL. Moyamoya disease in Washington State and California. Neurology. 2005 Sep 27;65(6):956-8.

[11] Kainth D, Chaudhry SA, Kainth H, Suri FK, Qureshi AI. Epidemiological and Clinical Features of Moyamoya Disease in the USA. Neuroepidemiology. 2013;40(4):282-7.

[12] Miao W, Zhao PL, Zhang YS, Liu HY, Chang Y, Ma J, et al. Epidemiological and clinical features of Moyamoya disease in Nanjing, China. Clin Neurol Neurosurg. 2010 Apr;112(3):199-203.

[13] Chen PC, Yang SH, Chien KL, Tsai IJ, Kuo MF. Epidemiology of Moyamoya Disease in Taiwan A Nationwide Population-Based Study. Stroke. 2014 May;45(5):1258-63.

[14] Kim T, Lee H, Bang JS, Kwon OK, Hwang G, Oh CW. Epidemiology of moyamoya disease in Korea: Based on national health insurance service data. Journal of Korean Neurosurgical Society. 2015;57(6):390-5.

[15] Baba T, Houkin K, Kuroda S. Novel epidemiological features of moyamoya disease. J Neurol Neurosurg Psychiatry. 2008 Aug;79(8):900-4.

[16] Graham JF, Matoba A. A survey of Moyamoya disease in Hawaii. Clinical Neurology and Neurosurgery. 1997;99(SUPPL. 2):S31-S5.

[17] Hung CC, Tu YK, Su CF, Lin LS, Shih CJ. Epidemiological study of moyamoya disease in Taiwan. Clin Neurol Neurosurg. 1997 Oct;99 Suppl 2:S23-5.

[18] Fukui M. Guidelines for the diagnosis and treatment of spontaneous occlusion of the circle of Willis ('moyamoya' disease). Research Committee on Spontaneous Occlusion of the Circle of Willis (Moyamoya Disease) of the Ministry of Health and Welfare, Japan. Clin Neurol Neurosurg. 1997 Oct;99 Suppl 2:S238-40.

[19] Goyal MS, Hallemeier CL, Zipfel GJ, Rich KM, Grubb Jr RL, Chicoine MR, et al. Clinical features and outcome in North American adults with idiopathic basal arterial occlusive disease without moyamoya collaterals. Neurosurgery. 2010;67(2):278-85.

[20] Kraemer M, Heienbrok W, Berlit P. Moyamoya disease in Europeans. Stroke. 2008;39(12):3193-200.

[21] Chiu D, Shedden P, Bratina P, Grotta JC. Clinical features of Moyamoya disease in the United States. Stroke. 1998;29(7):1347-51.

[22] Starke RM, Komotar RJ, Hickman ZL, Paz YE, Pugliese AG, Otten ML, et al. Clinical features, surgical treatment, and long-term outcome in adult patients with moyamoya disease: Clinical article. Journal of Neurosurgery. 2009;111(5):936-42.

[23] Lin RH, Xie ZY, Zhang JF, Xu HW, Su H, Tan XR, et al. Clinical and Immunopathological Features of Moyamoya Disease. Plos One. 2012 Apr 27;7(4).

[24] Kuroda S, Houkin K. Moyamoya disease: current concepts and future perspectives. The Lancet Neurology. 2008;7(11):1056-66.

[25] Roder C, Nayak NR, Khan N, Tatagiba M, Inoue I, Krischek B. Genetics of Moyamoya disease. Journal of Human Genetics. 2010;55(11):711-6.

[26] Scott RM, Smith ER. Moyamoya disease and moyamoya syndrome. New England Journal of Medicine. 2009;360(12):1226-37.

[27] Mukawa M, Nariai T, Matsushima Y, Ohno K. Clinical features of familial juvenile cases of moyamoya disease: analysis of patients treated in a single institute over a 28-year period. J Neurosurg-Pediatr. 2013 Aug;12(2):175-80.

[28] Papavasiliou A, Bazigou-Fotopoulou H, Ikeda H. Familial Moyamoya disease in two European children. Journal of Child Neurology. 2007;22(12):1371-6.

[29] Han C, Feng H, Han YQ, Liu WW, Zhang ZS, Yang WZ, et al. Prospective screening of family members with moyamoya disease patients. PLoS ONE. 2014;9(2).

[30] Inoue TK, Ikezaki K, Sasazuki T, Matsushima T, Fukui M. Analysis of class II genes of human leukocyte antigen in patients with Moyamoya disease. Clinical Neurology and Neurosurgery. 1997 Oct;99:S234-S7.

[31] Han H, Pyo CW, Yoo DS, Huh PW, Cho KS, Kim DS. Associations of Moyamoya patients with HLA class I and class II alleles in the Korean population. J Korean Med Sci. 2003 Dec;18(6):876-80.

[32] Inoue TK, Ikezaki K, Sasazuki T, Ono T, Kamikawaji N, Matsushima T, et al. DNA typing of HLA in the patients with moyamoya disease. Jpn J Hum Genet. 1997 Dec;42(4):507-15.

[33] Hong SH, Wang KC, Kim SK, Cho BK, Park MH. Association of HLA-DR and -DQ Genes with Familial Moyamoya Disease in Koreans. Journal of Korean Neurosurgical Society. 2009 Dec;46(6):558-63.

[34] Ikeda H, Sasaki T, Yoshimoto T, Fukui M, Arinami T. Mapping of a familial moyamoya disease gene to chromosome 3p24.2-p26. Am J Hum Genet. 1999 Feb;64(2):533-7.

[35] Inoue TK, Ikezaki K, Sasazuki T, Matsushima T, Fukui M. Linkage analysis of moyamoya disease on chromosome 6. J Child Neurol. 2000 Mar;15(3):179-82.

[36] Yamauchi T, Tada M, Houkin K, Tanaka T, Nakamura Y, Kuroda S, et al. Linkage of familial moyamoya disease (spontaneous occlusion of the circle of Willis) to chromosome 17q25. Stroke. 2000 Apr;31(4):930-5.

[37] Kang HS, Kim SK, Cho BK, Kim YY, Hwang YS, Wang KC. Single nucleotide polymorphisms of tissue inhibitor of metalloproteinase genes in familial moyamoya disease. Neurosurgery. 2006 Jun;58(6):1074-80; discussion -80.

[38] Paez MT, Yamamoto T. Single nucleotide polymorphisms of tissue inhibitor of metalloproteinase genes in familial moyamoya disease. Neurosurgery. 2007 Mar;60(3):E582; author reply E.

[39] Liu W, Hashikata H, Inoue K, Matsuura N, Mineharu Y, Kobayashi H, et al. A rare Asian founder polymorphism of Raptor may explain the high prevalence of Moyamoya disease among East Asians and its low prevalence among Caucasians. Environ Health Prev Med. 2010 Mar;15(2):94-104.

[40] Sakurai K, Horiuchi Y, Ikeda H, Ikezaki K, Yoshimoto T, Fukui M, et al. A novel susceptibility locus for moyamoya disease on chromosome 8q23. J Hum Genet. 2004;49(5):278-81.

[41] Guo DC, Papke CL, Tran-Fadulu V, Regalado ES, Avidan N, Johnson RJ, et al. Mutations in smooth muscle alpha-actin (ACTA2) cause coronary artery disease, stroke, and

Moyamoya disease, along with thoracic aortic disease. Am J Hum Genet. 2009 May;84(5):617-27.

[42] Roder C, Peters V, Kasuya H, Nishizawa T, Takehara Y, Berg D, et al. Polymorphisms in TGFB1 and PDGFRB are associated with Moyamoya disease in European patients. Acta Neurochir (Wien). 2010 Dec;152(12):2153-60.

[43] Liu WY, Morito D, Takashima S, Mineharu Y, Kobayashi H, Hitomi T, et al. Identification of RNF213 as a Susceptibility Gene for Moyamoya Disease and Its Possible Role in Vascular Development. Plos One. 2011 Jul 20;6(7).

[44] Liu WY, Hitomi T, Kobayashi H, Harada KH, Koizumi A. Distribution of Moyamoya Disease Susceptibility Polymorphism p.R4810K in RNF213 in East and Southeast Asian Populations. Neurologia Medico-Chirurgica. 2012 May;52(5):299-303.

[45] Miyatake S, Miyake N, Touho H, Nishimura-Tadaki A, Kondo Y, Okada I, et al. Homozygous c.14576G>A variant of RNF213 predicts early-onset and severe form of moyamoya disease. Neurology. 2012;78(11):803-10.

[46] Wu ZY, Jiang HQ, Zhang L, Xu X, Zhang XJ, Kang ZH, et al. Molecular Analysis of RNF213 Gene for Moyamoya Disease in the Chinese Han Population. Plos One. 2012 Oct 23;7(10).

[47] Cecchi AC, Guo DC, Ren Z, Flynn K, Santos-Cortez RLP, Leal SM, et al. RNF213 Rare Variants in an Ethnically Diverse Population With Moyamoya Disease. Stroke. 2014 Nov;45(11):3200-7.

[48] Lee MJ, Chen YF, Fan PC, Wang KC, Wang K, Wang JY, et al. Mutation genotypes of RNF213 gene from moyamoya patients in Taiwan. Journal of the Neurological Sciences. 2015 Jun 15;353(1-2):161-5.

[49] Moteki Y, Onda H, Kasuya H, Yoneyama T, Okada Y, Hirota K, et al. Systematic Validation of RNF213 Coding Variants in Japanese Patients With Moyamoya Disease. J Am Heart Assoc. 2015 May;4(5).

[50] Walcott BP, Peterson RT. Zebrafish models of cerebrovascular disease. Journal of Cerebral Blood Flow and Metabolism. 2014 Apr;34(4):571-7.

[51] Ito A, Fujimura M, Niizuma K, Kanoke A, Sakata H, Morita-Fujimura Y, et al. Enhanced post-ischemic angiogenesis in mice lacking RNF213; A susceptibility gene for moyamoya disease. Brain Research. 2015;1594:310-20.

[52] Sonobe S, Fujimura M, Niizuma K, Fujimura T, Furudate S, Nishijima Y, et al. Increased vascular MMP-9 in mice lacking RNF213: moyamoya disease susceptibility gene. Neuroreport. 2014 Dec 17;25(18):1442-6.

[53] Miyatake S, Miyake N, Touho H, Nishimura-Tadaki A, Kondo Y, Okada I, et al. Homozygous c.14576G > A variant of RNF213 predicts early-onset and severe form of moyamoya disease. Neurology. 2012 Mar;78(11):803-10.

[54] Hitomi T, Habu T, Kobayashi H, Okuda H, Harada KH, Osafune K, et al. The moyamoya disease susceptibility variant RNF213 R4810K (rs112735431) induces genomic instability by mitotic abnormality. Biochem Bioph Res Co. 2013 Oct 4;439(4):419-26.

[55] Koizumi A, Kobayashi H, Liu WY, Fujii Y, Senevirathna STMLD, Nanayakkara S, et al. P.R4810K, a polymorphism of RNF213, the susceptibility gene for moyamoya disease, is associated with blood pressure. Environ Health Prev. 2013 Mar;18(2):121-9.

[56] Fujimura M, Sonobe S, Nishijima Y, Niizuma K, Sakata H, Kure S, et al. Genetics and Biomarkers of Moyamoya Disease: Significance of RNF213 as a Susceptibility Gene. J Stroke. 2014 May;16(2):65-72.

[57] Miyawaki S, Imai H, Shimizu M, Yagi S, Ono H, Nakatomi H, et al. Genetic Analysis of RNF213 c.14576G > A Variant in Nonatherosclerotic Quasi-Moyamoya Disease. J Stroke Cerebrovasc. 2015 May;24(5):1075-9.

[58] Yoshimoto T, Houkin K, Takahashi A, Abe H. Angiogenic factors in moyamoya disease. Stroke. 1996;27(12):2160-5.

[59] Kang HS, Moon YJ, Kim YY, Park WY, Park AK, Wang KC, et al. Smooth-muscle progenitor cells isolated from patients with moyamoya disease: novel experimental cell model. J Neurosurg. 2014 Feb;120(2):415-25.

[60] Masuda J, Ogata J, Yutani C. Smooth muscle cell proliferation and localization of macrophages and T cells in the occlusive intracranial major arteries in moyamoya disease. Stroke. 1993 Dec;24(12):1960-7.

[61] Yamamoto M, Aoyagi M, Fukai N, Matsushima Y, Yamamoto K. Differences in cellular responses to mitogens in arterial smooth muscle cells derived from patients with moyamoya disease. Stroke. 1998 Jun;29(6):1188-93.

[62] Reid AJ, Bhattacharjee MB, Regalado ES, Mlewicz AL, El-Hakam LM, Dauser RC, et al. Diffuse and uncontrolled vascular smooth muscle cell proliferation in rapidly progressing pediatric moyamoya disease Case report. J Neurosurg-Pediatr. 2010 Sep;6(3):244-9.

[63] Kang HS, Moon YJ, Kim YY, Park WY, Park AK, Wang KC, et al. Smooth-muscle progenitor cells isolated from patients with moyamoya disease: novel experimental cell model. Journal of Neurosurgery. 2014 Feb;120(2):415-25.

[64] Jung KH, Chu K, Lee ST, Park HK, Kim DH, Kim JH, et al. Circulating endothelial progenitor cells as a pathogenetic marker of moyamoya disease. J Cerebr Blood F Met. 2008 Nov;28(11):1795-803.

[65] Jung KH, Chu K, Lee ST, Park HK, Kim DH, Kim JH, et al. Circulating endothelial progenitor cells as a pathogenetic marker of moyamoya disease (vol 28, pg 1795, 2008). J Cerebr Blood F Met. 2009 Apr;29(4):871-.

[66] He J, Wang R, Zhang D, Zhang Y, Zhang Q, Zhao J. Expression of circulating vascular endothelial growth factor-antagonizing cytokines and vascular stabilizing factors prior to and following bypass surgery in patients with moyamoya disease. Exp Ther Med. 2014 Jul;8(1):302-8.

[67] Sakamoto S, Kiura Y, Yamasaki F, Shibukawa M, Ohba S, Shrestha P, et al. Expression of vascular endothelial growth factor in dura mater of patients with moyamoya disease. Neurosurg Rev. 2008 Jan;31(1):77-81; discussion

[68] Nanba R, Kuroda S, Ishikawa T, Houkin K, Iwasaki Y. Increased expression of hepatocyte growth factor in cerebrospinal fluid and intracranial artery in moyamoya disease. Stroke. 2004 Dec;35(12):2837-42.

[69] Brisset AC, Hao H, Camenzind E, Bacchetta M, Geinoz A, Sanchez JC, et al. Intimal smooth muscle cells of porcine and human coronary artery express S100A4, a marker of the rhomboid phenotype in vitro. Circ Res. 2007 Apr 13;100(7):1055-62.

[70] Hsiung GY, Sotero de Menezes M. Moyamoya syndrome in a patient with congenital human immunodeficiency virus infection. J Child Neurol. 1999 Apr;14(4):268-70.

[71] Sharfstein SR, Ahmed S, Islam MQ, Najjar MI, Ratushny V. Case of moyamoya disease in a patient with advanced acquired immunodeficiency syndrome. J Stroke Cerebrovasc Dis. 2007 Nov-Dec;16(6):268-72.

[72] Sigdel TK, Shoemaker LD, Chen R, Li L, Butte AJ, Sarwal MM, et al. Immune response profiling identifies autoantibodies specific to Moyamoya patients. Orphanet J Rare Dis. 2013;8:45.

[73] Bonduel M, Hepner M, Sciuccati G, Torres AF, Tenembaum S. Prothrombotic disorders in children with moyamoya syndrome. Stroke. 2001 Aug;32(8):1786-92.

[74] Li H, Zhang ZS, Dong ZN, Ma MJ, Yang WZ, Han C, et al. Increased Thyroid Function and Elevated Thyroid Autoantibodies in Pediatric Patients With Moyamoya Disease A Case-Control Study. Stroke. 2011 Apr;42(4):1138-9.

[75] Ogawa K, Nagahiro S, Arakaki R, Ishimaru N, Kobayashi M, Hayashi Y. Anti-alpha-fodrin autoantibodies in moyamoya disease. Stroke. 2003 Dec;34(12):E244-E6.

[76] Kim JW, Kim SK, Wang KC, Kim HY, Jeoung D. SEREX identification of the autoantibodies that are prevalent in the cerebrospinal fluid of patients with moyamoya disease. Biotechnol Lett. 2004 Apr;26(7):585-8.

[77] Jeon JS, Ahn JH, Moon YJ, Cho WS, Son YJ, Kim SK, et al. Expression of cellular retinoic acid-binding protein-I (CRABP-I) in the cerebrospinal fluid of adult onset moyamoya disease and its association with clinical presentation and postoperative haemodynamic change. J Neurol Neurosur Ps. 2014 Jul;85(7):726-31.

[78] Kim SK, Yoo JI, Cho BK, Hong SJ, Kim YK, Moon JA, et al. Elevation of CRABP-I in the cerebrospinal fluid of patients with moyamoya disease. Stroke. 2003 Dec;34(12):2835-41.

[79] Aoki S, Hayashi N, Abe O, Shirouzu I, Ishigame K, Okubo T, et al. Radiation-induced arteritis: thickened wall with prominent enhancement on cranial MR images report of five cases and comparison with 18 cases of Moyamoya disease. Radiology. 2002 Jun;223(3):683-8.

[80] Desai SS, Paulino AC, Mai WY, Teh BS. Radiation-induced moyamoya syndrome. Int J Radiat Oncol Biol Phys. 2006 Jul 15;65(4):1222-7.

[81] Manion B, Sung WS. Radiation-induced moyamoya disease after childhood astrocytoma. J Clin Neurosci. 2011 Oct;18(10):1403-5.

[82] Kestle JR, Hoffman HJ, Mock AR. Moyamoya phenomenon after radiation for optic glioma. J Neurosurg. 1993 Jul;79(1):32-5.

[83] Serdaroglu A, Simsek F, Gucuyener K, Oguz A, Karadeniz C, Balibey M. Moyamoya syndrome after radiation therapy for optic pathway glioma: case report. J Child Neurol. 2000 Nov;15(11):765-7.

[84] Kondoh T, Morishita A, Kamei M, Okamura Y, Tamaki M, Kohmura E. Moyamoya syndrome after prophylactic cranial irradiation for acute lymphocytic leukemia. Pediatr Neurosurg. 2003 Nov;39(5):264-9.

[85] Ishikawa N, Tajima G, Yofune N, Nishimura S, Kobayashi M. Moyamoya syndrome after cranial irradiation for bone marrow transplantation in a patient with acute leukemia. Neuropediatrics. 2006 Dec;37(6):364-6.

[86] Kikuchi A, Maeda M, Hanada R, Okimoto Y, Ishimoto K, Kaneko T, et al. Moyamoya syndrome following childhood acute lymphoblastic leukemia. Pediatr Blood Cancer. 2007 Mar;48(3):268-72.

[87] Kansal R, Mahore A, Nadkarni T, Goel A. Fetal radiation exposure and moyamoya disease. J Clin Neurosci. 2010 Mar;17(3):406-7.

[88] Jimenez Caballero PE. Adult-onset Moyamoya disease in a patient with neurofibromatosis type 1. Neurologia. 2014 May 3.

[89] Hayashi K, Morofuji Y, Horie N, Izumo T. A Case of Neurofibromatosis Type 1 Complicated with Repeated Intracerebral Hemorrhage due to Quasi-Moyamoya Disease. J Stroke Cerebrovasc Dis. 2015 May;24(5):e109-13.

[90] Kawamura K, Jono M, Katsuragi M, Baba S, Shida K. A case of neurofibromatosis with occlusion of multiple cerebral artery, moyamoya phenomenon and scoliosis. No To Shinkei. 1994 Dec;46(12):1163-8.

[91] Vargiami E, Sapountzi E, Samakovitis D, Batzios S, Kyriazi M, Anastasiou A, et al. Moyamoya syndrome and neurofibromatosis type 1. Ital J Pediatr. 2014;40:59.

[92] Delvoye F, Herve D, Chabriat H, Mawet J. Moyamoya syndrome related to neurofibromatosis of type 1: a case report. Acta Neurol Belg. 2013 Dec;113(4):539-41.

[93] Lamas E, Diez Lobato R, Cabello A, Abad JM. Multiple intracranial arterial occlusions (moyamoya disease) in patients with neurofibromatosis. One case report with autopsy. Acta Neurochir (Wien). 1978;45(1-2):133-45.

[94] Duat-Rodriguez A, Carceller Lechon F, Lopez Pino MA, Rodriguez Fernandez C, Gonzalez-Gutierrez-Solana L. Neurofibromatosis type 1 associated with moyamoya syndrome in children. Pediatr Neurol. 2014 Jan;50(1):96-8.

[95] Drew JM, Scott JA, Chua GT. General case of the day. Moyamoya syndrome in a child with sickle cell disease. Radiographics. 1993 Mar;13(2):483-4.

[96] Hogan AM, Kirkham FJ, Isaacs EB, Wade AM, Vargha-Khadem F. Intellectual decline in children with moyamoya and sickle cell anaemia. Dev Med Child Neurol. 2005 Dec;47(12):824-9.

[97] Komur M, Unal S, Okuyaz C, Ozgur A. Moyamoya syndrome associated with sickle cell trait in a child. Brain Dev. 2014 Jun;36(6):545-7.

[98] Soares D, Bullock R, Ali S. Moyamoya syndrome in sickle cell anaemia: a cause of recurrent stroke. BMJ Case Rep. 2014;2014.

[99] Agrawal R, Berube C, Steinberg G, George TI. Moyamoya syndrome with sickle cell trait. Int J Lab Hematol. 2013 Oct;35(5):e8-9.

[100] Lo Presti A, Weil AG, Fallah A, Peterson EC, Niazi TN, Bhatia S. Treatment of a cerebral pial arteriovenous fistula in a patient with sickle cell disease-related moyamoya syndrome: case report. J Neurosurg Pediatr. 2015 Aug;16(2):207-11.

[101] See AP, Ropper AE, Underberg DL, Robertson RL, Scott RM, Smith ER. Down syndrome and moyamoya: clinical presentation and surgical management. J Neurosurg Pediatr. 2015 Jul;16(1):58-63.

[102] Chong PF, Ogata R, Kobayashi H, Koizumi A, Kira R. Early onset of moyamoya syndrome in a Down syndrome patient with the genetic variant RNF213 p.R4810K. Brain Dev. 2014 Dec 26.

[103] Takanashi J, Sugita K, Ishii M, Iai M, Goto M, Tanabe Y, et al. A girl with Down syndrome complicated by moyamoya disease and symptomatic atlanto-axial instability. No To Hattatsu. 1993 May;25(3):248-52.

[104] Hernandez Ch M, Huete LI, Concha GM, Mendez CJ, Sanchez DN, Cuellar GM, et al. Moyamoya disease in a girl with Down syndrome. Report of one case. Rev Med Chil. 2009 Aug;137(8):1066-70.

[105] Vimalesvaran S, Nachiappan N, Sithamparanathan Y. Moyamoya syndrome in a Malaysian child with Down syndrome. J Paediatr Child Health. 2013 Oct;49(10):865-7; quiz 7-8.

[106] Kainth DS, Chaudhry SA, Kainth HS, Suri FK, Qureshi AI. Prevalence and characteristics of concurrent down syndrome in patients with moyamoya disease. Neurosurgery. 2013 Feb;72(2):210-5; discussion 5.

[107] Troll S, Dietrich W, Robke M, Bar I, Erbguth FJ. Moyamoya disease associated with Grave's disease. J Neurol. 2006 May;253:44-.

[108] Ajimi Y, Uchida K, Kawase T, Toya S. A case of Turner's syndrome associated with moyamoya disease. No Shinkei Geka. 1992 Sep;20(9):1021-4.

[109] Manjila S, Miller BR, Rao-Frisch A, Otvos B, Mitchell A, Bambakidis NC, et al. Moyamoya disease associated with asymptomatic mosaic Turner syndrome: a rare cause of hemorrhagic stroke. J Stroke Cerebrovasc Dis. 2014 May-Jun;23(5):1242-4.

[110] Lo FS, Wang CJ, Wong MC, Lee NC. Moyamoya disease in two patients with Noonan-like syndrome with loose anagen hair. Am J Med Genet A. 2015 Jun;167(6):1285-8.

[111] Hosoda Y, Ikeda E, Hirose S. Histopathological studies on spontaneous occlusion of the circle of Willis (cerebrovascular Moyamoya disease). Clinical Neurology and Neurosurgery. 1997 Oct;99:S203-S8.

[112] Huang APH, Tu YK. Progressive PCA steno-occlusive changes after revascularization for moyamoya disease: A neglected phenomenon. Neurosurgery. 2010;67(6):E1865-E6.

[113] Lee JY, Kim SK, Cheon JE, Choi JW, Phi JH, Kim IO, et al. Posterior cerebral artery involvement in moyamoya disease: Initial infarction and angle between PCA and basilar artery. Child's Nervous System. 2013;29(12):2263-9.

[114] Mugikura S, Higano S, Shirane R, Fujimura M, Shimanuki Y, Takahashi S. Posterior Circulation and High Prevalence of Ischemic Stroke among Young Pediatric Patients with

Moyamoya Disease: Evidence of Angiography-Based Differences by Age at Diagnosis. American Journal of Neuroradiology. 2011 Jan;32(1):192-8.

[115] Lee JY, Kim SK, Phi JH, Wang KC. Posterior cerebral artery insufficiency in pediatric moyamoya disease. Journal of Korean Neurosurgical Society. 2015;57(6):436-9.

[116] Takagi Y, Kikuta K, Nozaki K, Hashimoto N. Histological features of middle cerebral arteries from patients treated for Moyamoya disease. Neurol Med Chir (Tokyo). 2007 Jan;47(1):1-4.

[117] Takekawa Y, Umezawa T, Ueno Y, Sawada T, Kobayashi M. Pathological and immunohistochemical findings of an autopsy case of adult moyamoya disease. Neuropathology. 2004;24(3):236-42.

[118] Weinberg DG, Arnaout OM, Rahme RJ, Aoun SG, Batjer HH, Bendok BR. Moyamoya disease: a review of histopathology, biochemistry, and genetics. Neurosurg Focus. 2011 Jun;30(6):E20.

[119] Yamashita M, Oka K, Tanaka K. Histopathology of the brain vascular network in moyamoya disease. Stroke. 1983 Jan-Feb;14(1):50-8.

[120] Fujimura M, Tominaga T. Lessons learned from moyamoya disease: Outcome of direct/indirect revascularization surgery for 150 affected hemispheres. Neurologia Medico-Chirurgica. 2012;52(5):327-32.

[121] Fujimura M, Tominaga T. Diagnosis of Moyamoya Disease: International Standard and Regional Differences. Neurologia Medico-Chirurgica. 2015 Mar;55(3):189-93.

[122] Kim JE, Jeon JS. An update on the diagnosis and treatment of adult Moyamoya disease taking into consideration controversial issues. Neurol Res. 2014 May;36(5):407-16.

[123] Research Committee on the P, Treatment of Spontaneous Occlusion of the Circle of W, Health Labour Sciences Research Grant for Research on Measures for Infractable D. Guidelines for diagnosis and treatment of moyamoya disease (spontaneous occlusion of the circle of Willis). Neurol Med Chir (Tokyo). 2012;52(5):245-66.

[124] Houkin K, Aoki T, Takahashi A, Abe H. Diagnosis of moyamoya disease with magnetic resonance angiography. Stroke; a journal of cerebral circulation. 1994 Nov;25(11):2159-64.

[125] Czabanka M, Pena-Tapia P, Schubert GA, Heppner FL, Martus P, Horn P, et al. Proposal for a new grading of Moyamoya disease in adult patients. Cerebrovasc Dis. 2011;32(1):41-50.

[126] Yoon HK, Shin HJ, Chang YW. "Ivy sign" in childhood moyamoya disease: Depiction on FLAIR and contrast-enhanced T1-weighted MR images. Radiology. 2002;223(2):384-9.

[127] Seo KD, Suh SH, Kim YB, Kim JH, Ahn SJ, Kim DS, et al. Ivy Sign on Fluid-Attenuated Inversion Recovery Images in Moyamoya Disease: Correlation with Clinical Severity and Old Brain Lesions. Yonsei Med J. 2015 Sep;56(5):1322-7.

[128] Sawada T, Yamamoto A, Miki Y, Kikuta K, Okada T, Kanagaki M, et al. Diagnosis of moyamoya disease using 3-T MRI and MRA: value of cisternal moyamoya vessels. Neuroradiology. 2012 Oct;54(10):1089-97.

[129] Horie N, Morikawa M, Nozaki A, Hayashi K, Suyama K, Nagata I. "Brush Sign" on susceptibility-weighted MR imaging indicates the severity of moyamoya disease. AJNR Am J Neuroradiol. 2011 Oct;32(9):1697-702.

[130] Uchino H, Ito M, Fujima N, Kazumata K, Yamazaki K, Nakayama N, et al. A novel application of four-dimensional magnetic resonance angiography using an arterial spin labeling technique for noninvasive diagnosis of Moyamoya disease. Clin Neurol Neurosurg. 2015 Jul 7;137:105-11.

[131] Smith ER, Scott RM. Spontaneous occlusion of the circle of Willis in children: pediatric moyamoya summary with proposed evidence-based practice guidelines A review. J Neurosurg-Pediatr. 2012 Apr;9(4):353-60.

[132] Schubert GA, Biermann P, Weiss C, Seiz M, Vajkoczy P, Schmiedek P, et al. Risk profile in Extracranial/intracranial bypass surgery - The role of antiplatelet agents, disease pathology, and surgical technique in 168 direct revascularization procedures. World Neurosurgery. 2014;82(5):672-7.

[133] Kim JE, Kim KM, Kim JG, Kang HS, Bang JS, Son YJ, et al. Clinical features of adult moyamoya disease with special reference to the diagnosis. Neurol Med Chir (Tokyo). 2012;52(5):311-7.

[134] Scott RM, Smith ER. Moyamoya disease and moyamoya syndrome. N Engl J Med. 2009 Mar 19;360(12):1226-37.

[135] Guey S, Tournier-Lasserve E, Herve D, Kossorotoff M. Moyamoya disease and syndromes: from genetics to clinical management. Appl Clin Genet. 2015;8:49-68.

[136] Gross BA, Thomas AJ, Frerichs KU. Endovascular treatment of symptomatic moyamoya. Neurosurg Rev. 2014 Oct;37(4):579-83.

[137] Khan N, Dodd R, Marks MP, Bell-Stephens T, Vavao J, Steinberg GK. Failure of Primary Percutaneous Angioplasty and Stenting in the Prevention of Ischemia in Moyamoya Angiopathy. Cerebrovasc Dis. 2011;31(2):147-53.

[138] Eicker S, Etminan N, Turowski B, Steiger HJ, Hanggi D. Intracranial carotid artery stent placement causes delayed severe intracranial haemorrhage in a patient with moyamoya disease. Journal of Neurointerventional Surgery. 2011 Jun;3(2):160-2.

[139] Kornblihtt LI, Cocorullo S, Miranda C, Lylyk P, Heller PG, Molinas FC. Moyamoya syndrome in an adolescent with essential thrombocythemia: successful intracranial carotid stent placement. Stroke. 2005 Aug;36(8):E71-3.

[140] Santirso D, Oliva P, Gonzalez M, Murias E, Vega P, Gil A, et al. Intracranial stent placement in a patient with moyamoya disease. J Neurol. 2012 Jan;259(1):170-1.

[141] Natarajan SK, Karmon Y, Tawk RG, Hauck EF, Hopkins LN, Siddiqui AH, et al. Endovascular treatment of patients with intracranial stenosis with moyamoya-type collaterals. J Neurointerv Surg. 2011 Dec 1;3(4):369-74.

[142] Chen Y, Dai D, Fang Y, Yang P, Huang Q, Zhao W, et al. Endovascular Treatment of Ruptured Large or Wide-Neck Basilar Tip Aneurysms Associated with Moyamoya Disease Using the Stent-Assisted Coil Technique. J Stroke Cerebrovasc Dis. 2015 Jul 24.

[143] Bechan RS, van Rooij WJ. Endovascular treatment of a ruptured flow aneurysm of the heubner artery as part of a moyamoya collateral network in a young patient with an occluded middle cerebral artery. Interv Neuroradiol. 2014 Dec;20(6):791-5.

[144] Amin-Hanjani S, Goodin S, Charbel FT, Alaraj A. Resolution of bilateral moyamoya associated collateral vessel aneurysms: Rationale for endovascular versus surgical intervention. Surg Neurol Int. 2014;5(Suppl 4):S155-60.

[145] Yu JL, Wang HL, Xu K, Li Y, Luo Q. Endovascular treatment of intracranial aneurysms associated with moyamoya disease or moyamoya syndrome. Interv Neuroradiol. 2010 Sep;16(3):240-8.

[146] Yang S, Yu JL, Wang HL, Wang B, Luo Q. Endovascular embolization of distal anterior choroidal artery aneurysms associated with moyamoya disease. A report of two cases and a literature review. Interv Neuroradiol. 2010 Dec;16(4):433-41.

[147] Kim SH, Kwon OK, Jung CK, Kang HS, Oh CW, Han MH, et al. Endovascular treatment of ruptured aneurysms or pseudoaneurysms on the collateral vessels in patients with moyamoya disease. Neurosurgery. 2009 Nov;65(5):1000-4; discussion 4.

[148] Nishio A, Hara M, Otsuka Y, Tsuruno T, Murata T. Endovascular treatment of posterior cerebral aneurysm associated with Moyamoya disease. J Neuroradiol. 2004 Jan;31(1):60-2.

[149] Murakami K, Midorikawa H, Takahashi N, Suzuki Y, Nomura H, Nishijima M. [Endovascular treatment of a ruptured aneurysm associated with unilateral moyamoya disease]. No Shinkei Geka. 2004 Feb;32(2):167-71.

[150] Arita K, Kurisu K, Ohba S, Shibukawa M, Kiura H, Sakamoto S, et al. Endovascular treatment of basilar tip aneurysms associated with moyamoya disease. Neuroradiology. 2003 Jul;45(7):441-4.

[151] Massoud TF, Guglielmi G, Vinuela F, Duckwiler GR. Saccular aneurysms in moyamoya disease: endovascular treatment using electrically detachable coils. Surg Neurol. 1994 Jun;41(6):462-7.

[152] Arias EJ, Derdeyn CP, Dacey RG, Zipfel GJ. Advances and surgical considerations in the treatment of moyamoya disease. Neurosurgery. 2014;74(2 SUPPL.):S116-S25.

[153] Donaghy RM, Yasargil G. Microangeional surgery and its techniques. Prog Brain Res. 1968;30:263-7.

[154] Group TEIBS. Failure of extracranial-intracranial arterial bypass to reduce the risk of ischemic stroke. Results of an international randomized trial. The EC/IC Bypass Study Group. N Engl J Med. 1985 Nov 7;313(19):1191-200.

[155] Powers WJ, Clarke WR, Grubb RL, Jr., Videen TO, Adams HP, Jr., Derdeyn CP, et al. Extracranial-intracranial bypass surgery for stroke prevention in hemodynamic cerebral ischemia: the Carotid Occlusion Surgery Study randomized trial. JAMA. 2011 Nov 9;306(18):1983-92.

[156] Roach ES, Golomb MR, Adams R, Biller J, Daniels S, Deveber G, et al. Management of stroke in infants and children: a scientific statement from a Special Writing Group of the American Heart Association Stroke Council and the Council on Cardiovascular Disease in the Young. Stroke. 2008 Sep;39(9):2644-91.

[157] Xu B, Song DL, Mao Y, Gu YX, Xu H, Liao YJ, et al. Superficial temporal artery-middle cerebral artery bypass combined with encephalo-duro-myo-synangiosis in treating moyamoya disease: surgical techniques, indications and midterm follow-up results. Chinese medical journal. 2012 Dec;125(24):4398-405.

[158] Newell DW, Vilela MD, Sekhar LN, Tabrizi P, Spetzler RF. Superficial temporal artery to middle cerebral artery bypass. Neurosurgery. 2004;54(6):1441-9.

[159] Ishikawa T, Kamiyama H, Kuroda S, Yasuda H, Nakayama N, Takizawa K. Simultaneous superficial temporal artery to middle cerebral or anterior cerebral artery bypass with pan-synangiosis for Moyamoya disease covering both anterior and middle cerebral artery territories. Neurol Med Chir (Tokyo). 2006 Sep;46(9):462-8.

[160] Kawashima A, Kawamata T, Yamaguchi K, Hori T, Okada Y. Successful superficial temporal artery-anterior cerebral artery direct bypass using a long graft for moyamoya disease: technical note. Neurosurgery. 2010 Sep;67(3 Suppl Operative):ons145-9; discussion ons9.

[161] Kuroda S, Houkin K. Bypass surgery for moyamoya disease: concept and essence of sugical techniques. Neurol Med Chir (Tokyo). 2012;52(5):287-94.

[162] Hayashi T, Shirane R, Tominaga T. Additional surgery for postoperative ischemic symptoms in patients with moyamoya disease: the effectiveness of occipital artery-posterior cerebral artery bypass with an indirect procedure: technical case report. Neurosurgery. 2009 Jan;64(1):E195-6; discussion E6.

[163] Pandey P, Steinberg GK. Neurosurgical Advances in the Treatment of Moyamoya Disease. Stroke. 2011 Nov;42(11):3304-10.

[164] Horiuchi T, Kusano Y, Asanuma M, Hongo K. Posterior auricular artery-middle cerebral artery bypass for additional surgery of moyamoya disease. Acta Neurochir (Wien). 2012 Mar;154(3):455-6.

[165] Tokugawa J, Naka Y, Kudo K, Iimura K, Esaki T, Yamamoto T, et al. Posterior Auricular Artery-Middle Cerebral Artery Bypass: A Rare Superficial Temporal Artery Variant with Well-developed Posterior Auricular Artery-Case Report. Neurologia Medico-Chirurgica. 2014 Oct;54(10):841-4.

[166] Germans MR, Regli L. Posterior auricular artery as an alternative donor vessel for extracranial-intracranial bypass surgery. Acta Neurochirurgica. 2014 Nov;156(11):2095-101.

[167] Roh SW, Ahn JS, Sung HY, Jung YJ, Kwun BD, Kim CJ. Extracranial-intracranial bypass surgery using a radial artery interposition graft for cerebrovascular diseases. J Korean Neurosurg Soc. 2011 Sep;50(3):185-90.

[168] Bisson EF, Visioni AJ, Tranmer B, Horgan MA. External carotid artery to middle cerebral artery bypass with the saphenous vein graft. Neurosurgery. 2008 Jun;62(6 Suppl 3):1419-24.

[169] Zipfel GJ, Fox DJ, Jr., Rivet DJ. Moyamoya disease in adults: the role of cerebral revascularization. Skull Base. 2005 Feb;15(1):27-41.

[170] Starke RM, Komotar RJ, Connolly ES. Optimal surgical treatment for moyamoya disease in adults: direct versus indirect bypass. Neurosurg Focus. 2009 Apr;26(4):E8.

[171] Kim DS, Huh PW, Kim HS, Kim IS, Choi S, Mok JH, et al. Surgical treatment of moyamoya disease in adults: combined direct and indirect vs. indirect bypass surgery. Neurol Med Chir (Tokyo). 2012;52(5):333-8.

[172] Oliveira RS, Amato MC, Simao GN, Abud DG, Avidago EB, Specian CM, et al. Effect of multiple cranial burr hole surgery on prevention of recurrent ischemic attacks in children with moyamoya disease. Neuropediatrics. 2009 Dec;40(6):260-4.

[173] Baaj AA, Agazzi S, Sayed ZA, Toledo M, Spetzler RF, van Loveren H. Surgical management of moyamoya disease: a review. Neurosurg Focus. 2009 Apr;26(4):E7.

[174] Saito N, Imai H. Insights on the revascularization mechanism for treatment of Moyamoya disease based on the histopathologic concept of angiogenesis and arteriogenesis. World Neurosurg. 2011 Feb;75(2):204-5.

[175] Nakamura M, Imai H, Konno K, Kubota C, Seki K, Puentes S, et al. Experimental investigation of encephalomyosynangiosis using gyrencephalic brain of the miniature pig: histopathological evaluation of dynamic reconstruction of vessels for functional anastomosis Laboratory investigation. J Neurosurg-Pediatr. 2009 Jun;3(6):488-95.

[176] McLaughlin N, Martin NA. Effectiveness of Burr Holes for Indirect Revascularization in Patients with Moyamoya Disease-A Review of the Literature. World Neurosurgery. 2014 Jan;81(1):91-8.

[177] Thines L, Petyt G, Aguettaz P, Bodenant M, Himpens FX, Lenci H, et al. Surgical management of Moyamoya disease and syndrome: Current concepts and personal experience. Rev Neurol (Paris). 2015 Jan;171(1):31-44.

[178] Ishii K, Fujiki M, Kobayashi H. Invited article: surgical management of Moyamoya disease. Turk Neurosurg. 2008 Apr;18(2):107-13.

[179] Houkin K, Kuroda S, Ishikawa T, Abe H. Neovascularization (angiogenesis) after revascularization in moyamoya disease. Which technique is most useful for moyamoya disease? Acta Neurochir (Wien). 2000;142(3):269-76.

[180] Li Y, Cikla U, Baggott C, Yilmaz T, Chao C, Baskaya MK. Surgical treatment of adult moyamoya disease with combined STA-MCA bypass and EDAS: demonstration of technique in video presentation. Turk Neurosurg. 2015;25(1):126-31.

[181] Starke RM, Komotar RJ, Hickman ZL, Paz YE, Pugliese AG, Otten ML, et al. Clinical features, surgical treatment, and long-term outcome in adult patients with moyamoya disease. Clinical article. J Neurosurg. 2009 Nov;111(5):936-42.

[182] Bao XY, Duan L, Li DS, Yang WZ, Sun WJ, Zhang ZS, et al. Clinical features, surgical treatment and long-term outcome in adult patients with Moyamoya disease in China. Cerebrovasc Dis. 2012;34(4):305-13.

[183] Jiang H, Ni W, Xu B, Lei Y, Tian Y, Xu F, et al. Outcome in adult patients with hemorrhagic moyamoya disease after combined extracranial-intracranial bypass. J Neurosurg. 2014 Nov;121(5):1048-55.

[184] Matsushima T, Inoue T, Suzuki SO, Fujii K, Fukui M, Hasuo K. Surgical treatment of moyamoya disease in pediatric patients--comparison between the results of indirect and direct revascularization procedures. Neurosurgery. 1992 Sep;31(3):401-5.

[185] Kronenburg A, Braun KP, van der Zwan A, Klijn CJ. Recent advances in moyamoya disease: pathophysiology and treatment. Curr Neurol Neurosci Rep. 2014 Jan;14(1):423.

[186] Fung LWE, Thompson D, Ganesan V. Revascularisation surgery for paediatric moyamoya: A review of the literature. Child's Nervous System. 2005;21(5):358-64.

[187] Kazumata K, Ito M, Tokairin K, Ito Y, Houkin K, Nakayama N, et al. The frequency of postoperative stroke in moyamoya disease following combined revascularization: a single-university series and systematic review. J Neurosurg. 2014 Aug;121(2):432-40.

[188] Amin-Hanjani S, Singh A, Rifai H, Thulborn KR, Alaraj A, Aletich V, et al. Combined direct and indirect bypass for moyamoya: quantitative assessment of direct bypass flow over time. Neurosurgery. 2013 Dec;73(6):962-7; discussion 7-8.

[189] Langer DJ, Vajkoczy P. ELANA: Excimer laser-assisted nonocclusive anastomosis for extracranial-to-intracranial and intracranial-to-intracranial bypass: A review. Skull Base-Interd Ap. 2005 Aug;15(3):191-205.

[190] van Doormaal TPC, van der Zwan A, van der Tweel I, Verdaasdonk R, Verweij BH, Regli L, et al. Optimization of the Excimer Laser Assisted Non-Occlusive Anastomosis (ELANA) Flap Retrieval Rate. Laser Surg Med. 2010 Jul;42(5):418-24.

[191] Streefkerk HJ, Bremmer JP, Tulleken CA. Extracranial-intracranial bypass - The ELANA technique: high flow revascularization of the brain. Act Neur S. 2005;94:143-8.

[192] Langer DJ, Vajkoczy P, Chakraborty S, Tymianski M, Amin-Hanjani S, Charbel FT, et al. Final Results of the ELANA FDA-IDE Study on High Flow Cerebral Bypasses for Surgical Treatment of Anterior Circulation Aneurysms. Neurosurgery. 2012 Aug;71(2):E551-E.

[193] van Doormaal TPC, van der Zwan A, Verweij BH, Biesbroek M, Regli L, Tulleken CAF. Experimental Simplification of the Excimer Laser-Assisted Nonocclusive Anastomosis (ELANA) Technique. Neurosurgery. 2010 Sep;67(3):283-90.

[194] Matsushima T, Inoue K, Kawashima M, Inoue T. History of the development of surgical treatments for moyamoya disease. Neurologia Medico-Chirurgica. 2012;52(5):278-86.

[195] Kim SK, Wang KC, Kim IO, Lee DS, Cho BK. Combined encephaloduroarteriosynangiosis and bifrontal encephalogaleo (periosteal) synangiosis in pediatric moyamoya disease. Neurosurgery. 2008 Jun;62(6 Suppl 3):1456-64.

[196] Navarro R, Chao K, Gooderham PA, Bruzoni M, Dutta S, Steinberg GK. Less invasive pedicled omental-cranial transposition in pediatric patients with moyamoya disease and failed prior revascularization. Neurosurgery. 2014;10(1):1-14.

[197] Gross BA, Stone SS, Smith ER. Occipital pial synangiosis. Acta Neurochirurgica. 2014;156(7):1297-300.

[198] Esposito G, Kronenburg A, Fierstra J, Braun KPJ, Klijn CJM, van der Zwan A, et al. “STA-MCA bypass with encephalo-duro-myo-synangiosis combined with bifrontal encephalo-duro-periosteal-synangiosis” as a one-staged revascularization strategy for pediatric moyamoya vasculopathy. Child's Nervous System. 2015.

[199] Kikuta K, Takagi Y, Fushimi Y, Ishizu K, Okada T, Hanakawa T, et al. "Target bypass": a method for preoperative targeting of a recipient artery in superficial temporal artery-to-middle cerebral artery anastomoses. Neurosurgery. 2006 Oct;59(4 Suppl 2):ONS320-6; discussion ONS6-7.

[200] Nakagawa I, Kurokawa S, Tanisaka M, Kimura R, Nakase H. Virtual surgical planning for superficial temporal artery to middle cerebral artery bypass using three-dimensional digital subtraction angiography. Acta Neurochirurgica. 2010;152(9):1535-40.

[201] Riva M, Kamouni R, Schoovaerts F, Bruneau M. A neuronavigation-based method for locating the superficial temporal artery during extra-intracranial bypass surgery. Neurosurg Rev. 2015;38(2):373-9.

[202] Cabrilo I, Schaller K, Bijlenga P. Augmented reality-assisted bypass surgery: Embracing minimal invasiveness. World Neurosurgery. 2015;83(4):596-602.

[203] Almefty RO, Nakaji P. Augmented, Reality-Enhanced Navigation for Extracranial-Intracranial Bypass. World Neurosurg. 2015 Jul;84(1):15-7.

[204] Awano T, Sakatani K, Yokose N, Kondo Y, Igarashi T, Hoshino T, et al. Intraoperative EC-IC bypass blood flow assessment with indocyanine green angiography in moyamoya and non-moyamoya ischemic stroke. World Neurosurg. 2010 Jun;73(6):668-74.

[205] Woitzik J, Horn P, Vajkoczy P, Schmiedek P. Intraoperative control of extracranial-intracranial bypass patency by near-infrared indocyanine green videoangiography. J Neurosurg. 2005 Apr;102(4):692-8.

[206] Schuette AJ, Dannenbaum MJ, Cawley CM, Barrow DL. Indocyanine green videoangiography for confirmation of bypass graft patency. J Korean Neurosurg Soc. 2011 Jul;50(1):23-9.

[207] Denault A, Deschamps A, Murkin JM. A proposed algorithm for the intraoperative use of cerebral near-infrared spectroscopy. Semin Cardiothorac Vasc Anesth. 2007 Dec;11(4):274-81.

[208] Murata Y, Katayama Y, Sakatani K, Fukaya C, Kano T. Evaluation of extracranial-intracranial arterial bypass function by using near-infrared spectroscopy. J Neurosurg. 2003 Aug;99(2):304-10.

[209] Wu JS, Zhang J, Zhuang DX, Yao CJ, Qiu TM, Lu JF, et al. Current status of cerebral glioma surgery in China. Chin Med J (Engl). 2011 Sep;124(17):2569-77.

[210] Wu JS, Zhu FP, Zhuang DX, Yao CJ, Qiu TM, Liu JF, et al. Preliminary application of 3. 0 T intraoperative magnetic resonance imaging neuronavigation system in China. Chinese Journal of Surgery. 2011;49(8):683-7.

[211] Wu JS, Shou XF, Yao CJ, Wang YF, Zhuang DX, Mao Y, et al. Transsphenoidal Pituitary Macroadenomas Resection Guided by Polestar N20 Low-Field Intraoperative Magnetic Resonance Imaging: Comparison with Early Postoperative High-Field Magnetic Resonance Imaging. Neurosurgery. 2009 Jul;65(1):63-71.

[212] Zhu FP, Wu JS, Yao CJ, Lang LQ, Xu G, Mao Y. Intraoperative neurophysiological monitoring in low-field MRI environment. Chinese Journal of Neurosurgery. 2010;26(4):303-5.

[213] Buchfelder M, Ganslandt O, Fahlbusch R, Nimsky C. Intraoperative magnetic resonance imaging in epilepsy surgery. J Magn Reson Imaging. 2000 Oct;12(4):547-55.

[214] Moriarty TM, Quinones-Hinojosa A, Larson PS, Alexander E, 3rd, Gleason PL, Schwartz RB, et al. Frameless stereotactic neurosurgery using intraoperative magnetic resonance imaging: stereotactic brain biopsy. Neurosurgery. 2000 Nov;47(5):1138-45; discussion 45-6.

[215] Daniel BL, Birdwell RL, Butts K, Nowels KW, Ikeda DM, Heiss SG, et al. Freehand iMRI-guided large-gauge core needle biopsy: a new minimally invasive technique for diagnosis of enhancing breast lesions. J Magn Reson Imaging. 2001 Jun;13(6):896-902.

[216] Sakurada K, Kuge A, Takemura S, Funiu H, Kokubo Y, Kondo R, et al. Intraoperative magnetic resonance imaging in the successful surgical treatment of an arteriovenous malformation--case report. Neurol Med Chir (Tokyo). 2011;51(7):512-4.

[217] Sutherland GR, Kaibara T, Wallace C, Tomanek B, M R. Intraoperative assessment of aneurysm clipping using magnetic resonance angiography and diffusion-weighted imaging: Technical case report. Neurosurgery. 2002;50:893-8.

[218] Fahlbusch R, Nimsky C. Intraoperative MRI developments. Neurosurgery clinics of North America. 2005 Jan;16(1):xi-xiii.

[219] Szabo K, Kern R, Gass A, Hirsch J, Hennerici M. Acute stroke patterns in patients with internal carotid artery disease: a diffusion-weighted magnetic resonance imaging study. Stroke; a journal of cerebral circulation. 2001 Jun;32(6):1323-9.

[220] Neumann-Haefelin T, Wittsack HJ, Fink GR, Wenserski F, Li TQ, Seitz RJ, et al. Diffusion- and perfusion-weighted MRI: influence of severe carotid artery stenosis on the DWI/PWI mismatch in acute stroke. Stroke; a journal of cerebral circulation. 2000 Jun;31(6):1311-7.

[221] Matsushima Y, Inaba Y. Moyamoya disease in children and its surgical treatment. Introduction of a new surgical procedure and its follow-up angiograms. Childs Brain. 1984;11(3):155-70.

[222] Miyamoto S, Yoshimoto T, Hashimoto N, Okada Y, Tsuji I, Tominaga T, et al. Effects of extracranial-intracranial bypass for patients with hemorrhagic moyamoya disease: results of the Japan Adult Moyamoya Trial. Stroke. 2014 May;45(5):1415-21.

[223] Houkin K, Nakayama N, Kuroda S, Ishikawa T, Nonaka T. How does angiogenesis develop in pediatric moyamoya disease after surgery? A prospective study with MR angiography. Childs Nerv Syst. 2004 Oct;20(10):734-41.

[224] Sasoh M, Ogasawara K, Kuroda K, Okuguchi T, Terasaki K, Yamadate K, et al. Effects of EC-IC bypass surgery on cognitive impairment in patients with hemodynamic cerebral ischemia. Surgical Neurology. 2003 Jun;59(6):455-60.

[225] Takagi Y, Hashimoto N, Iwama T, Hayashida K. Improvement of oxygen metabolic reserve after extracranial-intracranial bypass surgery in patients with severe haemodynamic insufficiency. Acta Neurochirurgica. 1997;139(1):52-6.

[226] Hoshino T, Sakatani K, Kano T, Murata Y, Katayama Y. Cerebral blood oxygenation changes induced by bypass blood flow in moyamoya disease and non-moyamoya cerebral ischaemic disease. Acta Neurochirurgica. 2006 May;148(5):551-7.

[227] Derdeyn CP. Direct bypass reduces the risk of recurrent haemorrhage in moyamoya syndrome, but effect on functional outcome is less certain. Stroke. 2014 May;45(5):1245-6.

[228] Guzman R, Lee M, Achrol A, Bell-Stephens T, Kelly M, Do HM, et al. Clinical outcome after 450 revascularization procedures for moyamoya disease. Clinical article. J Neurosurg. 2009 Nov;111(5):927-35.

[229] Hyun SJ, Kim JS, Hong SC. Prognostic factors associated with perioperative ischemic complications in adult-onset moyamoya disease. Acta Neurochir (Wien). 2010 Jul;152(7):1181-8.

[230] Funaki T, Takahashi JC, Takagi Y, Kikuchi T, Yoshida K, Mitsuhara T, et al. Unstable moyamoya disease: clinical features and impact on perioperative ischemic complications. J Neurosurg. 2015 Feb;122(2):400-7.

[231] Funaki T, Takahashi JC, Takagi Y, Yoshida K, Araki Y, Kikuchi T, et al. Incidence of late cerebrovascular events after direct bypass among children with moyamoya disease: a descriptive longitudinal study at a single center. Acta Neurochir (Wien). 2014 Mar;156(3):551-9; discussion 9.

[232] Kobayashi E, Saeki N, Oishi H, Hirai S, Yamaura A. Long-term natural history of hemorrhagic moyamoya disease in 42 patients. J Neurosurg. 2000 Dec;93(6):976-80.

[233] Ryan RW, Chowdhary A, Britz GW. Hemorrhage and risk of further hemorrhagic strokes following cerebral revascularization in Moyamoya disease: A review of the literature. Surg Neurol Int. 2012;3:72.

[234] Lee M, Guzman R, Bell-Stephens T, Steinberg GK. Intraoperative blood flow analysis of direct revascularization procedures in patients with moyamoya disease. J Cereb Blood Flow Metab. 2011 Jan;31(1):262-74.

[235] Cho WS, Kim JE, Kim CH, Ban SP, Kang HS, Son YJ, et al. Long-term outcomes after combined revascularization surgery in adult moyamoya disease. Stroke. 2014 Oct;45(10):3025-31.

[236] Andoh T, Sakai N, Yamada H, Yano H, Hirayama H, Imao Y, et al. Chronic subdural hematoma following bypass surgery--report of three cases. Neurol Med Chir (Tokyo). 1992 Aug;32(9):684-9.

[237] Narisawa A, Fujimura M, Shimizu H, Tominaga T. Seizure following superficial temporal-middle cerebral artery anastomosis in patients with moyamoya disease: possible contribution of postoperative cerebral hyperperfusion. No Shinkei Geka. 2007 May;35(5):467-74.

[238] Kawabori M, Kuroda S, Nakayama N, Hirata K, Shiga T, Houkin K, et al. Effective surgical revascularization improves cerebral hemodynamics and resolves headache in pediatric Moyamoya disease. World Neurosurg. 2013 Nov;80(5):612-9.

[239] Hayashi T, Kashiwazaki D, Akioka N, Kuwayama N, Kuroda S. [Recurrent hyperperfusion after revascularization surgery for adult moyamoya disease: a case report]. No Shinkei Geka. 2014 Jul;42(7):621-7.

[240] Kwon H, Kim HJ, Yim YM, Jung SN. Reconstruction of scalp defect after Moyamoya disease surgery using an occipital pedicle V-Y advancement flap. J Craniofac Surg. 2008 Jul;19(4):1075-9.

[241] Kim DS, Yoo DS, Huh PW, Kang SG, Cho KS, Kim MC. Combined direct anastomosis and encephaloduroarteriogaleosynangiosis using inverted superficial temporal artery-galeal flap and superficial temporal artery-galeal pedicle in adult moyamoya disease. Surg Neurol. 2006 Oct;66(4):389-94; discussion 95.

[242] Sanada Y, Yabuuchi T, Yoshioka H, Kubota H, Kato A. Zigzag skin incision effectively camouflages the scar and alopecia for moyamoya disease: Technical note. Neurologia Medico-Chirurgica. 2015;55(3):210-3.

[243] Hwang JW, Yang HM, Lee H, Lee HK, Jeon YT, Kim JE, et al. Predictive factors of symptomatic cerebral hyperperfusion after superficial temporal artery-middle cerebral artery

anastomosis in adult patients with moyamoya disease. Brit J Anaesth. 2013 May;110(5):773-9.

[244] Nossek E, Langer DJ. How I do it: combined direct (STA-MCA) and indirect (EDAS) EC-IC bypass. Acta Neurochir (Wien). 2014 Nov;156(11):2079-84.

[245] van Mook WN, Rennenberg RJ, Schurink GW, van Oostenbrugge RJ, Mess WH, Hofman PA, et al. Cerebral hyperperfusion syndrome. Lancet Neurol. 2005 Dec;4(12):877-88.

[246] Kim JE, Oh CW, Kwon OK, Park SQ, Kim SE, Kim YK. Transient hyperperfusion after superficial temporal artery/middle cerebral artery bypass surgery as a possible cause of postoperative transient neurological deterioration. Cerebrovasc Dis. 2008;25(6):580-6.

[247] Nyamekye IK, Begum S, Slaney PL. Post-carotid endarterectomy cerebral hyperperfusion syndrome. J R Soc Med. 2005 Oct;98(10):472-4.

[248] Fujimura M, Kaneta T, Mugikura S, Shimizu H, Tominaga T. Temporary neurologic deterioration due to cerebral hyperperfusion after superficial temporal artery-middle cerebral artery anastomosis in patients with adult-onset moyamoya disease. Surg Neurol. 2007 Mar;67(3):273-82.

[249] Ohue S, Kumon Y, Kohno K, Watanabe H, Iwata S, Ohnishi T. Postoperative temporary neurological deficits in adults with moyamoya disease. Surg Neurol. 2008 Mar;69(3):281-6; discussion 6-7.

[250] Lee M, Zaharchuk G, Guzman R, Achrol A, Bell-Stephens T, Steinberg GK. Quantitative hemodynamic studies in moyamoya disease: a review. Neurosurg Focus. 2009 Apr;26(4):E5.

[251] Kawamata T, Kawashima A, Yamaguchi K, Hori T, Okada Y. Usefulness of intraoperative laser Doppler flowmetry and thermography to predict a risk of postoperative hyperperfusion after superficial temporal artery-middle cerebral artery bypass for moyamoya disease. Neurosurg Rev. 2011 Jul;34(3):355-62; discussion 62.

[252] Fujimura M, Niizuma K, Endo H, Sato K, Inoue T, Shimizu H, et al. Quantitative analysis of early postoperative cerebral blood flow contributes to the prediction and diagnosis of cerebral hyperperfusion syndrome after revascularization surgery for moyamoya disease. Neurol Res. 2015;37(2):131-8.

[253] Wintermark M, Sesay M, Barbier E, Borbely K, Dillon WP, Eastwood JD, et al. Comparative overview of brain perfusion imaging techniques. J Neuroradiol. 2005 Dec;32(5):294-314.

[254] Zhang J, Wang J, Geng D, Li Y, Song D, Gu Y. Whole-brain CT perfusion and CT angiography assessment of Moyamoya disease before and after surgical revascularization: preliminary study with 256-slice CT. Plos One. 2013;8(2):e57595.

[255] Petrella JR, Provenzale JM. MR perfusion imaging of the brain: techniques and applications. AJR Am J Roentgenol. 2000 Jul;175(1):207-19.

[256] Calamante F, Ganesan V, Kirkham FJ, Jan W, Chong WK, Gadian DG, et al. MR perfusion imaging in Moyamoya Syndrome: potential implications for clinical evaluation of occlusive cerebrovascular disease. Stroke. 2001 Dec 1;32(12):2810-6.

[257] Hayashi H, Kawatani M, Ohta G, Kometani H, Ohshima Y. [Assessment of brain perfusion by arterial spin-labeling MR imaging in qusai-moyamoya disease associated with Graves' disease]. No To Hattatsu. 2014 Jul;46(4):297-300.

[258] Togao O, Mihara F, Yoshiura T, Tanaka A, Noguchi T, Kuwabara Y, et al. Cerebral hemodynamics in Moyamoya disease: correlation between perfusion-weighted MR imaging and cerebral angiography. AJNR Am J Neuroradiol. 2006 Feb;27(2):391-7.

[259] Yun TJ, Cheon JE, Na DG, Kim WS, Kim IO, Chang KH, et al. Childhood moyamoya disease: quantitative evaluation of perfusion MR imaging-correlation with clinical outcome after revascularization surgery. Radiology. 2009 Apr;251(1):216-23.

[260] Jefferson AL, Glosser G, Detre JA, Sinson G, Liebeskind DS. Neuropsychological and perfusion MR imaging correlates of revascularization in a case of moyamoya syndrome. AJNR Am J Neuroradiol. 2006 Jan;27(1):98-100.

[261] Lee SK, Kim DI, Jeong EK, Kim SY, Kim SH, In YK, et al. Postoperative evaluation of moyamoya disease with perfusion-weighted MR imaging: initial experience. AJNR Am J Neuroradiol. 2003 Apr;24(4):741-7.

[262] Zhao WG, Luo Q, Jia JB, Yu JL. Cerebral hyperperfusion syndrome after revascularization surgery in patients with moyamoya disease. Br J Neurosurg. 2013 Jun;27(3):321-5.

[263] Fujimura M, Niizuma K, Endo H, Sato K, Inoue T, Shimizu H, et al. Quantitative analysis of early postoperative cerebral blood flow contributes to the prediction and diagnosis of cerebral hyperperfusion syndrome after revascularization surgery for moyamoya disease. Neurol Res. 2015 Feb;37(2):131-8.

[264] Sakata H, Fujimura M, Mugikura S, Sato K, Tominaga T. Local Vasogenic Edema without Cerebral Hyperperfusion after Direct Revascularization Surgery for Moyamoya Disease. J Stroke Cerebrovasc Dis. 2015 Jul;24(7):e179-84.

[265] Qiu TM, Yao CJ, Wu JS, Pan ZG, Zhuang DX, Xu G, et al. Clinical experience of 3T intraoperative magnetic resonance imaging integrated neurosurgical suite in Shanghai Huashan Hospital. Chinese Medical Journal. 2012;125(24):4328-33.

[266] Wu JS, Zhu FP, Zhuang DX, Yao CJ, Qiu TM, Lu JF, et al. Preliminary application of 3.0 T intraoperative magnetic resonance imaging neuronavigation system in China. Zhonghua wai ke za zhi [Chinese journal of surgery]. 2011;49(8):683-7.

[267] Ostergaard L, Weisskoff RM, Chesler DA, Gyldensted C, Rosen BR. High resolution measurement of cerebral blood flow using intravascular tracer bolus passages. Part I: Mathematical approach and statistical analysis. Magnetic resonance in medicine : official journal of the Society of Magnetic Resonance in Medicine / Society of Magnetic Resonance in Medicine. 1996 Nov;36(5):715-25.

[268] Wu O, Ostergaard L, Weisskoff RM, Benner T, Rosen BR, Sorensen AG. Tracer arrival timing-insensitive technique for estimating flow in MR perfusion-weighted imaging using singular value decomposition with a block-circulant deconvolution matrix. Magnetic resonance in medicine : official journal of the Society of Magnetic Resonance in Medicine / Society of Magnetic Resonance in Medicine. 2003 Jul;50(1):164-74.

[269] Oppenheim AV, Schafer RW. Discrete-time signal processing. Englewood Cliffs, N.J.: Prentice Hall 1989.

[270] Hamberg LM, Hunter GJ, Halpern EF, Hoop B, Gazelle GS, Wolf GL. Quantitative high-resolution measurement of cerebrovascular physiology with slip-ring CT. AJNR American journal of neuroradiology. 1996 Apr;17(4):639-50.

[271] Lee BK. Computational fluid dynamics in cardiovascular disease. Korean Circ J. 2011 Aug;41(8):423-30.

[272] Farnoush A, Avolio A, Qian Y. A growth model of saccular aneurysms based on hemodynamic and morphologic discriminant parameters for risk of rupture. Journal of Clinical Neuroscience. 2014;21(9):1514-9.

[273] Kamoda A, Yagi T, Sato A, Qian Y, Iwasaki K, Umezu M, et al. Biomedical Engineering Analysis of the Rupture Risk of Cerebral Aneurysms: Flow Comparison of Three Small Pre-ruptured Versus Six Large Unruptured Cases. *IFMBE Proceedings* 2009:1600-3.

[274] Qian Y, Takao H, Umezu M, Murayama Y. Risk analysis of unruptured aneurysms using computational fluid dynamics technology: Preliminary results. American Journal of Neuroradiology. 2011;32(10):1948-55.

[275] Sen Y, Qian Y, Avolio A, Morgan M. Image segmentation methods for intracranial aneurysm haemodynamic research. Journal of biomechanics. 2014;47(5):1014-9.

[276] Shojima M, Morita A, Kimura T, Oshima M, Kin T, Saito N. Computational fluid dynamic simulation of a giant basilar tip aneurysm with eventual rupture after Hunterian ligation. World neurosurgery. 2014;82(3-4):535.e5-9.

[277] Cheng SWK, Lam ESK, Fung GSK, Ho P, Ting ACW, Chow KW. A computational fluid dynamic study of stent graft remodeling after endovascular repair of thoracic aortic dissections. Journal of Vascular Surgery. 2008;48(2):303-10.

[278] Alnaes MS, Isaksen J, Mardal KA, Romner B, Morgan MK, Ingebrigtsen T. Computation of hemodynamics in the circle of Willis. Stroke. 2007 Sep;38(9):2500-5.

[279] Alaraj A, Amin-Hanjani S, Shakur SF, Aletich VA, Ivanov A, Carlson AP, et al. Quantitative assessment of changes in cerebral arteriovenous malformation hemodynamics after embolization. Stroke. 2015 Apr;46(4):942-7.

[280] Alaraj A, Shakur SF, Amin-Hanjani S, Mostafa H, Khan S, Aletich VA, et al. Changes in wall shear stress of cerebral arteriovenous malformation feeder arteries after embolization and surgery. Stroke. 2015 May;46(5):1216-20.

[281] Seol HJ, Shin DC, Kim YS, Shim EB, Kim SK, Cho BK, et al. Computational analysis of hemodynamics using a two-dimensional model in moyamoya disease Laboratory investigation. J Neurosurg-Pediatr. 2010 Mar;5(3):297-301.

[282] Charbel FT, Misra M, Clarke ME, Ausman JI. Computer simulation of cerebral blood flow in moyamoya and the results of surgical therapies. Clin Neurol Neurosurg. 1997 Oct;99 Suppl 2:S68-73.

[283] Karunanithi K, Han C, Lee CJ, Shi W, Duan L, Qian Y. Identification of a hemodynamic parameter for assessing treatment outcome of EDAS in Moyamoya disease. Journal of Biomechanics. 2015;48(2):304-9.

[284] Kim T, Bang JS, Kwon OK, Hwang G, Kim JE, Kang HS, et al. Morphology and related hemodynamics of the internal carotid arteries of moyamoya patients. Acta Neurochir (Wien). 2015 May;157(5):755-61.

[285] Burleson AC, Strother CM, Turitto VT. Computer Modeling of Intracranial Saccular and Lateral Aneurysms for the Study of Their Hemodynamics. Neurosurgery. 1995 Oct;37(4):774-82.

[286] Cebral JR, Mut F, Raschi M, Scrivano E, Ceratto R, Lylyk P, et al. Aneurysm rupture following treatment with flow-diverting stents: computational hemodynamics analysis of treatment. AJNR Am J Neuroradiol. 2011 Jan;32(1):27-33.

[287] Chien A, Castro MA, Tateshima S, Sayre J, Cebral J, Vinuela F. Quantitative hemodynamic analysis of brain aneurysms at different locations. AJNR Am J Neuroradiol. 2009 Sep;30(8):1507-12.

[288] Hoi Y, Meng H, Woodward SH, Bendok BR, Hanel RA, Guterman LR, et al. Effects of arterial geometry on aneurysm growth: three-dimensional computational fluid dynamics study. J Neurosurg. 2004 Oct;101(4):676-81.

[289] Steinman DA, Thomas JB, Ladak HM, Milner JS, Rutt BK, Spence JD. Reconstruction of carotid bifurcation hemodynamics and wall thickness using computational fluid dynamics and MRI. Magn Reson Med. 2002 Jan;47(1):149-59.

[290] Valencia A, Zarate A, Galvez M, Badilla L. Non-Newtonian blood flow dynamics in a right internal carotid artery with a saccular aneurysm. Int J Numer Meth Fl. 2006 Feb 28;50(6):751-64.

[291] Amin-Hanjani S, Shin JH, Zhao M, Du X, Charbel FT. Evaluation of extracranial-intracranial bypass using quantitative magnetic resonance angiography. Journal of neurosurgery. 2007 Feb;106(2):291-8.

[292] Amin-Hanjani S, Singh A, Rifai H, Thulborn KR, Alaraj A, Aletich V, et al. Combined Direct and Indirect Bypass for Moyamoya: Quantitative Assessment of Direct Bypass Flow over Time. Neurosurgery. 2013 Aug 13.

[293] Wang Y, Chen L, Pan H, Xu B, Liao Y. Hemodynamic study with duplex ultrasonography on combined (direct/indirect) revascularization in adult moyamoya disease. J Stroke Cerebrovasc Dis. 2014 Nov-Dec;23(10):2573-9.

[294] Pelc NJ. Flow quantification and analysis methods. Magn Reson Imaging Clin N Am. 1995 Aug;3(3):413-24.

[295] Battal B, Kocaoglu M, Bulakbasi N, Husmen G, Tuba Sanal H, Tayfun C. Cerebrospinal fluid flow imaging by using phase-contrast MR technique. Br J Radiol. 2011 Aug;84(1004):758-65.

[296] Neff KW, Horn P, Schmiedek P, Duber C, Dinter DJ. 2D cine phase-contrast MRI for volume flow evaluation of the brain-supplying circulation in moyamoya disease. AJR Am J Roentgenol. 2006 Jul;187(1):W107-15.

[297] Zhao M, Charbel FT, Alperin N, Loth F, Clark ME. Improved phase-contrast flow quantification by three-dimensional vessel localization. Magnetic Resonance Imaging. 2000;18(6):697-706.

[298] Calderon-Arnulphi M, Amin-Hanjani S, Alaraj A, Zhao M, Du X, Ruland S, et al. In vivo evaluation of quantitative MR angiography in a canine carotid artery stenosis model. American Journal of Neuroradiology. 2011;32(8):1552-9.

[299] Amin-Hanjani S, Du X, Zhao M, Walsh K, Malisch TW, Charbel FT. Use of quantitative magnetic resonance angiography to stratify stroke risk in symptomatic vertebrobasilar disease. Stroke. 2005;36(6):1140-5.

[300] Prabhakaran S, Warrior L, Wells KR, Jhaveri MD, Chen M, Lopes DK. The utility of quantitative magnetic resonance angiography in the assessment of intracranial in-stent stenosis. Stroke. 2009 Mar;40(3):991-3.

[301] Marzo A, Singh P, Reymond P, Stergiopulos N, Patel U, Hose R. Influence of inlet boundary conditions on the local haemodynamics of intracranial aneurysms. Comput Methods Biomech Biomed Engin. 2009 Aug;12(4):431-44.

[302] Zhao SZ, Xu XY, Hughes AD, Thom SA, Stanton AV, Ariff B, et al. Blood flow and vessel mechanics in a physiologically realistic model of a human carotid arterial bifurcation. Journal of Biomechanics. 2000 Aug;33(8):975-84.

[303] Kim M, Taulbee DB, Tremmel M, Meng H. Comparison of two stents in modifying cerebral aneurysm hemodynamics. Annals of biomedical engineering. 2008 May;36(5):726-41.

[304] Ford MD, Stuhne GR, Nikolov HN, Lownie SP, Holdsworth DW, Steinman DA. Virtual angiography for visualization and validation of computational fluid dynamics models of aneurysm hemodynamics. P Soc Photo-Opt Ins. 2005;5744:329-37.

[305] Acevedo-Bolton G, Jou LD, Dispensa BP, Lawton MT, Higashida RT, Martin AJ, et al. Estimating the hemodynamic impact of interventional treatments of aneurysms: numerical simulation with experimental validation: technical case report. Neurosurgery. 2006 Aug;59(2):E429-30; author reply E-30.

[306] Ford MD, Nikolov HN, Milner JS, Lownie SP, DeMont EM, Kalata W, et al. PIV-measured versus CFD-predicted flow dynamics in anatomically realistic cerebral aneurysm models. J Biomech Eng-T Asme. 2008 Apr;130(2).

[307] Kuroda S, Houkin K. Moyamoya disease: current concepts and future perspectives. Lancet Neurol. 2008 Nov;7(11):1056-66.

[308] Fujimura M, Kaneta T, Mugikura S, Shimizu H, Tominaga T. Temporary neurologic deterioration due to cerebral hyperperfusion after superficial temporal artery-middle cerebral artery anastomosis in patients with adult-onset moyamoya disease. Surg Neurol. 2007 Mar;67(3):273-82.

[309] Ivens S, Gabriel S, Greenberg G, Friedman A, Shelef I. Blood-brain barrier breakdown as a novel mechanism underlying cerebral hyperperfusion syndrome. Journal of neurology. 2010 Apr;257(4):615-20.

[310] van Mook WN, Rennenberg RJ, Schurink GW, van Oostenbrugge RJ, Mess WH, Hofman PA, et al. Cerebral hyperperfusion syndrome. Lancet Neurol. 2005 Dec;4(12):877-88.

[311] Fujimura M, Inoue T, Shimizu H, Saito A, Mugikura S, Tominaga T. Efficacy of prophylactic blood pressure lowering according to a standardized postoperative management protocol to prevent symptomatic cerebral hyperperfusion after direct revascularization surgery for moyamoya disease. Cerebrovasc Dis. 2012;33(5):436-45.

[312] Uchino H, Nakamura T, Houkin K, Murata J, Saito H, Kuroda S. Semiquantitative analysis of indocyanine green videoangiography for cortical perfusion assessment in superficial temporal artery to middle cerebral artery anastomosis. Acta Neurochir (Wien). 2013 Apr;155(4):599-605.

[313] Avants BB, Tustison, N., & Song, G. Advanced Normalization Tools (ANTS). Insight J. 2009.

[314] Tatu L, Moulin T, Vuillier F, Bogousslavsky J. Arterial territories of the human brain. Frontiers of neurology and neuroscience. 2012;30:99-110.

[315] Eastwood JD, Lev MH, Azhari T, Lee TY, Barboriak DP, Delong DM, et al. CT perfusion scanning with deconvolution analysis: pilot study in patients with acute middle cerebral artery stroke. Radiology. 2002 Jan;222(1):227-36.

[316] Kudo K, Sasaki M, Yamada K, Momoshima S, Utsunomiya H, Shirato H, et al. Differences in CT perfusion maps generated by different commercial software: quantitative analysis by using identical source data of acute stroke patients. Radiology. 2010 Jan;254(1):200-9.

[317] Butcher KS, Parsons M, MacGregor L, Barber PA, Chalk J, Bladin C, et al. Refining the perfusion-diffusion mismatch hypothesis. Stroke; a journal of cerebral circulation. 2005 Jun;36(6):1153-9.

[318] Ikezaki K, Matsushima T, Kuwabara Y, Suzuki SO, Nomura T, Fukui M. Cerebral circulation and oxygen metabolism in childhood moyamoya disease: a perioperative positron emission tomography study. Journal of neurosurgery. 1994 Dec;81(6):843-50.

[319] Fricke E, Fricke H, Weise R, Kammeier A, Hagedorn R, Lotz N, et al. Attenuation correction of myocardial SPECT perfusion images with low-dose CT: evaluation of the method by comparison with perfusion PET. Journal of nuclear medicine : official publication, Society of Nuclear Medicine. 2005 May;46(5):736-44.

[320] Sakamoto S, Ohba S, Shibukawa M, Kiura Y, Arita K, Kurisu K. CT perfusion imaging for childhood moyamoya disease before and after surgical revascularization. Acta Neurochir (Wien). 2006 Jan;148(1):77-81; discussion

[321] Rohde V, Rohde I, Thiex R, Kuker W, Ince A, Gilsbach JM. The role of intraoperative magnetic resonance imaging for the detection of hemorrhagic complications during surgery

for intracerebral lesions an experimental approach. Surg Neurol. 2001 Oct;56(4):266-74; discussion 74-5.

[322] Nair AK, Drazin D, Yamamoto J, Boulos AS. Computed tomographic perfusion in assessing postoperative revascularization in moyamoya disease. World neurosurgery. 2010 Feb;73(2):93-9; discussion e13.

[323] Kim SK, Wang KC, Oh CW, Kim IO, Lee DS, Song IC, et al. Evaluation of cerebral hemodynamics with perfusion MRI in childhood moyamoya disease. Pediatric neurosurgery. 2003 Feb;38(2):68-75.

[324] Takeuchi K SK. Hypoplasia of the bilateral internal carotid arteries. No To Shinkei. 1957;9:37-43.

[325] Fukui M. Current state of study on moyamoya disease in Japan. Surg Neurol. 1997 Feb;47(2):138-43.

[326] Suzuki J TA. Cerebrovascular 'Moyamoya disease':Adisease showing abnormal net-like vessels in base of brain. Arch Neurol. 1969;20:288-99.

[327] Kuroda S, Houkin K. Moyamoya disease: current concepts and future perspectives. Lancet Neurol. 2008 Nov;7(11):1056-66.

[328] Zhao M, Amin-Hanjani S, Ruland S, Curcio AP, Ostergren L, Charbel FT. Regional cerebral blood flow using quantitative MR angiography. AJNR American journal of neuroradiology. 2007 Sep;28(8):1470-3.

[329] Jamali AA, Deuel C, Perreira A, Salgado CJ, Hunter JC, Strong EB. Linear and angular measurements of computer-generated models: are they accurate, valid, and reliable? Comput Aided Surg. 2007 Sep;12(5):278-85.

[330] Qian Y LJ, Itatani K, Miyaji K, Umezu M. Computational hemodynamic analysis in congenital heart disease: simulation of the Norwood procedure. Ann Biomed Eng. 2010;38(7):2302–13.

[331] Zhang Y, Furusawa T, Sia SF, Umezu M, Qian Y. Proposition of an outflow boundary approach for carotid artery stenosis CFD simulation. Comput Methods Biomech Biomed Engin. 2012 Jan 30.

[332] Brater FE, King HW, eds. Handbook of hydraulics for the solution of hydraulic engineering problems. New York McGraw-Hill 1976.

[333] Allan CR. Effect of Collateral and Peripheral Resistance on Blood Flow Through Arterial Stenoses. J Biomech. 1976;9:367-75.

[334] Goldman S, Zadina K, Moritz T, Ovitt T, Sethi G, Copeland JG, et al. Long-term patency of saphenous vein and left internal mammary artery grafts after coronary artery

bypass surgery: results from a Department of Veterans Affairs Cooperative Study. J Am Coll Cardiol. 2004 Dec 7;44(11):2149-56.

[335] Lajos TZ, Graham SP, Guntupalli M, Raza ST, Hasnain S. Comparison of long-term patency of "horseshoe" saphenous vein grafts with and without valves. Eur J Cardiothorac Surg. 1996;10(10):846-51.

[336] Eguchi T. EC/IC bypass using a long-vein graft. International Congress Series 1247. 2002:421– 35.

[337] Sia SF, Davidson AS, Assaad NN, Stoodley M, Morgan MK. Comparative patency between intracranial arterial pedicle and vein bypass surgery. Neurosurgery. 2011;69(2):308-14.

[338] Gu Y, Ni W, Jiang H, Ning G, Xu B, Tian Y, et al. Efficacy of extracranial-intracranial revascularization for non-moyamoya steno-occlusive cerebrovascular disease in a series of 66 patients. J Clin Neurosci. 2012 Oct;19(10):1408-15.

[339] Nuki Y MM, Tsang E, Young WL, van Rooijen, N, Kurihara C, Hashimoto T. Roles of macrophages in flow-induced outward vascular remodeling. J Cereb Blood Flow Metab. 2009;29:495-503.

[340] Ota R, Kurihara C, Tsou TL, Young WL, Yeghiazarians Y, Chang M, et al. Roles of matrix metalloproteinases in flow-induced outward vascular remodeling. Journal of cerebral blood flow and metabolism : official journal of the International Society of Cerebral Blood Flow and Metabolism. 2009 Sep;29(9):1547-58.

[341] Zhang Y, Furusawa T, Sia SF, Umezu M, Qian Y. Proposition of an outflow boundary approach for carotid artery stenosis CFD simulation. Comput Methods Biomech Biomed Engin. 2013;16(5):488-94.

[342] Markl M, Wegent F, Zech T, Bauer S, Strecker C, Schumacher M, et al. In vivo wall shear stress distribution in the carotid artery: effect of bifurcation geometry, internal carotid artery stenosis, and recanalization therapy. Circ Cardiovasc Imaging. 2010 Nov;3(6):647-55.

[343] Shi ZD, Winoto SH, Lee TS. Experimental investigation of pulsatile flows in tubes. J Biomech Eng. 1997 May;119(2):213-6.

[344] Gibbons GH DV. The emerging concept of vascular remodeling. N Engl J Med. 1994;330:1431-8.

[345] Kuroda S, Houkin K. Moyamoya disease: current concepts and future perspectives. Lancet Neurol. 2008 Nov;7(11):1056-66.

[346] Iwama T, Morimoto M, Hashimoto N, Goto Y, Todaka T, Sawada M. Mechanism of intracranial re-bleeding in moyamoya disease. Clin Neurol Neurosurg. 1997 Oct;99 Suppl 2:S187-90.

[347] Miyamoto S, Yoshimoto T, Hashimoto N, Okada Y, Tsuji I, Tominaga T, et al. Effects of extracranial-intracranial bypass for patients with hemorrhagic moyamoya disease: results of the Japan Adult Moyamoya Trial. Stroke. 2014 May;45(5):1415-21.

[348] Zhang Y, Sia SF, Morgan MK, Qian Y. Flow resistance analysis of extracranial-to-intracranial (EC-IC) vein bypass. J Biomech. 2012 May 11;45(8):1400-5.

[349] Lee CJ, Zhang Y, Takao H, Murayama Y, Qian Y. A fluid-structure interaction study using patient-specific ruptured and unruptured aneurysm: the effect of aneurysm morphology, hypertension and elasticity. J Biomech. 2013 Sep 27;46(14):2402-10.

[350] Wong GK, Poon WS. Current status of computational fluid dynamics for cerebral aneurysms: the clinician's perspective. Journal of clinical neuroscience : official journal of the Neurosurgical Society of Australasia. 2011 Oct;18(10):1285-8.

[351] Sia SF, Qian Y, Zhang Y, Morgan MK. Mean arterial pressure required for maintaining patency of extracranial-to-intracranial bypass grafts: An investigation with computational hemodynamic models-case series. Neurosurgery. 2012;71(4):826-31.

[352] Zhu FP, Zhang Y, Higurashi M, Xu B, Gu YX, Mao Y, et al. Haemodynamic analysis of vessel remodelling in STA-MCA bypass for Moyamoya disease and its impact on bypass patency. J Biomech. 2014 Jun 3;47(8):1800-5.

[353] Karunanithi K, Han C, Lee CJ, Shi W, Duan L, Qian Y. Identification of a hemodynamic parameter for assessing treatment outcome of EDAS in Moyamoya disease. J Biomech. 2014 Jan 21;48(2):304-9.

[354] Vilela MD, Newell DW. Superficial temporal artery to middle cerebral artery bypass: past, present, and future. Neurosurgical Focus. 2008 Feb;24(2):-.

[355] Seol HJ, Shin DC, Kim YS, Shim EB, Kim SK, Cho BK, et al. Computational analysis of hemodynamics using a two-dimensional model in moyamoya disease. J Neurosurg Pediatr. 2010 Mar;5(3):297-301.

[356] Hertza J, Loughan A, Perna R, Davis AS, Segraves K, Tiberi NL. Moyamoya disease: a review of the literature. Applied neuropsychology Adult. 2014;21(1):21-7.

[357] Im SH, Cho CB, Joo WI, Chough CK, Park HK, Lee KJ, et al. Prevalence and epidemiological features of moyamoya disease in Korea. Journal of cerebrovascular and endovascular neurosurgery. 2012 Jun;14(2):75-8.

[358] Fung LW, Thompson D, Ganesan V. Revascularisation surgery for paediatric moyamoya: a review of the literature. Child's nervous system : ChNS : official journal of the International Society for Pediatric Neurosurgery. 2005 May;21(5):358-64.

[359] Isono M, Ishii K, Kamida T, Inoue R, Fujiki M, Kobayashi H. Long-term outcomes of pediatric moyamoya disease treated by encephalo-duro-arterio-synangiosis. Pediatric neurosurgery. 2002 Jan;36(1):14-21.

[360] Sekhon LHS, Spence I, Morgan MK, Weber NC. Long-term potentiation saturation in chronic cerebral hypoperfusion. Journal of Clinical Neuroscience. 1998;5(3):323-8.

[361] Robertson RL, Burrows PE, Barnes PD, Robson CD, Poussaint TY, Scott RM. Angiographic changes after pial synangiosis in childhood moyamoya disease. AJNR American journal of neuroradiology. 1997 May;18(5):837-45.

[362] Ross IB, Shevell MI, Montes JL, Rosenblatt B, Watters GV, Farmer JP, et al. Encephaloduroarteriosynangiosis (EDAS) for the treatment of childhood moyamoya disease. Pediatric neurology. 1994 May;10(3):199-204.

[363] Uno M, Nakajima N, Nishi K, Shinno K, Nagahiro S. Hyperperfusion syndrome after extracranial-intracranial bypass in a patient with moyamoya disease--case report. Neurol Med Chir (Tokyo). 1998 Jul;38(7):420-4.

[364] Phi JH, Wang KC, Lee JY, Kim SK. Moyamoya Syndrome: A Window of Moyamoya Disease. Journal of Korean Neurosurgical Society. 2015 Jun;57(6):408-14.

[365] Houkin K, Kamiyama H, Abe H, Takahashi A, Kuroda S. Surgical therapy for adult moyamoya disease. Can surgical revascularization prevent the recurrence of intracerebral haemorrhage? Stroke. 1996 Aug;27(8):1342-6.

[366] Ishii K, Morishige M, Anan M, Sugita K, Abe E, Kubo T, et al. Superficial temporal artery-to-middle cerebral artery anastomosis with encephalo-duro-myo-synangiosis as a modified operative procedure for moyamoya disease. Acta neurochirurgica Supplement. 2010;107:95-9.

[367] Miyamoto S, Japan Adult Moyamoya Trial G. Study design for a prospective randomized trial of extracranial-intracranial bypass surgery for adults with moyamoya disease and hemorrhagic onset--the Japan Adult Moyamoya Trial Group. Neurol Med Chir (Tokyo). 2004 Apr;44(4):218-9.

[368] Karunanithi K, Han C, Lee CJ, Shi W, Duan L, Qian Y. Identification of a hemodynamic parameter for assessing treatment outcome of EDAS in Moyamoya disease. Journal of biomechanics. 2015 Jan 21;48(2):304-9.

[369] Jamali AA, Deuel C, Perreira A, Salgado CJ, Hunter JC, Strong EB. Linear and angular measurements of computer-generated models: are they accurate, valid, and reliable? Computer aided surgery : official journal of the International Society for Computer Aided Surgery. 2007 Sep;12(5):278-85.

[370] Kato M, Suzuki T, Ogino T, Kimura T. Compliance of the peripheral capacitance vessels in patients with congestive heart failure. Angiology. 1976 Dec;27(12):698-706.

[371] Qian Y, Takao H, Umezu M, Murayama Y. Risk analysis of unruptured aneurysms using computational fluid dynamics technology: preliminary results. AJNR American journal of neuroradiology. 2011 Nov-Dec;32(10):1948-55.

[372] Zhang Y, Chong W, Qian Y. Investigation of intracranial aneurysm hemodynamics following flow diverter stent treatment. Medical engineering & physics. 2013 May;35(5):608-15.

[373] Kuroda S, Hashimoto N, Yoshimoto T, Iwasaki Y, Research Committee on Moyamoya Disease in J. Radiological findings, clinical course, and outcome in asymptomatic moyamoya disease: results of multicenter survey in Japan. Stroke; a journal of cerebral circulation. 2007 May;38(5):1430-5.

[374] Wang D, Zhu F, Fung KM, Zhu W, Luo Y, Chu WC, et al. Predicting Cerebral Hyperperfusion Syndrome Following Superficial Temporal Artery to Middle Cerebral Artery Bypass based on Intraoperative Perfusion-Weighted Magnetic Resonance Imaging. Sci Rep. 2015;5:14140.

[375] Dhar S, Tremmel M, Mocco J, Kim M, Yamamoto J, Siddiqui AH, et al. Morphology parameters for intracranial aneurysm rupture risk assessment. Neurosurgery. 2008 Aug;63(2):185-96; discussion 96-7.

[376] Doenitz C, Schebesch KM, Zoephel R, Brawanski A. A mechanism for the rapid development of intracranial aneurysms: a case study. Neurosurgery. 2010 Nov;67(5):1213-21; discussion 21.

[377] Shin DC, Seol HJ, Kim SK, Wang KC, Cho BK, Shim EB. Computational analysis of the hemodynamics in cerebral arteries related to Moyamoya disease. Ifmbe Proc. 2007;14:155-8.

[378] Iwama T, Hashimoto N, Murai BN, Tsukahara T, Yonekawa Y. Intracranial re-bleeding in moyamoya disease. Journal of clinical neuroscience : official journal of the Neurosurgical Society of Australasia. 1997 Apr;4(2):169-72.

[379] Zhang C, Wang L, Li X, Li S, Pu F, Fan Y, et al. Modeling the circle of Willis to assess the effect of anatomical variations on the development of unilateral internal carotid artery stenosis. Bio-medical materials and engineering. 2014;24(1):491-9.

[380] Fraser KH, Taskin ME, Griffith BP, Wu ZJ. The use of computational fluid dynamics in the development of ventricular assist devices. Med Eng Phys. 2011 Apr;33(3):263-80.

[381] Garcia D, Pibarot P, Dumesnil JG, Sakr F, Durand LG. Assessment of aortic valve stenosis severity - A new index based on the energy loss concept. Circulation. 2000 Feb 22;101(7):765-71.

[382] Pekkan K, Kitajima HD, de Zelicourt D, Forbess JM, Parks WJ, Fogel MA, et al. Total cavopulmonary connection flow with functional left pulmonary artery stenosis - Angioplasty and fenestration in vitro. Circulation. 2005 Nov 22;112(21):3264-71.

[383] Shojima M, Morita A, Kimura T, Oshima M, Kin T, Saito N. Computational fluid dynamic simulation of a giant basilar tip aneurysm with eventual rupture after Hunterian ligation. World Neurosurgery. 2014;82(3):535.E5-.E9.

[384] Morlacchi S, Keller B, Arcangeli P, Balzan M, Migliavacca F, Dubini G, et al. Hemodynamics and In-stent restenosis: Micro-CT images, histology, and computer simulations. Annals of Biomedical Engineering. 2011;39(10):2615-26.

[385] Takao H, Murayama Y, Otsuka S, Qian Y, Mohamed A, Masuda S, et al. Hemodynamic differences between unruptured and ruptured intracranial aneurysms during observation. Stroke. 2012;43(5):1436-9.

[386] Sia SF, Zhang Y, Qian Y, Kadir KAA, Nor HM, Morgan MK. Hemodynamic effects resulting from a common carotid to middle cerebral bypass with varying degrees of proximal internal carotid stenosis. Neurology Asia. 2014;19(3):241-7.